Doctoral Thesis
June 6, 2023

Casimir forces, entanglement and conformal invariance in inhomogeneous quantum chains

Author: Begoña Mula Martín

Supervisors: Javier Rodríguez-Laguna y Silvia N. Santalla

Programa de Doctorado en Ciencias

Einstein said that if quantum mechanics were correct then the world would be crazy. Einstein was right - the world is crazy.

D.M. Greenberger

About this thesis

This document collects part of the work developed during my Ph.D. at UNED, UC3M and SISSA under the supervision of Prof. Javier Rodríguez-Laguna and Prof. Silvia N. Santalla. The main goal of this thesis is to improve our understanding of physics of low-dimensional inhomogeneous systems, such as ground state Casimir forces and conformal symmetry breaking. Besides, the relation between quantum thermodynamics and the entanglement structure of ground states of homogeneous systems have also been object of study. This thesis is based on the following publications:

- B. Mula, S.N. Santalla, J. Rodríguez-Laguna, *Casimir forces on deformed fermionic chains*, Phys. Rev. Research **3**, 013062 (2021).
- B. Mula, N. Samos Sáenz de Buruaga, G. Sierra, S.N. Santalla, J. Rodríguez-Laguna, *Depletion in fermionic chains with inhomogeneous hoppings*, Phys. Rev. B **106**, 224204 (2022).
- B. Mula, E.M. Fernández, J.E. Alvarellos, J.J. Fernández, D. García-Aldea, S.N. Santalla, J. Rodríguez-Laguna, *Ergotropy and entanglement in critical spin chains*, Phys. Rev. B **107**, 075116 (2023).

I declare that this thesis is the result of my own original work and that it has not been submitted for any other degree or academic award. In cases where the work of others is presented, appropriate citations are used.

All figures presented in this paper have been created expressly or belong to the aforementioned papers. Otherwise, they are properly cited. All the numerical results have been obtained using codes written by me in C++ with the Hvb library[1].

Additionally, I have been part of the project *Mathematical modeling of infectious disease focused on COVID-19*, funded by Instituto de Salud Carlos III, which led to the following publication:

- O. Toledano, B. Mula, S.N. Santalla, J. Rodríguez-Laguna, O. Gálvez, *Effects of confinement and vaccination on an epidemic outburst: a statistical mechanics approach*, Phys. Rev. E **104**, 034310 (2021).

[1] Hvb is free software developed by my supervisors and his co-workers, and is released under the GPL. You can download it from the github repository:
http://github.com/jvrlag/hvb

Agradecimientos

No puedo imaginar ninguna otra forma de empezar que agradeciendo a Silvia y a Javi por todo el esfuerzo y tiempo puestos en este trabajo. No hay jamones suficientes en el mundo para daros las gracias. Habéis sido los mejores directores que se puede tener y me siento enormemente afortunada. Lo que empezó siendo un pequeño proyecto de unos meses, termina hoy en una tesis cuyo principal responsable ha sido el optimismo de Javi y su "*¡Esto ya lo tenemos, compañeras!*". Sí, han pasado cuatro años... Ha sido un viaje muy largo y no puedo decir que haya sido fácil, pero con vosotros ha sido menos difícil. Gracias por enseñarme que la programación no da miedo, o al menos intentarlo. Gracias por renormalizar las *catástrofes* y por vuestro maravilloso sentido del humor para hacerles frente. Gracias por vuestra infinita disponibilidad, vuestra ilusión y vuestras ganas constantes. Pero, sobre todo, gracias por confiar en mí aun cuando yo misma he tenido dudas.

Me gustaría dar las gracias también a Germán Sierra y a Nadir Samos por toda la ayuda recibida para que este trabajo salga adelante. Gracias a Erik Tonni y a Francesco Gentile por las reuniones, en Madrid y en Trieste, donde he tenido la oportunidad de aprender tanto. Además, agradezco a Sudipto Singha Roy por sus comentarios para mejorar este manuscrito.

Gracias a todas las personas de la UNED que, de una manera u otra, me han acompañado en este largo camino. Me gustaría agradecer de forma especial a los departamentos de Física Fundamental y de Física Interdisciplinar, donde he pasado algunos de los mejores momentos de estos años. La lista de nombres es larga y el miedo a olvidarme de alguno me previene de tratar de escribirlos todos. Aun así, estoy segura de que os llegará mi agradecimiento a todos aquellos con los que he tenido el placer de trabajar y compartir este tiempo. Gracias por vuestro apoyo, ayuda y preocupación hasta por las goteras de mi coche. No he podido pasarlo mejor con vosotros.

Gracias a mis amigos por su constante interés y entusiasmo aun sin entender nada de este trabajo. Gracias en especial a Pilar y a Inés por estar siempre y por ser las mejores compañeras de vida que se puede tener. Gracias también a Marina porque, sin vernos todo lo que nos gustaría, has hecho que me sienta comprendida en los momentos no tan bonitos de la tesis. Espero que me perdonéis los demás por no daros las gracias uno a uno, ojalá pudiera hacerlo.

Gracias a mi familia porque, sin ellos, el agobio y el estrés de estos últimos cuatro años se hubiese reducido a la mitad. Gracias a ti, mamá, por tus consejos y por escuchar las crisis existenciales durante este tiempo. Gracias, papá, por las lavadoras, las empanadillas y las salchichas. Gracias, Nacho, por nuestros viajes. Gracias también, a los dos, por todos los kilómetros corridos. Dicen que tan solo diez minutos de carrera ayudan a despejar y ordenar la mente y, aun así, ha hecho falta una maratón para llegar a este día. Espero que sea la primera de muchas.

Por último, gracias a todos los que me animasteis a embarcarme en mi aventura a Indonesia mientras me encontraba en el período de escritura. Acabo este viaje llena de energía y con muchas ganas de lo que sea que está por venir, aunque no sin pena por el fin de este largo y bonito camino llamado tesis.

Resumen

El principal objetivo de la física de la materia condensada es el estudio del comportamiento macroscópico de un sistema dado, que resulta de la interacción de las muchas partículas que lo constituyen. Las partículas que componen estos sistemas presentan naturaleza cuántica, es decir, existen correlaciones cuánticas entre ellas: están entrelazadas.

En general, los sistemas cuánticos de muchos cuerpos son difíciles de tratar dado que no se pueden describir en términos de las partículas que los conforman de manera individual. La descripción de los sistemas de muchos cuerpos viene determinada por una función de onda global cuyos coeficientes, en una base dada, pertenecen a un espacio de Hilbert que presenta una dimensión que crece exponencialmente con el número de constituyentes del sistema. Esto implica una gran dificultad a la hora de determinarlos cuando el número de partículas del sistema es grande.

No obstante, no todos los estados cuánticos pertenecientes al espacio de Hilbert correspondiente presentan la misma relevancia. Afortunadamente, existen ciertos estados cuánticos que satisfacen la denominada *ley del área*. Si, por ejemplo, consideramos dos regiones de un sistema, A y B, las correlaciones cuánticas entre ambos subsistemas vienen determinadas por la *entropía de entrelazamiento* (EE). Un estado cuántico elegido aleatoriamente en el espacio de Hilbert presenta una entropía de entrelazamiento volumétrica, es decir, que escala con el volumen mínimo entre A y B. Sin embargo, algunos estados cuánticos presentan una entropía de entrelazamiento que escala con el área de la frontera de separación entre las dos regiones que estamos considerando. Estos estados cuánticos resultan ser los estados fundamentales de ciertos Hamiltonianos que presentan una longitud de correlación finita y solo tienen en cuenta interacciones locales, que son las que encontramos en la naturaleza. El estado fundamental no es más que el estado de mínima energía del sistema, que constituye el escenario principal para el estudio de la física a bajas temperaturas.

Por el contrario, existen algunos estados fundamentales que violan la ley del área. Esto ocurre cuando la longitud de correlación del sistema es infinita y, por tanto, las correlaciones cuánticas de largo alcance, incluso lejos de la frontera de separación entre las regiones A y B, deben ser tenidas en cuenta. La entropía de entrelazamiento en estos casos puede presentar una correción logarítmica, que es predicha por la *teoría de campos conformes* (CFT), cuando el sistema es unidimensional. Otro ejemplo de violación de la ley del área en una dimensión lo consituyen los estados fundamentales de algunos modelos de cadenas fermiónicas con *amplitudes de salto* inhomogéneas.

Las cadenas fermiónicas son objetos matemáticos unidimensionales cuyos sitios pueden estar ocupados, o no, por una sola partícula. Estos sitios de la cadena están relacionados entre sí mediante unas amplitudes de salto que se pueden manipular. Si estas amplitudes son iguales y homogéneas, el sistema representa un fermión de Dirac en un espacio-tiempo plano, o de Minkowski, cuando el número de partículas del sistema equivale a la mitad de los sitios de la cadena. En este caso, decimos que el sistema está a *llenado mitad*.

Por otro lado, los enlaces entre los distintos sitios de la cadena pueden depender de la posición de estos, es decir, podemos tener amplitudes de salto inhomogéneas.

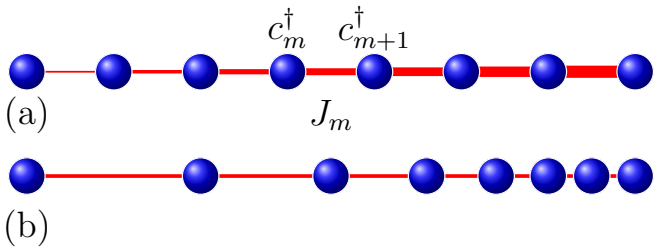

Figure 1: El sistema (a) representa una cadena fermiónica con amplitudes de enlace inhomogéneas: los sitios (azul) situados a la derecha de la cadena presentan una mayor amplitud de enlace (rojo) que aquellos situados hacia la izquierda. En la cadena (b), todas las amplitudes de enlace corresponden a una dinámica homogénea pero la geometría del sistema se ha visto modificada.

Las amplitudes de salto inhomogéneas tienen una interpretación geométrica directa. Dos sitios de la cadena que están fuertemente vinculados pueden considerarse como aquellos situados muy próximos entre sí en el espacio. Por el contrario, dos sitios que presentan una amplitud de salto débil se corresponderán con aquellos localizados a una mayor distancia espacial. Por este motivo, es posible realizar un cambio de coordenadas que transforme un sistema inhomogéneo en otro cuya dinámica es homogénea, donde la geometría inicial del sistema se ve alterada (ver Fig. 1). Es decir, no todos los sitios de la cadena están equiespaciados: es lo que denominamos *espacio-tiempos curvos*.

Además, cuando estas cadenas se pueden describir mediante Hamiltonianos que son cuadráticos en los operadores fermiónicos, es posible estudiar el sistema en términos de una sola partícula que se comporta de manera independiente al resto de constituyentes. En este caso, el Hamiltoniano se puede diagonalizar de manera exacta encontrando los autoestados y energías de una partícula individual que recoge la física del sistema completo. Estos sistemas son los denominados modelos de *fermiones libres* y son los que vamos a utilizar a lo largo de este trabajo.

Los modelos de fermiones libres son especialmente interesantes en el estudio de sistemas de muchos espines, los cuales presentan una gran relevancia en el análisis de diversas propiedades magnéticas de los materiales, así como las transiciones de fase y los puntos críticos. Algunos de estos sistemas, como el conocido modelo de Ising, se pueden convertir a un modelo de fermiones libres mediante la conocida transformación de Jordan-Wigner.

Una vez dicho esto, la primera parte de esta tesis pretende ser un resumen de los conocimientos necesarios para entender el trabajo que se ha realizado, el cual será expuesto en la segunda parte. El Capítulo 1 es una breve introducción a conceptos clave en esta tesis como son el efecto Casimir y el vacío cuántico, el entrelazamiento, la entropía de entrelazamiento y la ley del área. El Capítulo 2 constituye un resumen del formalismo de matriz densidad. La descripción detallada de los sistemas de fermiones libres así como los modelos de espines, se encuentran en el Capítulo 3. Además, concluyendo la primera parte, el Capítulo 4 pretende exponer de una forma accesible los resultados más relevantes de la teoría de campos conformes que serán

necesarios para la comprensión del trabajo desarrollado en esta tesis.

La segunda parte de este documento recoge los objetivos principales que se han llevado a cabo en esta tesis en los respectivos Capítulos 5, 6 y 7:

- **Anális de las fuerzas de Casimir simuladas en cadenas fermiónicas inhomogéneas.**
  La expresión de la energía de Casimir para el estado fundamental de una cadena fermiónica homogénea presenta una contribución no universal proporcional al tamaño del sistema N, más correcciones de tamaño finito de orden $O(1/N)$. Las correciones de tamaño finito vienen fijadas por la CFT cuando el sistema está sujeto a invariancia conforme. En este trabajo estudiamos cómo varian estas correcciones cuando el sistema está deformado, es decir, presenta amplitudes de enlace inhomogéneas.

- **Estudio de la densidad fermiónica en cadenas inhomogéneas cuando nos encontramos fuera del llenado mitad.**
  El estado fundamental de una cadena de fermiones libres con amplitudes de enlace inhomogéneas presenta una ocupación homogénea. Es decir, todos los sitios de la cadena tienen la misma probabilidad de estar ocupados, o vacíos, incluso en espacio-tiempos curvos, siempre que nos encontremos en el estado de mínima energía. Sin embargo, cuando el sistema no se encuentra en su estado fundamental, es decir, no estamos a llenado mitad, aparece nueva física que requiere de una aproximación continua para ser explicada.

- **Caracterización de la estructura de entrelazamiento de un estado fundamental de una cadena crítica en términos de las relaciones energéticas de un subsistema con su entorno.**
  En general, un subsistema de un estado fundamental dado no se encuentra en su respectivo estado fundamental sino que presenta un exceso de energía. Parte de esta energía se puede extraer por medio de operaciones unitarias y es lo que denominamos *ergotropía*. Para sistemas unidimensionales con invariancia conforme, la parte de este exceso de energía que no se puede extraer está relacionada con el tamaño total de este y la entropía de entrelazamiento del subsistema.

Finalmente, el Capítulo 8 recoge las conslusiones y los resultados alcanzados en esta tesis, tanto en inglés como en castellano.

Abstract

The main goal of condensed matter physics is to study how the macroscopic behavior of matter arises from a large number of interacting particles. The particles involved in these systems show a quantum nature and, thus, have quantum correlations amongst them: they are entangled.

In general, many-body systems are difficult to work with as they can not be described in terms of single particles that behave independently of each other. The description of many-body systems requires a global wavefunction where its coefficients in a given basis belong to a certain Hilbert space whose dimension increases exponentially with the number of constituents of the system. For that reason, this becomes a really difficult task for large sizes.

However, some quantum states in the Hilbert space are more relevant than others. Fortunately, there exist certain quantum states that satisfy the so-called *area law*. Let us, for instance, consider two subregions of the system, A and B. We can measure the quantum correlations between the two regions through the so-called *entanglement entropy* (EE). One randomly chosen quantum state in the Hilbert space shows a volumetric law for the entanglement entropy, *i.e.*, it scales with the minimum volume between parts A and B. Nevertheless, some quantum states show an entanglement entropy which is proportional to the boundary between the two subsystems. These quantum states are the ground states (GS) of gapped local Hamiltonians which have a finite correlation length. The ground state is nothing else but the lowest possible energy state of the system, which is the perfect scenario for the study of low temperature physics.

On the contrary, there are also ground states that violate the area law. The violation of the area law usually takes place when the correlation length is infinite and, thus, long-range quantum correlations become relevant even far away from the border between the two regions we are considering. For these cases, the entanglement entropy may show a logarithmic correction for one-dimensional systems, which is predicted by *conformal field theory* (CFT). An example of violation of the area law is given by ground states of some fermionic chains with inhomogeneous *hopping amplitudes*.

A fermionic chain is a mathematical one-dimensional object in which each site may be occupied, or not, by a single particle. The sites in the chain are related among them by the so-called hopping amplitudes which can be tuned. If all the hopping amplitudes are equal and homogeneous, the system represents a Dirac fermion in a flat space-time, also called Minkowski space-time, when the number of particles is equal to half of the sites of the chain. This is what we called *half-filling*.

However, these coupling parameters can be position-dependent, *i.e.*, we can have inhomogeneous hopping amplitudes. Inhomogeneous hopping amplitudes possess a geometric interpretation. Two sites that have a strong hopping amplitude can be considered to be within close proximity. On the other hand, two sites that show a weak coupling can be interpreted as sites located spatially far away. For this reason, it is possible to find an appropriate change of coordinates that maps a chain with inhomogeneous hopping amplitudes to a system where certain sites are spatially closer than others but show the same coupling amplitude regardless of their position

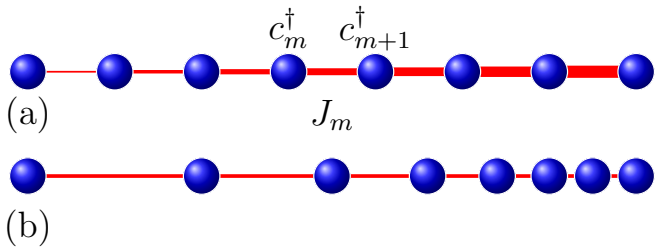

Figure 2: System (a) represents an inhomogeneous fermionic chain: sites (blue) located towards the right side show stronger hopping amplitudes (red) than those sites placed on the left side. In system (b) all hopping amplitudes represented correspond to a homogeneous dynamic but the geometry of the system has been deformed.

along the chain (see Fig. 2). This is what we call *curved space-times*.

In addition, these chains may be described by a Hamiltonian which is quadratic in the fermionic operators and, thus, can be solved exactly in terms of effective non-interacting fermions, *i.e.*, particles that move independently of each other. In this case, the Hamiltonian can be diagonalized analytically in terms of single-body modes and energies. These systems are called *free fermion* models and will be used throughout this work.

Free fermion models are specially interesting in the analysis of spin systems which are shown to be of great relevance in the study of magnetic properties of materials, phase transitions and critical points. Some spin systems, such as the well-known Ising model, can be mapped to a free fermion model by the so-called Jordan-Wigner transformation.

The first part of this thesis provides a review of the knowledge required to follow the work that has been developed, which will be exposed in the second part. Chapter 1 is an introduction to some important concepts such as the Casimir effect and the quantum vacuum, entanglement, the entanglement entropy and the area law. Chapter 2 summarizes the density matrix formalism. The description of both free fermionic models and spin models can be found in Chapter 3. In addition, to conclude this first part, Chapter 4 presents a review of some relevant conformal field theory results that are needed later on.

The second part of this document shows the main goals achieved in this thesis which constitute Chapters 5, 6 and 7, respectively:

- **Analysis of Casimir forces in inhomogeneous fermionic chains.**
  The Casimir energy expression for the ground state of a homogeneous fermionic chain shows a non-universal contribution proportional to the system size N, plus finite-size corrections of order $O(1/N)$. These finite-size corrections are fixed by CFT when the system is subject to conformal invariance. In this work, we study how these corrections behave under the deformation of the system, *i.e.*, when inhomogeneous hopping amplitudes are considered.

- **Study of the fermionic density in inhomogeneous chains away from half-filling.**

The ground state of an inhomogeneous free fermionic chain shows a homogeneous occupation: all sites in the chain have the same probability of being occupied, or empty. However, away from half-filling, a new physical phenomenon appears and it requires a continuum approximation to be explained.

- **Characterization of the ground state entanglement structure of a critical chain in terms of the energetic relations between a subsystem and its environment.**
  In general, a subsystem of a ground state is not in its ground state but presents an excess energy. Part of this excess energy can be extracted via unitary operations, which we call subsystem *ergotropy*. For one-dimensional systems with conformal invariance, the part of the excess energy that can not be extracted is related to its size and the entanglement entropy of the subsystem.

To conclude, Chapter 8 contains the final remarks and the results obtained in this thesis both in English and Spanish.

Contents

Part I

Background

Chapter 1

Introduction

Condensed matter physics is the area of knowledge that studies how the macroscopic behaviour of matter arises from a large number of interacting particles. As such, it is considered one of the widest fields in physics. Physicists in the quantum condensed matter area try to understand the behaviour of complex systems of atoms and molecules which include quantum phase transitions, high-temperature superconductivity, spin systems and other strongly correlated phenomena where quantum many-body techniques are extremely useful as it will be shown in this work [1].

In particular, the purpose of quantum many-body physics is the study of systems of many constituents which cannot be treated in an isolated way due to the strong correlations among them. Indeed, strongly correlated many-body systems are very difficult to describe. In 1956, Lev Landau proposed the theory of Fermi liquids which meant a huge step into modern theoretical physics [2]. Landau's theory of Fermi liquids states that some interacting many-particle systems can be described in terms of a collection of elementary excitations at low temperatures. These elementary excitations are called *quasiparticles* and, although they can be treated as single particles, they encode a much more complex behavior which represents the motion of many particles of the system simultaneously. The Fermi liquid theory provides a universal low energy description that applies to a wide range of condensed matter models, despite their differing high energy physics. The relation between microscopic models and Fermi liquid models is provided via the *renormalization group* (RG) approach which connects these models all together, even though RG may be applied in many other different contexts. However, the low energy physics of many interacting fermions models does not always reduce to a Fermi liquid theory. For instance, the quasiparticle picture fails in one dimension and, thus, a new paradigm of *strongly correlated systems* emerges naturally. Moreover, low-dimensional systems are interesting in themselves as they constitute the playground of a wide variety of theoretical physics methods and approaches such as quantum field theory (QFT), conformal field theory (CFT) and renormalization group techniques.

Specifically, the field of low dimensional magnetism was born with the one-dimensional Ising model [3] and the Heisenberg model [4] despite their simplicity. The corresponding Hamiltonians of some of these models, which at most involve

quadratic terms of spins of local interactions, capture a broad collection of magnetic phenomena. Moreover, this type of Hamiltonians in 1D can be mapped onto the so-called *free fermions* systems, which provide a natural language for describing integrable spin chains. Free fermionic chains, which are one of the most relevant basic models of quantum many-body systems, constitute the main object of study in this work.

Beyond the relevance of fermionic chains in condensed matter, they constitute one of the basic structures behind quantum simulators. Quantum simulators are devices designed specifically to provide insight about a certain physical problem which take advantage of two of the most relevant quantum properties: superposition and entanglement. For example, fermionic chains have been put forward to simulate the Dirac vacuum in curved space-times [5], leading us to perform experiments on the *Unruh effect* [6] and the *Casimir effect*. Such quantum simulators can be built using ultracold fermionic atoms on an optical lattice [7].

The main goal of this chapter is to provide a qualitative notion of important concepts that are extremely useful to follow this work. Section 1.1 develops a short introduction to quantum vacuum and its measurable effect: the Casimir force. Entanglement and entanglement entropy are introduced in Section 1.2, and Section 1.3 presents a brief review of quantum thermodynamics arising from the area law and accelerated observers.

1.1 Casimir effect

Probably, one of the most important and fundamental concepts to understand this work is the *quantum vacuum*. With that aim, let us imagine the ocean and its swell, which in our analogy represents particles. Now we slowly get rid of the waves. In the process, we are reducing the associated energy. When nothing else can be removed, one can say we have reached the lowest possible energy level. The calm sea represents the vacuum. The vacuum is, therefore, nothing else but the lowest energy state of the universe and it presents a quantum nature.

Yet, the nature of the vacuum state can be rather complex and bear measurable effects such as Casimir forces. The *Casimir effect* is a physical phenomenon, proposed for the first time in 1948 by Hendrik Casimir and Dirk Polder [8], which is predictable by theory and experimentally testable. Although there are several ways to describe this effect, the original experiment consisted in two neutral conducting parallel plates placed within close proximity. An attractive force arises between the plates due to quantum vacuum fluctuations [9] while the lack of an external field should imply no force in a classical description. The nature of this force directly depends on the configuration of the boundary conditions. Electric and magnetic fields vanish at the boundaries, therefore, only a subset of all possible quantum fluctuations of the vacuum can exist between the plates as one can see in Fig. 1.1: when two or more materials are placed within a close proximity, the vacuum modes are perturbed by the confinement of quantum fluctuations. Fluctuations with larger wavelengths simply do not fit. Quantum fluctuations of electromagnetic waves are a fascinating consequence of the quantization process that takes place when light is

pushed to the quantum regime.

In 1956, the chemist Boris Derjaguin set a new experimental background by replacing one of the plates with a sphere due to the fact that keeping the two plates parallel was not an easy task [10], becoming the first experimental measurement of the Casimir forces. However, Marcus Sparnaay confirmed in 1958 the existence of the Casimir effect in its initial set up [11]. In 1961, theorists Igor Dzyaloshinskii, Yevgueni Lifshitz and Lev Pitaevski generalized Casimir's results to the case where the plates are not perfect conductors [12]. This led to consider anisotropic plates in 1970, where the total free energy of the systems depends not only on the separation between the two parallel plates but also on the angle θ that defines their relative orientation. Casimir torque was introduced to describe the rotation exhibited by the plates towards the position of minimum energy [13]. Beyond the confirmation of a quantum effect predicted decades ago, the measurement of Casimir torque sets the perfect scenario for engineering vacuum fluctuations to modify how nanoscale and microscale devices work [14]. In the world of microelectromechanical systems (MEMS), the Casimir force is of great importance as it can lead to device malfunctioning or even break-up. Reducing, eliminating or even reversing the Casimir force could help to solve the problem.

Casimir's original proposal has been extended to some equilibrium systems where fluctuations arise from thermal effects instead of having quantum nature [15–17]. Moreover, the case of Casimir forces in equilibrium physical systems, where long-range correlations show due to a continuous symmetry breaking, is specially relevant such as in crystal liquids [18].

We can also define Casimir forces in physical systems of a different nature, such as a spin or fermionic chains, as long as we can define a stress-energy tensor. Indeed, lattice models have been proved to play an important role in the study of quantum many-body physics. These models allow us to manipulate the boundary conditions of the system and the geometry of the lattice which implies the perturbation of the vacuum modes giving rise to many physical phenomena which are objects of interest in this work.

In some cases, Casimir forces are fixed by symmetry considerations. For example, if the fields are subject to conformal invariance, which will be explain in Chapter 4, the Casimir force is associated to the *conformal anomaly*, measured by the central charge in 2D conformal field theory, c [19–22]. The expression for the energy contains a non-universal contribution proportional to the system size N, plus finite-size corrections of order $O(1/N)$ which are fixed by conformal invariance. Moreover, conformal invariance is strong enough to yield an analytical expression for the Casimir forces in presence of arbitrarily shaped boundaries [23].

The peculiarities of Casimir forces in curved space-times have been considered by several authors [24]. However, the problem is already difficult for static space-times and weak gravitational fields [25–28]. Even though our technological abilities do not allow us to access direct measurements of the Casimir effect in curved space-times, there are several proposals to develop quantum simulators using current technologies, such as ultracold atoms in optical lattices [7]. Concretely, it has been shown that the Dirac vacuum on certain static space-times can be characterized in such a quantum simulator [5]. The key insight is the use of so-called *curved optical lattices*, in which

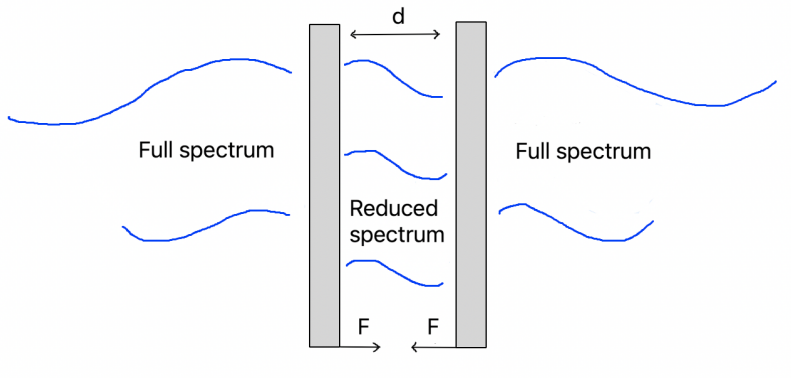

Figure 1.1: Casimir force: zero-point vacuum radiation arises from those modes whose wavelength is shorter than the distance between the parallel plates and, thus, fit into the system.

fermionic atoms are distributed on a flat optical lattice with inhomogeneous hopping amplitudes, thus simulating a position-dependence index of refraction or, in other terms, an optical metric.

1.2 Entanglement

Entanglement is a surprising physical phenomenon that takes place in quantum systems. Let us consider a system divided into two parts, A and B, within which our quantum state is defined. If one performs a measurement of a local observable on A, the probabilities of obtaining different results on B may be altered regardless of the distance between A and B and vice-versa.

1.2.1 A brief history of entanglement

Back in 1905, Einstein helped introduce quantum theory with his revolutionary discovery about light behaving both as a wave and a particle [29]. Niels Bohr explained later that this duality depends on how you observe light but it was not until 1924 that Louis De Broglie stated that if light waves could behave as particles then, perhaps, particles of matter could also behave as waves. Erwing Schrödinger developed the mathematics needed to explain this phenomenon in 1926 [30] and Max Born showed that Schrödinger's waves have a probabilistic interpretation, which is compatible with Heisenberg's uncertainty principle formulated in 1927 [31]: it is not possible to obtain exact information about both the position and the momentum of a particle at the same time in the quantum world, as it is also the case with energy and time. By 1935, conceptual understanding of the quantum theory was dominated by Bohr who was convinced that observing a quantum object involves an unknown interaction with a measurement device that affects both systems and it is responsible for the impossibility to co-measure other quantities with the same device.

In the framework of those debates, quantum entanglement was first described by Einstein, Podolski and Rosen (EPR) in their famous paper of 1935 [32], which was

intended to be an argument against the completeness of the quantum mechanical description of physical reality. The EPR argument consisted in considering a pair of particles prepared in what later would be known as an *entangled state*. Let us picture this with two electrons. If two electrons are prepared together in the laboratory so that they have zero total spin, then the principle of conservation of angular momentum leads to one electron with spin up and one electron with spin down. This state is called a *singlet state*, which means that all the electrons are paired. However, quantum theory says that there is 50% chance of one electron to have spin up and 50% chance of spin down. In this state, if the spin of the first electron is measured along any axis, then the spin of the second electron is predictable. However, since no information can travel faster than light and thus violate Einstein's relativity theory, no action taken on the first particle could instantly affect the other. Einstein, Podolski and Rosen proposed that a realist theory would require each spin to be determined from the beginning but it is only revealed when you look at it. Quantum spin then involves a hidden variable yet to be described by quantum theory.

On the other side, Bohr believed that nature was fundamentally random but Einstein did not. Hidden-variable theories of quantum mechanics were introduced to remove the randomness of quantum measurements by assuming that some deeper element of quantum phenomena explains each outcome. These hidden variables were also assumed not to be accessible to current experiments so, according to Einstein, Podolski and Rosen, the quantum theory of Bohr and Heisenberg was correct but not complete. There were still things that the theory could not predict nor explain: the hidden variables.

Schrödinger was the first to introduce the term *entanglement* the same year as the EPR paper was published [33]. Einstein's entanglement argument and Schrödinger's cat paradox, which were originally formulated to be arguments against the validity of the quantum theory, have become some of the best known established pedagogical tools in this area.

In 1950, Chien-Shiung Wu and Irving Shaknov found an oddly linked behaviour in pairs of photons [34]. However, they did not know at the time that they had performed the first real world experiment of quantum entanglement.

In 1951, David Bohm published a textbook about quantum mechanics where he took a close look at the EPR paradox [35]. He kept working on hidden-variable theories but realising the non-locality constraint Einstein had remarked. In addition, Bohm and Aharonov published in 1957 a description of a plausible experiment set up in which entangled spin correlations could be tested [36]. This would be later known as the EPRB experiment, although there were no attempts in this direction due to the technical difficulties involved in the process.

In 1964, John Bell proved that if local hidden-variable theories were indeed correct, then the probabilities of different measurements in the EPRB experiment should respect a certain inequality which now bears his name [37]. However, he proved that this inequality is violated by certain quantum states and thus showed that an experiment could rule out any possibility of any local hidden variable theory. Nevertheless, an experiment showing a violation of Bell's inequalities can not rule out a non-local theory of hidden variables such as the one developed by Bohm.

Some years later, John Clauser and his coworkers developed an alternative to

Bell's inequality, known as Clauser-Horne-Shimony-Holt (CHSH) inequality, that is easier to check experimentally and does not need hidden variables involved [38]. In 1972, the CHSH inequality was published and later tested. However, it was not until 1982 when Alan Aspect became the first physicist to verify the violation of Bell's inequalities [39].

In the meantime, Anton Zeilinger led notorious experiments involving entanglement of three particles which have strengthened the arguments in favor of quantum non-locality. Indeed, the so-called GHZ state, named after Greenberger, Horne and Zeilinger, has been very useful in the fields of quantum communication and cryptography [40].

1.2.2 The von Neumann and Shannon entropies

While all this debate about the validity of quantum theory was taking place, John von Neumann developed a new mathematical framework for quantum mechanics in 1932 [41]. Indeed, von Neumann and Landau were pioneers in introducing the density matrix formalism in the realm of quantum statistical mechanics which would turn out to be a measurement of entanglement some years later. The density matrix is an alternative way of expressing quantum states which, unlike the state-vector representation, allows us to use the same mathematical language to describe both the individual quantum states, *i.e.*, *pure states*, and the *mixed states* that consist of ensembles of pure states. Moreover, mixed states may also describe a part of a pure state.

However, it was not until almost 15 years later, in 1948, that Shannon introduced the concept of entropy in classical information theory [42]:

"My greatest concern was what to call it. I thought of calling it 'information', but the word was overly used, so I decided to call it 'uncertainty'. When I discussed it with John von Neumann, he had a better idea. Von Neumann told me, 'You should call it entropy, for two reasons. In the first place your uncertainty function has been used in statistical mechanics under that name, so it already has a name. In the second place, and more important, no one really knows what entropy really is, so in a debate you will always have the advantage".

Von Neumann used then the expression of Shannon's entropy to characterize entanglement for mixed states. In this context, von Neumann's entropy accounts for the probabilities of obtaining different pure states. For a quantum-mechanical system described by a density matrix ρ, the *von Neumann entropy* is

$$S = -\mathrm{Tr}\left(\rho \log \rho\right). \tag{1.1}$$

1.2.3 Entanglement entropy

Many efforts were put into the task of measuring entanglement and have made their appearance over the years. Entanglement is associated to the fact that a part of a pure state may be described as a mixed state. Given a pure bipartite quantum state ρ of a system divided into two regions A and B, $|\psi\rangle_{AB} \in \mathcal{H}_{AB}$ with $\mathcal{H}_{AB} = \mathcal{H}_A \bigotimes \mathcal{H}_B$, all the physical properties of subsystem A are contained in a reduced density matrix that accounts only for the degrees of freedom of the subsystem we are considering, $\rho_A = \mathrm{Tr}_B \rho_{AB}$. Its spectrum $\{\lambda_k\}$ encodes all the

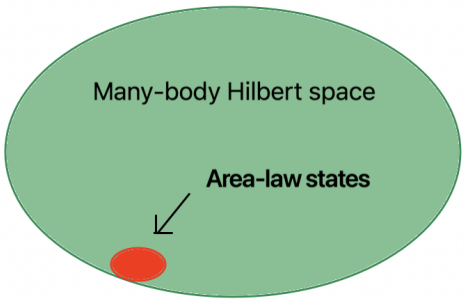

Figure 1.2: The number of quantum states in the Hilbert space that obeys the area law for the entanglement entropy corresponds to a very small corner of it.

entanglement properties of the subsystem. The *entanglement entropy* (EE) is the von Neumann entropy of the reduced density matrix for any of the subsystems and it is defined as

$$S(A) = -\mathrm{Tr}\left(\rho_A \log \rho_A\right). \tag{1.2}$$

The entanglement entropy $S(A)$ measures the amount of information associated to the fact that the state ρ_A is not pure. If this quantity is zero, the two subsystems are said to be *unentangled*. On the other hand, a non-zero entanglement entropy directly implies the presence of these quantum correlations.

1.2.4 Area law

The entanglement entropy is, then, a fundamental quantity that characterizes the quantum correlations between sub-regions belonging to a larger quantum system.

Let us consider two subsystems and focus on their boundary. The entanglement entropy between the two subsystems is proportional to the area of the separation surface, *i.e.*, the boundary. This leads to the so-called *area law*, which was first introduced in the field of black holes by Bekenstein [43].

In 1993, Srednicki calculated the reduced density matrix of a block within the vacuum by tracing out the degrees of freedom inside an imaginary surface [44]. He showed that the entanglement entropy is proportional to the entangling surface due to the short-distance correlations present in the system. According to this, only those degrees of freedom located in a small region close to the separation surface between subsystems contribute to the entropy.

Let us specialize in the case where the ground state of a gapped local Hamiltonian on a lattice in D spatial dimensions is a pure state. The entanglement between a region A of size L^D and the rest B of the lattice is often proportional to the size of the boundary $\mu(\partial A)$,

$$S_A \approx \mu(\partial A) \approx L^{D-1}. \tag{1.3}$$

Thus, the ground state (GS) entanglement entropy typically obeys the area law as opposed to the volumetric law, $S_A \approx L^D$, satisfied by generic states in the many-body Hilbert space [45].

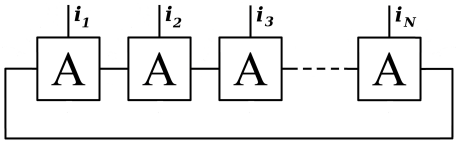

Figure 1.3: Graphical representation of a translational invariant MPS with interconnected tensors A.

1.2.5 Tensor Networks

The Hilbert space of a quantum many-body system contains an incredibly large number of quantum states. Let us consider the number of particles of the system to be $N \sim 10^{23}$, *i.e.*, the order of the Avogadro number. Then, the number of basis states in a d dimensional Hilbert space is $\sim d^{10^{23}}$ with , which is exponentially larger than the number of atoms in the observable universe that it is estimated to be 10^{80}.

Fortunately, some quantum states in the Hilbert space are more relevant than others. Hastings proved that ground states of gapped local Hamiltonians, *i.e.*,, Hamiltonians with a finite correlation length and, thus, a finite energy gap that separates the ground state from the excited states, obey the area law for the entanglement entropy under local interactions in 1D [46]. In addition, some gapless systems in $D > 1$ dimensions also obey Eq. (1.3) [47].

These ground states are not uniformly distributed in Hilbert space. Instead, they belong to a *small corner* of it (see Fig. 1.2). This means that finding the GS of a certain Hamiltonian which, in general, is completely out of reach due to the exponential growth of the underlying Hilbert space, may be a feasible task.

Moreover, the area law can be taken as a guideline for establishing classes of quantum states which can approximate the aforementioned ground states. A first attempt in this direction was proposed in 1988 by Affleck, Kennedy, Lieb and Tasaki as a way to understand the one dimensional antiferromagnetic spin-1 Heisenberg model [47] giving rise to the well known AKLT state. The idea consisted in designing wavefunctions for ground states which try to capture some physical properties of the system and finding appropriate Hamiltonians for them, which would be later known as *parent Hamiltonians*. Fannes, Nachtergaele and Werner generalized this construction in 1992 and introduced the so-called *finitely correlated states*, also finding a gapped local Hamiltonian for them [48].

Finitely correlated states would later lead to *tensor networks* (TN). Certainly, TN techniques have been used as an efficient description of quantum many-body states. The most famous example is the *density matrix renormalization group* (DMRG) algorithm, which was introduced in 1992 by Steve White to simulate 1D quantum lattice systems [49, 50] as the exact diagonalization of quantum Hamiltonians is restricted to systems of small size and, thus, far away from the thermodynamic limit where quantum phase transitions appear.

Indeed, the corresponding wavefunction is described by a network of interconnected tensors with entanglement playing the role of "glue" amongst pieces as it is shown in Fig 1.3. For instance, the AKLT state can be written as a product of matrices whose dimension is related to the correlation length and the entanglement

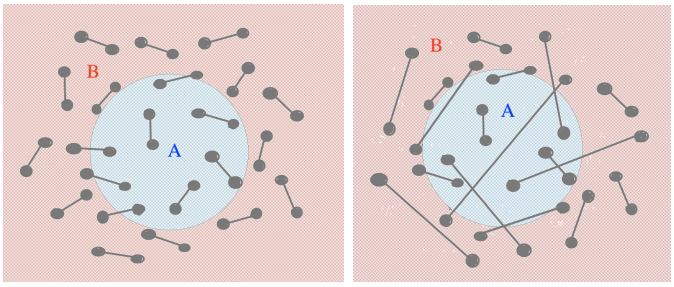

(a) Gapped. (b) Gapless.

Figure 1.4: This figure shows the boundary between regions A and B for two different cases. When the Hamiltonian of the system is gapped (a), long-range correlations are negligible and, thus, only those degrees of freedom close to the boundary contribute to the entanglement entropy between regions A and B: the area law is satisfied. For gapless Hamiltonians (b), not only short range correlations are relevant and this leads to a violation of the area law.

structure,

$$|\psi\rangle = \sum_i \mathrm{Tr}\left[A_{i_1} A_{i_2} \dots A_{i_N}\right] |i_1 i_2 \dots i_N\rangle \,, \tag{1.4}$$

where indices i_m go over the states in the computational basis and the trace comes from assuming periodic boundary conditions. Eq. (1.4) is called a *matrix product state* (MPS) [51]. The natural generalization of MPS to higher spatial dimensions are the so-called *projected entangled pair states* (PEPS), although they are not the only ones.

Tensor networks have become a very powerful tool in condensed matter physics and quantum information theory as they can target the small corner of the Hilbert space of relevant states and give a good intuition about the structure of entanglement between the constituents of a given wavefunction This information in terms of a network of quantum correlations leads to an effective lattice geometry in which states actually live. By pushing this idea to the limit, it has been proposed that geometry and curvature, *i.e* gravity, could emerge naturally from the entanglement structure contained in quantum states [52, 53].

1.2.6 Violations of area law

There are also ground states of local Hamiltonians which do not obey the area law. A ground state that violates this property for the entanglement entropy must break, at least, one of the hypothesis of Hastings theorem [46]. Thus, Hamiltonians with non-local interactions may violate this law.

In general, when the correlation length of the system is infinite, the ground state entanglement displays a logarithmic correction to the area law in gapless systems in $D = 1$ dimensions, as well as in certain fermionic gapless systems with $D > 1$ which present a Fermi surface of dimension $D - 1$. This logarithmic correction appears as quantum long-range correlations become relevant (see Fig. 1.4). Therefore,

$$S_A \approx L^{D-1} \log L. \tag{1.5}$$

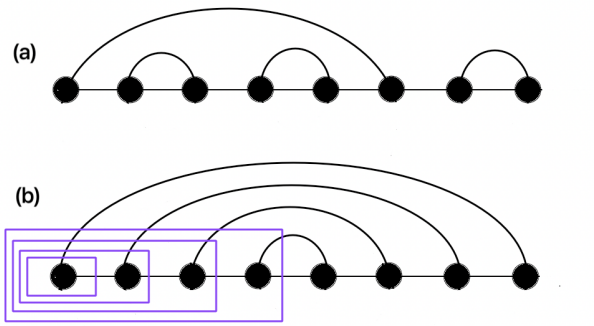

Figure 1.5: (a) Random singlet phase: each spin forms a singlet pair with another one. Some of them produce long distance correlations and, hence, the EE scales logarithmically at the critical point. (b) Concentric singlet phase: the EE scales with the size of the block. As translational invariance is broken, the EE also depends on the position of the block: if the blocks are centered in the middle of the chain, the EE would be zero as no bonds are cut.

Moreover, the ground states and low energy excitations of critical Hamiltonians are also expected to violate the area law as the correlation length diverges at the critical point implying the existence of quantum correlations of the system with the environment even far from the boundaries.

Furthermore, it is also possible to work with one-dimensional systems that maximally violate the area law. For instance, a simple spin 1/2 model with nearest neighbors interactions can lead to a highly entangled ground state by a suitable fine tuning of its coupling constants, *i.e.*, a volume law scaling for the EE. A way of achieving so is to generate a ground state with a concentric singlet phase [54, 55], as shown in Fig. 1.5. It is straightforward to see that the entanglement entropy of this configuration would scale with the size of the block since it corresponds to the number of bonds cut by the bipartition.

1.3 Entanglement and Thermodynamics

Let us return to Bekenstein's conjecture that black holes should have entropy and, furthermore, it should be proportional to the area of the event horizon A [43],

$$S_{BH} = \frac{k_B A}{4 l_p^2}, \tag{1.6}$$

where k_B is the Boltzmann constant and l_p is Planck length. The correct proportionality coefficient, 1/4, was later found by Hawking [56, 57]. Using Eq. (1.6), Bekenstein proposed a generalized version of the second law of thermodynamics [43]: *"When common entropy goes down a black hole, the common entropy in the black hole exterior plus the black hole entropy never decreases"*. This version provides a unique relation between thermodynamics, gravitation and quantum theory.

Bekenstein's thermodynamics of black holes received a strong support from

Hawking when he found that a black hole must emit radiation at a temperature

$$T_H = \frac{\hbar a}{2\pi c k_B}, \tag{1.7}$$

where a is the acceleration of gravity, c is the speed of light and $\hbar = h/2\pi$ is the Planck constant. From 1973 to 1976, Fulling, Davies and Unruh proposed that a similar effect existed in an essentially flat space-time: uniformly accelerated observers will feel a thermal bath of particles with a temperature proportional to their acceleration while inertial observers will not [58–60]. This is the so called *Unruh effect*.

Indeed, an observer undergoing constant acceleration moves in a hyperbolic trajectory which is described by Rindler coordinates (see Fig. 1.6). This means that accelerated observers will feel that they are moving through a different metric, called *Rindler metric*, which possesses an event horizon that prevents communication between different regions of space-time. Therefore, inertial and non-inertial observers will perceive the vacuum as a different quantum state. A uniformly accelerated observer will see the ground state of an inertial observer as a mixed state in thermodynamic equilibrium with a finite temperature. This temperature was stated by Unruh and it was shown to correspond to Hawking's temperature for black hole radiation.

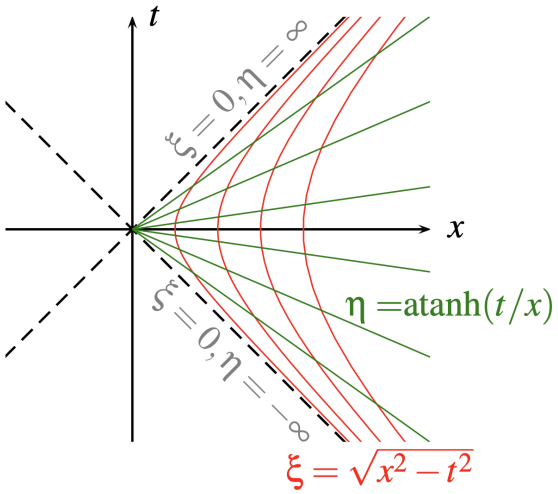

Figure 1.6: Space-time diagram corresponding to Rindler coordinates η and ξ which are the co-moving time and space coordinates, respectively, found by $t = \xi \sinh \eta$, $x = \xi \cosh \eta$. The pole $\xi = 0$ corresponds to a singularity in the coordinate system and it can be thought of as an event horizon. Constant η lines (green) are spacelike, and constant ξ lines (red) are timelike. We have considered an observer moving with constant acceleration $a = 1$ in the positive x-axis and assumed $c = 1$ for convenience. The observer is at rest at $t = 0$ and $x = 1$. This figure belongs to [6] and it is used under the authors' permission.

The Unruh effect bears a deep relation to entanglement [61] and black hole thermodynamics, what leads to the notion of a quantum equivalence principle [62].

The Unruh effect also plays an important role in Jacobson's derivation of Einstein's equations as equations of state for space-times in thermal equilibrium [63].

Many attempts have been performed in order to reproduce the Unruh effect experimentally due to its fundamental relevance, including quantum simulation of Dirac fermions using ultracold fermionic atoms in a 2D optical lattice [6]. Furthermore, the possibility of using accelerated electrons to exhibit the quantum field theoretic relation between acceleration and temperature has been considered [64,65].

Chapter 2

Density matrix formalism

This chapter constitutes a mathematical review of the density matrix formalism where concepts as pure states, reduced density matrix, entanglement entropy (EE) and entanglement contour are briefly discussed.

2.1 Pure states

Given a quantum system composed of two subsystems A and B with finite dimensional Hilbert spaces $\mathcal{H}_A$ and $\mathcal{H}_B$, respectively, a *pure state* is defined by the vector $|\psi\rangle \in \mathcal{H}_{AB}$ with $\mathcal{H}_{AB} = \mathcal{H}_A \bigotimes \mathcal{H}_B$. The state $|\psi\rangle$ is said to be *factorized* if $|\psi\rangle = |\phi\rangle \bigotimes |\varphi\rangle$ with $|\phi\rangle \in \mathcal{H}_A$ and $|\varphi\rangle \in \mathcal{H}_B$. Factorized states can be treated as if subsystems A and B were independent of each other. However, if $|\psi\rangle \neq |\phi\rangle \bigotimes |\varphi\rangle$ the system is said to be *entangled*.

The ground states (GS) of the systems we will consider along this work are always pure states. However, a subsystem of a pure state may not be in a pure state: it is said to be a *mixed state*.

2.2 Mixed states

Mixed states are statistical ensembles of m different quantum pure states, not necessarily orthogonal, and, thus, can be expressed as

$$\{|\psi_j\rangle\}_{j=1}^{m} = \{|\psi_1\rangle, |\psi_2\rangle, ..., |\psi_m\rangle\}, \tag{2.1}$$

where each term has a probability given by

$$\{p_j\}_{j=1}^{m} = \{p_1, p_2, ..., p_m\}, \tag{2.2}$$

whith $\sum_{j=1}^{m} p_j = 1$.

This way of expressing mixed states gives rise to certain difficulties when the number of pure states involved is large. For this reason, the density matrix formalism is introduced.

2.3 Density matrix

Let us consider a quantum system described by a Hilbert space $\mathcal{H}$. Then, the state of the system is a density matrix operator ρ of the form

$$\rho = \sum_j p_j \left|\psi_j\right\rangle \left\langle\psi_j\right| , \tag{2.3}$$

where $\left|\psi_j\right\rangle$ are pure states that occur with a probability p_j. These states $\left|\psi_j\right\rangle$ do not need to be orthogonal. Indeed, if they are, they will be the eigenvectors of the density matrix, and p_j the eigenvalues. Moreover, it satisfies $\rho = \rho^\dagger$, $\rho \geq 0$ and $\mathrm{Tr}\rho = 1$. If ρ is a one dimensional projector, *i.e.*, $\rho = \rho^2$, it is said to be a pure state. On the other hand, if $\rho \neq \rho^2$, it is said to be a mixed state.

In addition, there are several relevant aspects that are important to mention:

1. Observables are described by linear selfadjoint operators $A = A^\dagger$ and its expectation value can be calculated by

$$\langle A\rangle = \sum_j p_j \left\langle\psi_j|A|\psi_j\right\rangle = \sum_j p_j \mathrm{Tr}\left(\left|\psi_j\right\rangle \left\langle\psi_j\right| A\right) = \mathrm{Tr}\left(\sum_j p_j \left|\psi_j\right\rangle \left\langle\psi_j\right| A\right) . \tag{2.4}$$

   Therefore,

$$\langle A\rangle = \mathrm{Tr}\left(\rho A\right) . \tag{2.5}$$

   Moreover, A has a spectral decomposition $A = \sum_n \alpha_n P_n$. In this decomposition, α_n are real eigenvalues and P_n is a set of orthonormal projectors that satisfies $\sum_n P_n = 1$.

2. The measurement of an observable A is described by the measurement basis formed by the projectors of A. Let us consider the system prepared in a state ρ. Then, the possible outcomes are

$$\tilde{\rho}_n = \frac{P_n \rho P_n}{\mathrm{Tr} P_n \rho P_n}, \tag{2.6}$$

   with probability $\mathrm{Prob}(n) = \mathrm{Tr} P_n \rho P_n$. The state after the measurement is $\tilde{\rho}_n$.

3. The dynamics of the system is given by a unitary matrix U_t, acting on the states as

$$\rho(t) = U_t \rho(0) U_t^\dagger, \tag{2.7}$$

   where the initial condition $\rho(0)$ is given by Eq. (2.3).

4. Since ρ is a positive semi-definite operator, it has a spectral decomposition

$$\rho = \sum_n \lambda_n \left|\phi_n\right\rangle \left\langle\phi_n\right| , \tag{2.8}$$

   with $0 \leq \lambda_n \leq 1$ and $\sum_n \lambda_n = 1$, and $\left|\phi_n\right\rangle$ are orthonormal vectors. Notice that n takes values up to the dimension of the corresponding Hilbert space,

whereas j in Eq. (2.3) can take any values. Then, the von Neumann entropy of a state ρ is given by

$$S = -\mathrm{Tr}\left(\rho \log \rho\right) = -\sum_n \lambda_n \log \lambda_n. \tag{2.9}$$

Thus, the von Neumann entropy for any pure state is zero.

2.4 Reduced density matrix

A composite system $A \cup B$ can be in a pure state while its components are mixed. The density matrix that describes only a part of a given system, let us say subregion A, is called reduced density matrix and is given by

$$\rho_A = \mathrm{Tr}_B \rho, \tag{2.10}$$

where the partial trace is defined as follows:

$$\mathrm{Tr}_B \left(|a_i\rangle \langle a_j| \otimes |b_i\rangle \langle b_j| \right) = |a_i\rangle \langle a_j| \left(\mathrm{Tr}\, |b_i\rangle \langle b_j| \right) = \left(|a_i\rangle \langle a_j| \right) \langle b_j|b_i\rangle , \tag{2.11}$$

and where $|a_i\rangle$, $|a_j\rangle$ and $|b_i\rangle$, $|b_j\rangle$ are orthogonal basis of subspaces A and B, respectively. Let us assume

$$|\Psi\rangle = \sum_{ij} C_{ij} |a_i\rangle \otimes |b_j\rangle = \sum_{ij} C_{ij} |a_i b_j\rangle , \tag{2.12}$$

where $|a_i\rangle \in \mathcal{H}_A$ and $|b_j\rangle \in \mathcal{H}_B$. Then, the density matrix is given by

$$\rho = |\Psi\rangle \langle \Psi| = \sum_{ijkl} \bar{C}_{ij} C_{kl} |a_i b_j\rangle \langle a_k b_l| , \tag{2.13}$$

and the partial traces are

$$\rho_A = \mathrm{Tr}_B \rho = \sum_{ijkl} \bar{C}_{ij} C_{kl} |a_i\rangle \langle a_k| \langle b_l|b_j\rangle = \sum_{ik} \left(\sum_j \bar{C}_{ij} C_{kj} \right) |a_i\rangle \langle a_k| , \tag{2.14}$$

$$\rho_B = \mathrm{Tr}_A \rho = \sum_{ijkl} \bar{C}_{ij} C_{kl} |b_j\rangle \langle b_l| \langle a_k|a_i\rangle = \sum_{jl} \left(\sum_i \bar{C}_{ij} C_{il} \right) |b_j\rangle \langle b_l| . \tag{2.15}$$

For a composite system in the state ρ, the reduced density matrix ρ_A describes everything that is accessible by local operations in part A.

2.5 Schmidt decomposition

A pure state $|\Psi\rangle \in \mathcal{H}_{AB}$ can be written by means of the so-called *Schmidt decomposition* (see Appendix A)

$$|\Psi\rangle = \sum_{k=1}^{n_S} \sigma_k |\alpha_k\rangle |\beta_k\rangle , \tag{2.16}$$

where $\sigma_k > 0$ are the *Schmidt values*, $\{|\alpha_k\rangle\}_{k=1}^{N_A}$, $\{|\beta_k\rangle\}_{k=1}^{N_B}$ are orthogonal basis of $\mathcal{H}_A$ and $\mathcal{H}_B$, respectively, with dimensions N_A and N_B, and $n_S \leq \min(N_A, N_B)$ is the *Schmidt number*. The Schmidt number stands for the number of non-zero coefficients σ_k, including multiplicity, in the Schmidt decomposition of $|\Psi\rangle$. It also accounts for the number of non-zero eigenvalues of the reduced density matrices $\mathrm{Tr}_B |\Psi\rangle \langle\Psi|$ and $\mathrm{Tr}_A |\Psi\rangle \langle\Psi|$.

The reduced density matrices are given by

$$\rho_A = \sum_{k=1}^{n_S} \sigma_k^2 |\alpha_k\rangle \langle\alpha_k| , \tag{2.17}$$

$$\rho_B = \sum_{k=1}^{n_S} \sigma_k^2 |\beta_k\rangle \langle\beta_k| . \tag{2.18}$$

A factorized state has Schmidt number equal to 1. On the other hand, since an entangled state cannot be factored as a tensor product, its Schmidt number must be at least 2. The state is maximally entangled when, for all k, $\sigma_k^2 = 1/\min(N_A, N_B)$. This can be thought of as a first attempt to quantify entanglement.

The eigenvalues of the reduced density matrix codify the whole entanglement structure of a system. Since every density operator ρ_A has non-negative spectrum and it is Hermitian, it can be written as

$$\rho_A = e^{-K_A}, \tag{2.19}$$

where K_A is a Hermitian operator known as the *entanglement Hamiltonian* (EH). By taking the logarithm of Eq. (2.17), or equivalently of Eq. (2.18), we find the spectrum of the entanglement Hamiltonian which is also known as the *entanglement spectrum* (ES)

$$E_k = -2 \log \sigma_k. \tag{2.20}$$

2.6 Entanglement entropy

The entanglement entropy is the most widespread magnitude in the characterization of bipartite entanglement. For that purpose, the many-body system is virtually divided into two subregions, A and B. As we discussed in the previous chapter, the information entropy was first defined by Shannon. Von Neumann extended the concept of entropy to quantum physics and, in terms of the density matrix, it can

be expressed as in Eq. (1.1). Thus, the von Neumann entropy of the subsystem A is

$$S\left(\rho_A\right) = -\mathrm{Tr}\left(\rho_A \log \rho_A\right) = -\sum_{k=1}^{N_A} \lambda_k \log \lambda_k, \tag{2.21}$$

where ρ_A is the reduced density matrix of part A given by Eq. (2.10) and we assume the whole system is in a pure state. The $\{\lambda_k\}_{k=1}^{N_A}$ is the set of eigenvalues of ρ_A and N_A is the dimension of $\mathcal{H}_A$.

The perspective of Shannon theory leads to interpret von Neumann's entropy, $S(\rho_A)$, as the amount of information necessary to describe the subsystem A as a pure state starting with the mixed state ρ_A. Or, in other words, it quantifies the correlations that prevent describing A as a pure state. This is the reason why von Neumann entropy is often called entanglement entropy.

Eigenvalues $\lambda_k = 0$ do not contribute to the entanglement entropy given by Eq. (2.21), so it can be given in terms of the Schmidt singular values σ_k,

$$S(\rho_A) = -\sum_{k=1}^{n_S} \sigma_k^2 \log \sigma_k^2 = S(\rho_B). \tag{2.22}$$

Thus, $\sigma_k = \sqrt{\lambda_k}$. If the state is a product state, *i.e.*, $n_S = 1$, as we mentioned earlier, then $S(\rho_A) = 0$.

The entanglement entropy satisfies a series of mathematical inequalities which are the result of physical requirements [66]. For instance, additivity and subadditivity

$$S(\rho_A \otimes \rho_B) = S(\rho_A) + S(\rho_B), \tag{2.23}$$

$$S(\rho) \leq S(\rho_A) + S(\rho_B). \tag{2.24}$$

This last equation establishes that the entropy of a given state $\rho \in \mathcal{H}_A \otimes \mathcal{H}_B$ is bounded by the entropy of a product state $\rho_A \otimes \rho_B$.

2.7 Rényi entropies

Rényi entropies are an important generalization of the von Neumann entanglement entropy, both theoretically and experimentally, which fulfill all the properties of the entropy but with the relaxation of the subadditivity.

Analogously to the von Neumann EE, we can define Rényi entropies between a region A and its complementary as

$$S_A^{(n)} = \frac{1}{1-n} \log\left(\mathrm{Tr}\rho_A^n\right), \qquad n \in \mathbb{R}, \tag{2.25}$$

where ρ_A is, once again, the reduced density matrix of the subregion A. In the limit $n \to 1^+$ Eq. (2.25) is reduced to the von Neumann entanglement entropy

$$S_A = \lim_{n \to 1^+} S_A^{(n)} = -\mathrm{Tr}\left(\rho_A \log \rho_A\right). \tag{2.26}$$

Given a certain system, Rényi entropies have been shown to provide highly non-trivial information about, *e.g.*, topological properties [67, 68]. They are also very useful in quantum field theory since they can be computed directly with the so-called *replica trick* [69].

2.8 Entanglement contour

As we have seen, the entanglement entropy accounts for the amount of quantum correlations between two parts present in a certain system. For instance, the area law can be understood as resulting from entanglement that involves degrees of freedom located near the boundary between two regions A and B. Moreover, the logarithmic correction present in systems with infinite correlation length is argued to come from those degrees of freedom that are further away from the boundary between A and B.

Furthermore, Vidal and Chen [70] considered the possibility of introducing a function s_A, called *entanglement contour*, that assigns a real number $s_A(m) \geq 0$ to each lattice site m contained in region A such that the sum of $s_A(m)$ over all the sites $m \in A$ is equal to the entanglement entropy $S(A)$. The aim of the entanglement contour is, then, to quantify how much the degrees of freedom in site m contribute to the entanglement between subregions A and B. However, it is important to emphasize that $S(A) \neq \sum_{m \in A} S(m)$, where $S(A)$ is the von Neumann entanglement entropy. When site m is only entangled with neighboring sites contained within region A, and thus uncorrelated with region B, the entanglement contour $s_A(m)$ will be required to vanish. On the contrary, the one-site von Neumann entropy $S(m)$ still takes a non-zero value due to the presence of local entanglement within region A.

The entanglement contour is not uniquely defined. Yet, Vidal and Chen provided a list of reasonable requests to be made on any sensible contour function [70]:

- Positivity: $s_A(m) \geq 0$.
- Normalization: $\sum_{m \in A} s(m) = S(A)$.
- Symmetry: if T is a symmetry of ρ_A that interchanges the role of sites m and n, then $s(m) = s(n)$.
- Invariance under local unitary transformations: if a state $\tilde{\psi}$ is obtained from a state ψ by means of a unitary transformation U^X that acts on a subregion $X \subseteq A$, then the entanglement contour $s_A(X)$ must be the same for both states.
- Upper bound: the entanglement contour of a subregion $X \subseteq A$ cannot be larger than the entanglement entropy of the subregion X with the rest of the system.

Chapter 3

Free fermions and spin chains

The Hilbert space of quantum many-body systems grows exponentially with the number of elements, whether they are spins, sites or orbitals. Therefore, classical simulations of their dynamics constitute a difficult problem. However, in some cases, we can describe the system as a combination of single-body orbitals which may be either occupied or empty. This is the case of *free fermion* models which will be discussed in this section.

Free fermion models are those expressed by a Hamiltonian which is bilinear in the fermionic operators. Therefore, they can be exactly solved in terms of single-body modes and single-body energies so we can treat the system as constituted by a certain number of particles which move independently of each other.

3.1 Hopping model

Let us consider a fermionic chain with (even) N sites. We can define a hopping Hamiltonian,

$$H(\mathbf{J})_N = -\sum_{m=1}^{N-1} J_m \left(c_m^\dagger c_{m+1} + \text{h.c.} \right), \tag{3.1}$$

where $\mathbf{J} = \{J_m\}_{m=1}^{N-1}$ are called *hopping amplitudes*, $J_m \in \mathbb{R}^+$ referring to the link between sites m and $m+1$ as shown in Fig. 3.1, and $c_m^\dagger$, c_m are the creation and annihilation operators of site m, which satisfy the standard anticommutation relations

$$\{c_i, c_j^\dagger\} = \delta_{ij}, \tag{3.2}$$

$$\{c_i, c_j\} = \{c_i^\dagger, c_j^\dagger\} = 0. \tag{3.3}$$

The exact diagonalization of Hamiltonian (3.1) is a straightforward procedure which only involves the solution of the associated single-body problem. Let us define the hopping matrix, $T_{ij} = T_{ji} = -J_i \left(\delta_{i,j+1} + \delta_{i,j-1} \right)$, such that

$$H(\mathbf{J})_N = \sum_{ij} T_{ij} c_i^\dagger c_j. \tag{3.4}$$

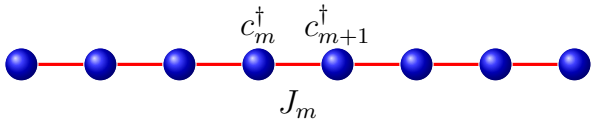

Figure 3.1: Chain with homogeneous hopping amplitudes.

Then, we can diagonalize the hopping matrix, $T_{ij} = \sum_k U_{ik}\varepsilon_k \bar{U}_{jk}$, where ε_k are the single-body energies and the columns of U_{ik} represent the single-body modes. These modes determine a canonical transformation

$$b_k^\dagger = \sum_i U_{ik} c_i^\dagger, \tag{3.5}$$

where U is a unitary matrix which implies that $b_k^\dagger$ are also fermionic operators and satisfy anticommutation relations given by Eq. (3.2) and (3.3). Therefore,

$$H(\mathbf{J})_N = \sum_{k=1}^{N} \varepsilon_k b_k^\dagger b_k, \tag{3.6}$$

where ε_k are arranged in ascending order. We can write a basis of eigenstates of $H(\mathbf{J})_N$ by fixing the occupation numbers of the $b_k^\dagger$ modes.

Let us consider the minimum energy eigenstate with a fixed number of particles m, which is obtained by filling up the lowest m single-particle modes. Then,

$$|\Psi_m\rangle = \prod_{k=1}^{m} b_k^\dagger |0\rangle , \tag{3.7}$$

where $|0\rangle$ is the Fock vacuum which is annihilated by the operators b_k and the filling fraction is defined as $\nu \equiv m/N$. The energy of this state is

$$E = \sum_{k=1}^{m} \varepsilon_k. \tag{3.8}$$

In this case, the graph associated to matrix T_{ij} is bipartite, *i.e.*, there are no diagonal nor even-ranged terms. Therefore, the Hamiltonian given in Eq. (3.1) presents particle-hole symmetry, $\varepsilon_k = -\varepsilon_{N+1-k}$, with $U_{ik} = (-1)^i U_{i,N+1-k}$. For every single-particle eigenstate with energy ε there is another eigenstate with energy $-\varepsilon$, as it is shown in Fig. 3.2 (a). Therefore, the ground state (GS) is given by filling up all the modes with negative energy if there are no zero modes, *i.e.*, $\nu = 1/2$, which is called *half-filling* and it is represented in Fig. 3.2 (b). The energy of the highest occupied mode is called the *Fermi energy*, ε_F.

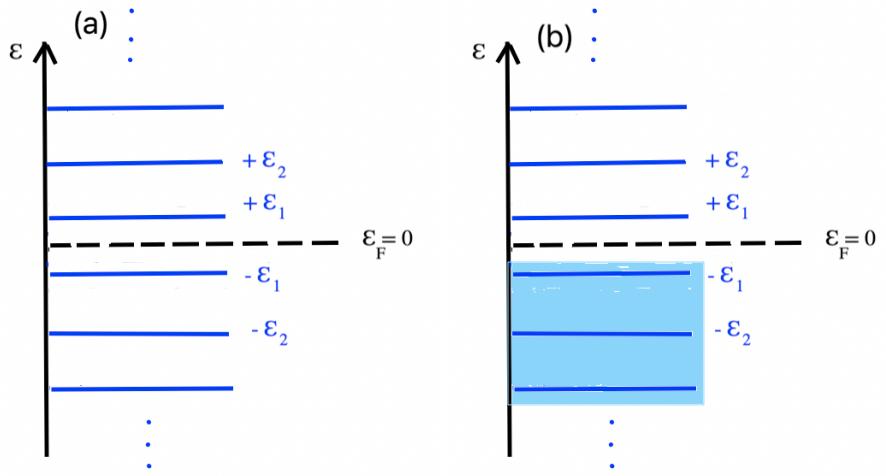

Figure 3.2: Particle-hole symmetry: (a) for every single-particle eigenstate with energy ε there is another eigenstate with energy $-\varepsilon$. (b) The GS is given by filling up all the modes with negative energy.

3.2 Correlation matrix and local density

The considered GS given by Eq. (3.7) is a Gaussian state, for which all observables can be obtained from the correlation matrix C, defined as

$$C = \begin{pmatrix} \left\langle c_1^\dagger c_1 \right\rangle & \cdots & \left\langle c_1^\dagger c_N \right\rangle \\ \vdots & \ddots & \vdots \\ \left\langle c_N^\dagger c_1 \right\rangle & \cdots & \left\langle c_N^\dagger c_N \right\rangle \end{pmatrix}. \tag{3.9}$$

In the case shown in the previous section where the number of particles is conserved, we can obtain any higher-order correlator, *e.g.*,

$$\left\langle c_m^\dagger c_n^\dagger c_k c_l \right\rangle = \left\langle c_m^\dagger c_l \right\rangle \left\langle c_n^\dagger c_k \right\rangle - \left\langle c_m^\dagger c_k \right\rangle \left\langle c_n^\dagger c_l \right\rangle. \tag{3.10}$$

Following from Eq. (3.5), one can write the inverse relations

$$c_i^\dagger = \sum_k \bar{U}_{ik} b_k^\dagger, \tag{3.11}$$

$$c_i = \sum_k U_{ik} b_k. \tag{3.12}$$

Thus, the elements of the correlation matrix C of a system with m particles are defined as

$$C_{ij} \equiv \left\langle c_i^\dagger c_j \right\rangle = \langle GS | \, c_i^\dagger c_j \, | GS \rangle = \sum_{k=1}^{m} \bar{U}_{ki} U_{kj}, \tag{3.13}$$

and, concretely, the local occupation or density is found as

$$\langle n_i \rangle = C_{ii}. \tag{3.14}$$

3.3 Computation of entanglement entropy

All the entanglement properties of a Gaussian state can be determined from the correlation matrix C. Indeed, the reduced density matrix of any block A of size ℓ, can be obtained diagonalizing the corresponding $\ell \times \ell$ submatrix, $C_A = \{C_{mn} | m, n \in A\}$. The set $\{\nu_k^A\}$ of eigenvalues of C_A, where each $\nu_k^A \in [0,1]$, determines uniquely the full entanglement spectrum. Then, we may diagonalize C_A

$$\sum_{m,n=1}^{\ell} \bar{V}_{mk} \left(C_A\right)_{mn} V_{kl} = \nu_{kl} \delta_{kl}, \tag{3.15}$$

where V are unitary matrices. So we can define a new set of fermionic operators $\{f_k\}_{k=1}^{N_A}$ with $f_k = \sum_{m=1}^{N_A} V_{mk} c_k$, whose correlator matrix is diagonal

$$\left\langle f_k^\dagger f_l \right\rangle = \nu_k \delta_{kl}. \tag{3.16}$$

Using the definition of the density matrix $\langle O \rangle = \mathrm{Tr}\left(O\rho\right)$, we can write

$$\left\langle f_k^\dagger f_l \right\rangle = \mathrm{Tr}\left(f_k^\dagger f_l \rho_A\right) = \nu_k \delta_{kl}. \tag{3.17}$$

Eq. (3.17) implies that $\rho_A = \rho_{A_1} \otimes \rho_{A_2} \otimes \cdots \otimes \rho_{A_l}$ which leads us to focus on the eigenvalues of ρ_{A_k}

$$\rho_{A_k} = \begin{pmatrix} \alpha_k & \beta_k \\ \beta_k^* & 1-\alpha_k \end{pmatrix}. \tag{3.18}$$

If we consider the matrix form of the fermionic operators

$$f_k = \begin{pmatrix} 0 & 0 \\ 1 & 0 \end{pmatrix}, \qquad f_k^\dagger = \begin{pmatrix} 0 & 1 \\ 0 & 0 \end{pmatrix}, \tag{3.19}$$

and impose $\langle f_k \rangle = 0$, we end up with $\mathrm{Tr}\left(f_k \rho_A\right) = \beta_k = 0$. On the other hand, from Eq. (3.17), $\alpha_k = \nu_k$. Therefore,

$$\rho_A = \bigotimes_{k=1}^{\ell} \rho_{A_k} = \bigotimes_{k=1}^{\ell} \begin{pmatrix} \nu_k & 0 \\ 0 & 1-\nu_k \end{pmatrix}. \tag{3.20}$$

We can now compute

$$\mathrm{Tr}\rho_A^n = \prod_{k=1}^{\ell} \mathrm{Tr}\rho_{A_k}^n = \prod_{k=1}^{\ell} \left(\nu_k^n + (1-\nu_k)^n\right). \tag{3.21}$$

The Rényi entropies are given by

$$S^{(n)}(A) = \frac{1}{1-n} \sum_{k=1}^{\ell} \log\left(\nu_k^n + (1-\nu_k)^n\right), \tag{3.22}$$

and the von Neumann entropy of block A can be expressed as

$$S(A) = \sum_{k=1}^{\ell} \left(\nu_k^A \log\left(\nu_k^A\right) + \left(1-\nu_k^A\right) \log\left(1-\nu_k^A\right)\right). \tag{3.23}$$

3.4 Analytical solution of the homogeneous chain

Let us consider a homogeneous fermionic chain described by Hamiltonian (3.1), where $J_m = 1$. In this particular case, it is possible to diagonalize analytically the hopping matrix T_{lj} in order to find the single-body modes and energies from Eq. (3.4).

3.4.1 Open chain

For open boundary conditions (OBC), the hopping matrix is given by

$$T_{lj} = -\begin{pmatrix} 0 & 1 & 0 & & \\ 1 & 0 & 1 & & \\ & \ddots & \ddots & \ddots & \\ & & 1 & 0 & 1 \\ & & 0 & 1 & 0 \end{pmatrix}, \tag{3.24}$$

and can be diagonalized using the Ansatz

$$\phi_l = Ae^{ikl} + Be^{-ikl}, \tag{3.25}$$

where k indicates the momentum. Thus, we can now write the corresponding bulk equations

$$T_{lj}\phi_j = \varepsilon\phi_l, \tag{3.26}$$

where we are using the summation over the set of repeated indexes. The eigenvalues ε represent the energy of each mode k. Therefore, taking into account Eq. (3.25) and Eq. (3.26),

$$A\left(e^{ik(l-1)} + e^{ik(l+1)}\right) + B\left(e^{ik(l-1)} + e^{ik(l+1)}\right) = \varepsilon_k\left(Ae^{ikl} + Be^{-ikl}\right), \tag{3.27}$$

with $\varepsilon_k = -2\cos(k)$.

If we consider expressions for the first and last sites of Eq. (3.27), *i.e.*, $l = 1$ and $l = N$, it is straightforward to see that $A = -B$ and

$$k_{\mathrm{OBC}} = \frac{\pi n}{N+1} \text{ with } n \in [1, N]\,. \tag{3.28}$$

The GS is obtained by filling up all the levels with negative energy so

$$\mathrm{GS} \to \left\{k_{\mathrm{OBC}} = \frac{\pi n}{N+1}, k \in \left[1, N/2\right]\right\}, \tag{3.29}$$

if the system has an even number of sites. However, if the size of the system is odd, the number of fermions of the ground state is odd and there is a state with zero energy corresponding to the *Fermi momentum* $k_F = \pi/2$, which is the momentum of the highest occupied mode. As a consequence, the ground state is degenerate since it is possible to define it with and without the zero mode.

3.4.2 Periodic chain

For closed boundary conditions we must distinguish two cases depending on the number of sites involved in the system.

For periodic boundary conditions (PBC), the hopping matrix follows from Eq. (3.24) but with $T_{1N} = T_{N1} = -1$. On the other side, for anti-periodic boundary conditions (APBC), one must have $T_{1N} = T_{N1} = 1$. The Ansatz for this configurations is $\phi_l = e^{ikl}$ and we proceed in the same way as for OBC.

For PBC, the allowed modes are

$$k = \frac{2m\pi}{N} \text{ with } \begin{cases} m \in \left[-\frac{N}{2}, \frac{N}{2}\right] \text{ for } N = 4n, \\ m \in \left[-\frac{(N-2)}{2}, \frac{(N-2)}{2}\right] \text{ for } N = 4n+2, \end{cases} \tag{3.30}$$

while for APBC,

$$k = \frac{(2m+1)\pi}{N} \text{ with } \begin{cases} m \in \left[-\frac{N}{2}, \frac{N}{2} - 1\right] \text{ for } N = 4n, \\ m \in \left[-\frac{(N-2)}{2}, \frac{(N-2)}{2} - 1\right] \text{ for } N = 4n+2. \end{cases} \tag{3.31}$$

The number of fermions, N_f, for the ground state is determined by particle-hole symmetry, $N_f = N/2$. Thus, the GS is determined by filling up half of the lowest energy modes. Therefore, for PBC, the GS modes are those with $k \in \left[-\frac{N}{4}, \frac{N}{4}\right]$ for $N = 4n$, and modes with $k \in \left[-\frac{(N-2)}{4}, \frac{N-2}{4}\right]$ for $N = 4n+2$. Equivalently, we definde the GS for APBC.

3.5 Energy

In this section, we will show that the expression for the energy contains a non-universal contribution proportional to the system size N, plus finite-size corrections of order $O(1/N)$. These corrections are fixed by conformal invariance which will be explained in the next chapter.

The energy of the system with a fixed number of particles m is given by Eq. (3.8)

$$E = \sum_{k=1}^{m} \varepsilon_k = -\sum_{k=1}^{m} 2\cos(k), \tag{3.32}$$

where k is given by Eq. (3.28) for OBC. Moreover, we can define the *Fermi velocity* as

$$v_F = \left.\frac{\partial \varepsilon_k}{\partial_k}\right|_{k_F} = 2, \tag{3.33}$$

with $k_F = \pi/2$.

Yet, the previous sum in Eq. (3.8) is difficult to compute so one can use the asymptotic expansion of Euler-Maclaurin expression, which provides a relation between the sum and the integral of a real or complex valued continuous function for real numbers x in the interval $[a, b]$ in terms of higher derivatives evaluated at the endpoints of the interval, in order to obtain the energy. Thus,

$$\sum_{n=a}^{b} f(n) \sim \int_a^b f(x)dx + \frac{f(a)+f(b)}{2} + \sum_{q=1}^{\infty} \frac{B_{2q}}{(2q)!}\left(f^{(2q-1)}(b) - f^{(2q-1)}(a)\right), \quad (3.34)$$

where a and b are integer numbers, B_{2q} are the Bernoulli numbers and $f^{(l)}$ is the l-th derivative. We will only compute the first term, $q = 1$, of the sum involving these numbers due to the fact that contributions to first order corrections to the energy in N^{-1} are fully determined by it. Therefore, we will only need $B_2 = 1/6$.

Taking into account the occupied modes for the GS for the different boundary configurations explained in Section 3.4, the energy of the ground state is given by

$$E^{\mathrm{OBC}}(N) \simeq -\frac{2N}{\pi} - \left(\frac{2}{\pi} - 1\right) - \frac{\pi}{12N}, \quad (3.35)$$

$$E^{\mathrm{PBC}}_{4n}(N) = E^{\mathrm{APBC}}_{4n+2}(N) \simeq -\frac{2N}{\pi} + \frac{2\pi}{3N}, \quad (3.36)$$

$$E^{\mathrm{PBC}}_{4n+2}(N) = E^{\mathrm{APBC}}_{4n}(N) \simeq -\frac{2N}{\pi} - \frac{\pi}{3N}. \quad (3.37)$$

A detailed calculation can be found in Appendix B.

3.5.1 General boundary conditions

Let us, for instance, focus on the case of $N = 4n$. We can observe from Eqs. (3.36) and (3.37) that the correction of order $O(1/N)$ of the energy for PBC and APBC switches its sign. This implies that there should be a phase θ for which the correction of $O(1/N)$ to the energy vanishes. With that aim, let us consider

$$k = \frac{2m\pi}{N} + \frac{\theta}{N}, \text{ with } m \in \left[-\frac{N}{4}, \frac{N}{4} - 1\right], \quad (3.38)$$

since we are focusing on the $N = 4n$ case. For $\theta = 0$, we recover $k = \dfrac{2m\pi}{N}$ as stated in Eq. (3.30) for PBC. On the other side, we obtain $k = \dfrac{2m\pi}{N} + \dfrac{\pi}{N}$, for $\theta = \pi$, which corresponds to APBC.

Indeed, we can compute the energy of the GS, with k given by Eq. (3.38), using the Euler-MacLaurin expression (3.34). Therefore,

$$E(\theta) \simeq -\frac{2N}{\pi} + \frac{2\pi}{3N} + \frac{\theta^2}{N\pi} - \frac{2\theta}{N}. \quad (3.39)$$

We recover Eqs. (3.36) and (3.37) for $\theta = 0$ and $\theta = \pi$, respectively, as it was expected.

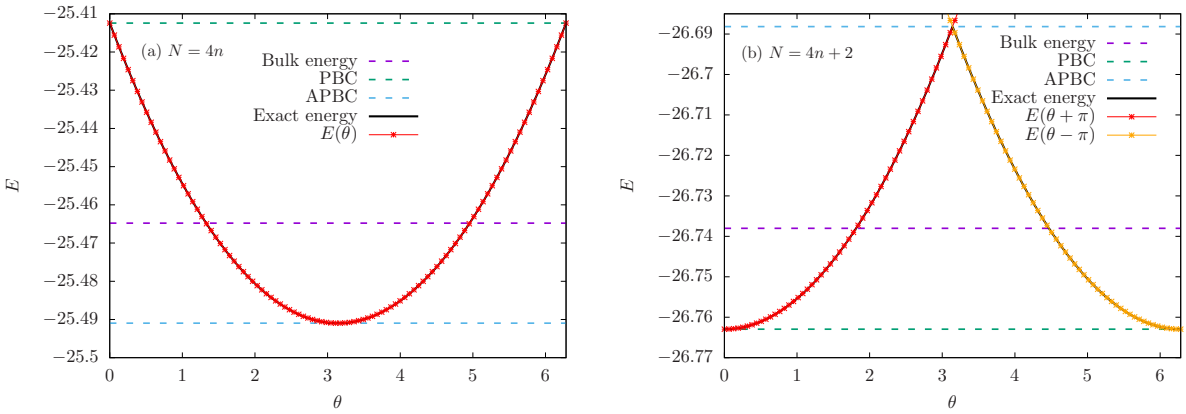

Figure 3.3: (a) The validity of Eq. (3.39) is checked in this panel for $N = 40$, where we recover PBC for $\theta = 0$ and $\theta = 2\pi$, whereas APBC are obtained when $\theta = \pi$. The corrections of order $O(1/N)$ to the energy vanish when θ takes the values of Eq. (3.40), which have also been checked numerically. (b) The validity of Eq. (3.39), which has to be shifted, is checked in this panel for $N = 42$. As it is seen, PBC become APBC and vice-versa. The values of θ which give no contribution to the energy of order $O(1/N)$ (Eq. (3.41)) have been also checked numerically.

Furthermore, from Eq. (3.39) we can find the values of θ that lead to no corrections of order $O(1/N)$:

$$\theta_1 = \pi\left(1 + \frac{1}{\sqrt{3}}\right), \quad \theta_2 = \pi\left(1 - \frac{1}{\sqrt{3}}\right). \tag{3.40}$$

In panel (a) of Fig. 3.3 we have compared Eq. (3.39) for $N = 4n$, with the energy obtained numerically. Aditionally, we have plot the PBC and APBC energies given by Eqs. (3.36) and (3.37), together with the bulk energy which is determined by the term proportional to the size of the system N. Indeed, when Eq. (3.39) has no correction of order $O(1/N)$, *i.e.*, θ takes the values given by Eq. (3.40), $E(\theta)$ is equal to the bulk energy.

Moreover, if we consider $N = 4n + 2$, the role of PBC and APBC is exchanged as it is shown in panel (b) of Fig. 3.3. Thus, since Eq. (3.39) was obtained for $N = 4n$, we need to shift it by $\pm\pi$ in order to reproduce the data for $N = 4n + 2$. As a consequence,

$$\theta_1' = \frac{\pi}{\sqrt{3}}, \quad \theta_2' = 2\pi - \frac{\pi}{\sqrt{3}}. \tag{3.41}$$

3.6 Spin models

Magnetism is one of the most relevant forces in nature and the magnetic properties of materials have long been considered object of interest [71]. The ferromagnetic behaviour of certain materials, such as iron, which remain magnetized even when the external field is removed showing all the spins aligned in the same direction, led to the introduction of the so-called spin systems. Shortly after the electron spin

was hypothesized in 1925, Lenz proposed to one of his students, Ising, to consider a model in which an interaction was introduced between spins placed on a lattice. Each spin is limited to take values ± 1, and interacts with neighbors such that spins with the same sign have a lower energy than those that disagree. Since all systems tend to their lowest possible energy state, this model captures a tendency towards ferromagnetism which is disturbed by temperature.

Indeed, magnetic materials exhibit interesting temperature-dependent behaviour. As the temperature increases, thermal motion becomes relevant and competes with the tendency of spins to be aligned. When the temperature reaches a certain point, called the *critical temperature* or the *Curie temperature* T_c, a second order phase transition takes place and the system can no longer maintain a spontaneous magnetization. However, for $T > T_c$ the system still responds paramagnetically to an external field: spins align in the direction of the applied magnetic field. Unlike ferromagnets, paramagnets do not retain any magnetization in the absence of an external field as thermal fluctuations randomize the spin orientations. Below T_c, there is a spontaneous symmetry breaking and spins become aligned with their neighbors resulting in stable magnetization regions.

In addition, the Ising model presents a $\mathbb{Z}_2$ symmetry group which means it is invariant under the unitary transformation of flipping all the spins in the z direction.

Ising was able to solve the one-dimensional version of the model exactly in the absence of an external magnetic field. He found that, even for very low temperatures, the model never undergoes a phase transition to an ordered ferromagnetic state which means that the spins become parallel only at $T = 0$. For finite T, the correlations between neighboring spins decay exponentially and the system is disordered. Furthermore, Onsager published an exact solution to the problem for a two dimensional square lattice, as represented in Fig. 3.4, and proved that the 2D model has a critical point at a non-zero temperature [72]. He was the first to describe the critical exponents of the phase transition, which are currently well understood by conformal field theory (CFT).

The quantum version of the classical Ising model presents a phase transition at zero temperature due to the interaction with a transverse magnetic field. In order to express the Ising Hamiltonian using a quantum mechanical description, we replace the spin variables with their respective Pauli matrices. In this case, spin projections align or anti-align along the z-axis and the external magnetic field is considered to be perpendicular as in the x-axis. In the quantum sense, the spin projections along the x and z axis do not commute so they can not be observed simultaneously. This means classical statistical mechanics is unable to explain the transition.

The one-dimensional quantum model admits two phases depending on whether the GS breaks or preserves the $\mathbb{Z}_2$ symmetry. At the critical point, the system undergoes a quantum phase transition. The $(1+1)$D transverse field Ising model is the quantum version of the two dimensional Ising model and can also be described by a 2D CFT.

There are also other spin models that have been put forward to study critical points and phase transitions of magnetic systems such as the model proposed by

Heisenberg and which takes the name after him. This model describes, quantum mechanically, the exchange interaction between particles of spin 1/2. The key difference between the Ising and Heisenberg models is that the Ising model, as we already said, presents a Hamiltonian which is invariant under a simultaneous flip of all spins, *i.e.*, a $\mathbb{Z}_2$ symmetry, whereas the Heisenberg Hamiltonian is rotationally symmetric, *i.e.*, possesses the full $SU(2)$ symmetry. This means that the Heisenberg model has a continuous symmetry opposed to the discrete symmetry present in the Ising system.

In two spatial dimensions, the Mermin-Wagner theorem [73] shows rigorously that such a continuous symmetry cannot be broken spontaneously at any finite temperature. Therefore, the Heisenberg model cannot have an ordered phase at low temperature like the Ising model. However, this theorem does not apply at $T = 0$.

For the ferromagnetic case, the total spin of the system commutes with the Hamiltonian and then is conserved. However, the ferromagnetic GS is not invariant under rotations. When the symmetry that is broken is continuous, there are infinitely many ground states. On the contrary, the number of GS in the Ising model is finite because the symmetry is discrete.

On the other side, in 1932 Néel identified a possible antiferromagnetic behaviour of the system below a certain transition temperature in which nearest neighbors order themselves in such a way that spins point in opposite directions [74]. However, this is not an eigenstate of the Heisenberg Hamiltonian and thus the GS is not trivial. Few rigorous results are known for the ground state of the antiferromagnetic Heisenberg model.

As we have seen, spin models are a very powerful tool in the study of magnetism. However, these spins systems represent quantum-many body models and analytical approaches are not always feasible. Nevertheless, there exists a powerful method for understanding the behaviour of quantum many-body spin systems which consists in mapping to non-interacting effective fermions. When this mapping is possible, it can be said that we have restricted the model's essential behaviour to the low-dimensional subspace of a single fermion. This means the model is solvable in terms of single-body modes, *i.e.*, free fermions, and the physics of the system is well understood.

The best known mapping to free fermions is the Jordan-Wigner transformation where non-local Pauli operators are identified with fermionic ladder operators. This method was successfully employed by Lieb, Schultz and Mattis to solve the one dimensional XY model [75] and the Ising model in a transverse field [3].

3.6.1 Jordan-Wigner transformation

Let us consider a single spin 1/2 and the three components of the spin-operators S^α with $\alpha = x, y, z$,

$$S^x = \frac{1}{2}\begin{pmatrix} 0 & 1 \\ 1 & 0 \end{pmatrix}, \quad S^y = \frac{1}{2}\begin{pmatrix} 0 & -i \\ i & 0 \end{pmatrix}, \quad S^z = \frac{1}{2}\begin{pmatrix} 1 & 0 \\ 0 & -1 \end{pmatrix}. \tag{3.42}$$

These spin operator are related to Pauli matrices as $S^\alpha = \sigma^\alpha/2$ ($\hbar = 1$).

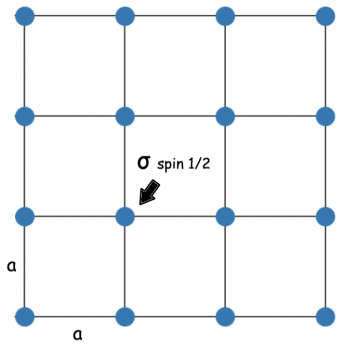

Figure 3.4: Ising model in 2D.

The Hilbert space of a single spin 1/2 is two-dimensional and the spin operators commute when they act on different sites of the chain, *i.e.*, different Hilbert spaces. However, acting on the same site, the commutator of spin operators leads to

$$\left[S_j^x, S_j^y\right] = iS_j^z, \tag{3.43}$$

and cyclic permutations. Spin operators (3.42) are related to raising and lowering operators as

$$a_j^+ = S_j^x + iS_j^y, \; a_j = S_j^x - iS_j^y. \tag{3.44}$$

So,

$$S_j^x = \frac{\left(a_j^+ + a_j\right)}{2}, \; S_j^y = \frac{\left(a_j^+ - a_j\right)}{2i}, \; S_j^z = a_j^+ a_j - 1/2. \tag{3.45}$$

The Jordan-Wigner transformation [76] relates spin and fermionic degrees of freedom as [3]

$$a_j = \exp\left[-\pi i \sum_{k=1}^{j-1} c_k^\dagger c_k\right] c_j, \tag{3.46}$$

$$a_j^\dagger = c_j^\dagger \exp\left[\pi i \sum_{k=1}^{j-1} c_k^\dagger c_k\right]. \tag{3.47}$$

The inverse relations are

$$c_j = \exp\left[\pi i \sum_{k=1}^{j-1} a_k^\dagger a_k\right] a_j, \tag{3.48}$$

$$c_j^\dagger = a_j^\dagger \exp\left[-\pi i \sum_{k=1}^{j-1} a_k^\dagger a_k\right]. \tag{3.49}$$

where c_j and $c_j^\dagger$ are fermionic operators and hence satisfy $\{c_j, c_k^\dagger\} = \delta_{jk}$, $\{c_j, c_k\} = \{c_j^\dagger, c_k^\dagger\} = 0$.

3.6.2 XY and XX models

Let us consider N spins 1/2's located in a 1D chain with nearest-neighbor interactions and general boundary conditions. The corresponding Hamiltonian is given by [75]

$$H_\Gamma = -\sum_{i=1}^{N-1} J\left[(1+\Gamma)\,S_i^x S_{i+1}^x + (1-\Gamma)\,S_i^y S_{i+1}^y - \Theta\left((1+\Gamma)\,S_N^x S_1^x + (1-\Gamma)\,S_N^y S_1^y\right)\right], \tag{3.50}$$

where J is the coupling amplitude, Γ is a parameter that characterizes the anisotropy in XY-plane and S^α with $\alpha = x, y, z$, are the spin operators of Eq. (3.42). The last term in Eq. (3.50) has been added to take into account all the possible boundary conditions of the system through parameter Θ. When $\Theta = 0$, we deal with the open chain. On the other hand, $\Theta = 1$ stands for the periodic boundary conditions where $S_{N+1}^\alpha = S_1^\alpha$, and Hamiltonian (3.50) is translational invariant.

If $|\Gamma| \neq 1$, the model behaves quantum mechanically as the different components of S_i appearing in (3.50) do not commute. The second term of Hamiltonian (3.50) opposes the ordering of the x component to favor the ordering of the y component. We will focus on the case with $|\Gamma| = 0$, which describes the isotropic XX model given by

$$H_{\mathrm{XX}} = -\sum_{i=1}^{N-1} J\left(S_i^x S_{i+1}^x + S_i^y S_{i+1}^y\right) - \Theta J\left(S_N^x S_1^x + S_N^y S_1^y\right). \tag{3.51}$$

The XX Hamiltonian commutes with the total magnetization $\mathcal{M}$, $[H, \mathcal{M}] = 0$, which is defined as $\mathcal{M} = \sum_{i=1}^N S_i^z$. As a consequence, H_{XX} is invariant under rotations around the z axis. Hamiltonian (3.51) also commutes with the parity operator $P = 2\prod_{i=1}^N S_i^z$, so it is invariant under spin inversion. This means that the number of particles in the system, and thus the parity, are fixed.

From Eq. (3.45), one can rewrite Hamiltonian (3.51) as

$$H = -\sum_{i=1}^{N-1} \frac{J}{2}\left(a_i^\dagger a_{i+1} + a_i a_{i+1}^\dagger\right) - \Theta\frac{J}{2}\left(a_N^\dagger a_1 + a_N a_1^\dagger\right). \tag{3.52}$$

Due to the fact that $a_i^\dagger a_{i+1} = c_i^\dagger c_{i+1}$, for OBC we recover Hamiltonian (3.1)

$$H^{\mathrm{OBC}} = -\frac{1}{2}\sum_{i=1}^{N-1} J\left(c_i^\dagger c_{i+1} + c_{i+1}^\dagger c_i\right). \tag{3.53}$$

However, for PBC, $a_N a_1^\dagger = (-1)^{N_f+1} c_N^\dagger c_1$, where N_f is the total number of fermions of the system given by $N_f = \sum_{i=1}^N c_i^\dagger c_i$. We must distinguish then between N_f even and odd.

$$N_f \text{ even} \rightarrow H_e^{\mathrm{PBC}} = H^{\mathrm{OBC}} + \frac{J}{2}\left(c_N^\dagger c_1 + c_N c_1^\dagger\right), \tag{3.54}$$

$$N_f \text{ odd} \rightarrow H_o^{\mathrm{PBC}} = H^{\mathrm{OBC}} - \frac{J}{2}\left(c_N^\dagger c_1 + c_N c_1^\dagger\right). \tag{3.55}$$

For N_f even it is straightforward to see that $c_{N+1} = -c_1$ which means anti-periodic boundary conditions. When N_f is odd, $c_{N+1} = c_1$ and thus the chain is closed with PBC. This shows that boundary conditions are affected by the fermion parity.

Notice that we have mapped the XX spin model into a Hamiltonian which is quadratic in fermionic operators so free fermions techniques may be applied. Yet, boundary conditions are affected by the fermion parity: PBC becomes APBC when N is even. No problem is present, instead, when the boundary conditions are open because there is no link between operators at site N and $N + 1 \equiv 1$.

3.6.3 Ising model

The 1D classical Ising model in the absence of an external magnetic field is given by the Hamiltonian

$$H_{\text{Ising}} = -\sum_{i=1}^{N-1} J\sigma_i\sigma_{i+1}, \tag{3.56}$$

where each site is occupied by one single particle and it is represented by the discrete variable σ_i. Each spin can only take a value of $\sigma_i = \pm 1$ and we have restricted the interaction to nearest-neighbors. The magnetic behaviour of the system is determined by the parameter J. When $J > 0$, the Ising model is ferromagnetic and spins desire to be aligned. On the other hand, the system becomes antiferromagnetic when $J < 0$.

For the one-dimensional case, there is no phase transition, contrary to the 2D classical system [77].

The Ising model can be extended into a quantum mechanical description when a transverse external magnetic field is considered. In this case, spin variables are replaced by their respective Pauli matrices and the Hamiltonian is defined as

$$H_{\text{Ising}} = -\sum_{i=1}^{N-1} J\sigma_i^z\sigma_{i+1}^z - \Delta\sum_{i=1}^{N} \sigma_i^x. \tag{3.57}$$

We have considered that spin projections align or anti-align along the z axis and the magnetic field is applied in the perpendicular direction of the x axis. When $\Delta > 0$, spins tend to line up in the direction of the positive x axis.

The one-dimensional quantum Ising model presents two distinguished phases based on whether the ground state breaks or preserves the $\mathbb{Z}_2$ symmetry. When $|\Delta| < 1$, the GS breaks the spin-flip symmetry and the system is said to be in the ordered phase. When $|\Delta| > 1$, the GS preserves the symmetry and the system is said to be in a disordered phase. Both of these phases are gapped [3]. At the boundary between these two gapped phases we find a quantum phase transition, or a critical point, which can be described by a CFT as we will see in the next chapter.

3.6.4 Heisenberg model

The Heisenberg model explains the exchange interaction between particles of spin 1/2, which has a quantum mechanical origin.

The spin-1/2 Heisenberg model in 1D is one of the simplest critical interacting systems and is defined by [4]

$$H_{\text{Heisenberg}} = -J \sum_{i=1}^{N-1} \left[\left(S_i^x S_{i+1}^x + S_i^y S_{i+1}^y \right) + \Delta S_i^z S_{i+1}^z \right], \tag{3.58}$$

The exchange interaction is controlled by J, and the ratio Δ is the anisotropy parameter. When $\Delta = 1$, Hamiltonian (5.32) is known as the Heisenberg model or XXX model. On the other hand, it is said to be the XXZ model for $\Delta \neq 1$, or, equivalently, XYZ when the coupling parameter J is different in the three directions.

The exchange interaction term present in Heisenberg Hamiltonian has no effect over the state where all spins align in the same direction. Therefore, this state is a ground state when the Heisenberg model is ferromagnetic. For the antiferromagnetic Heisenberg model the ground state is more complicated than the simple configuration of anti-parallel spins [78].

Under the Jordan-Wigner transformation, Hamiltonian (3.58) can be written in fermionic language as

$$H = -\sum_{i=1}^{N-1} J_i \left(c_i^\dagger c_{i+1} + \text{h.c.} \right) + 2 \sum_{i=1}^{L} J_i \, n_i^\dagger n_{i+1}, \tag{3.59}$$

where $n_i = c_i^\dagger c_i$ is the fermion number operator. We can see that fermionic particles at nearby sites repel each other, making it impossible to use free fermion techniques. Yet, the GS energy of this Hamiltonian can be accurately obtained using the density matrix renormalization group (DMRG) algorithm [49, 50] or the Bethe Ansatz.

Chapter 4

Conformal Field Theory

The aim of this chapter is to briefly introduce conformal field theory (CFT) and its relevance in condensed matter physics. CFT predictions have been crucial in this work as it will be shown in the next chapters.

In order to have a good understanding of this thesis, we will focus on 2D CFT results so we will leave the cases where $D > 2$ out of this text. A 2D CFT is strongly constrained by its symmetries because the algebra of conformal transformations is infinite-dimensional. Conformal field theories in two dimensions are a powerful tool in many topics as scale invariance is directly related to conformal invariance.

4.1 Motivation

One of the main purposes of condensed matter physics is the distinction and characterization of phases of matter. For that aim, the *renormalization group* (RG) procedure has proved to be very useful [79]. The RG focuses on how the physical phenomena change with the length scale of a given system. Let us consider a Hamiltonian $H\left(\{g\}\right)$, parametrized by a certain set of coupling constants $\{g\}$. The RG characterizes how $H\left(\{g\}\right)$ varies under a re-scaling $\mathcal{R}$ of the corresponding lattice spacing a, *i.e.*, $a \to ba$ with $b > 1$. The RG transformation $\{g'\} = \mathcal{R}\left(\{g\}\right)$ can be seen as a flow from point $\{g\}$ to point $\{g'\}$. When $\{g^*\} = \mathcal{R}\left(\{g^*\}\right)$, we say we have reached a fixed point and thus, the correlation length of the system does not change under the re-scaling transformation. However, this correlation length must be measured with respect to the new scale so $\mathcal{R}\left(\xi\right) = \xi/b$. Therefore, there are two values for ξ at the fixed point: $\xi = 0$ and $\xi = \infty$. The first case is trivial, and leads to a factorized state. The second case, $\xi = \infty$, leads to critical points, where short-distance behaviour is irrelevant and phase transitions take place.

A conformal field theory is a field theory that is invariant under conformal transformations, *i.e.*, transformations that preserve angles [21]. An example of these transformations is *scaling*: the theory remains the same both at small and long distances. For instance, due to their scale invariance, critical points can be characterized with conformal field theories [80].

We will focus on relativistic conformal field theories, which play an important

role in the space of quantum field theories as they describe fixed points of the renormalization group flow in a relativistic quantum field theory [81]. The symmetry group of a relativistic conformal field theory is encoded by Poincaré transformations, dilations and special conformal transformations. Special relativity establishes that all of physics is invariant under Poincaré transformations: physics remain the same regarding where an observer is (translation), the direction they are facing (rotation) or how fast they are moving (boost).

Two of the simplest examples of conformal field theories are classical Maxwell's equations in the absence of sources (charged particles) and the free massless Dirac fermion in dimension $D = 4$ [81], which are both non-interacting fields with no mass so the associated Lagrangians have no dimensional coupling parameters. This means that the action is invariant under conformal transformations. There are also examples of interacting theories with classical conformal invariance [82] with massless fields. However, if the associated Lagrangian has a mass parameter the theory can not be conformally invariant: the mass introduces a characteristic length scale in the system that is not invariant under scale transformations.

The quantum version of conformal invariance presents certain peculiarities, due to the need of regularization, which introduces a length scale, giving rise to the so-called *conformal anomaly*, which will be discussed in the following paragraphs.

CFT has found applications beyond the characterization of fundamental fields. It describes critical points in statistical mechanics, both classical and quantum, with special success in 2D classical [77] or $(1 + 1)D$ quantum cases, due to the special properties of the conformal group in this case. Moreover, CFT provides an interesting route to quantize gravity, such as string theory or the holographic principle, through the AdS/CFT correspondence [83]. A theory of gravity in an anti-de Sitter space, *i.e.*, space-time with a negative cosmological constant corresponds to a CFT on the boundary. In string theory, the worldsheet theory describing the excitations of a string is a CFT.

The following sections constitute an overview of CFT in $(1 + 1)D$, which it is enough for the applications we employ in this thesis. For a more general review see [21, 22].

4.2 Conformal transformations

As previously stated, conformal transformations in 2D are spatial maps that preserve angles (see Fig. 4.1). In terms of a certain metric, a conformal transformation is a change of coordinates, $r \to \tilde{r}$, that yields a local rescaling of the metric [21]:

$$g^{\mu\nu}(r) \to \tilde{g}^{\mu\nu}(\tilde{r}) = \Omega(r) g^{\mu\nu}(r). \tag{4.1}$$

Focusing on 2D, we may consider coordinates (x^0, x^1), in Euclidean metric, and the change of coordinates $x^\mu \to w^\mu(x)$. Thus, the metric transforms as

$$g^{\mu\nu} \to \tilde{g}^{\mu\nu} = \frac{\partial w^\mu}{\partial x^\alpha} \frac{\partial w^\nu}{\partial x^\beta} g^{\alpha\beta}. \tag{4.2}$$

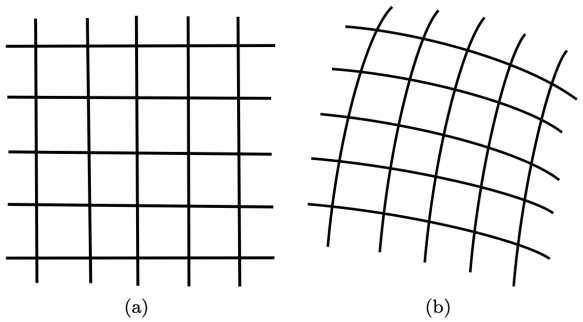

Figure 4.1: A conformal mapping transforms Cartesian coordinates (a) into curvilinear coordinates (b) while preserving angles.

For a Euclidean metric, $g^{00} = g^{11} = 1$, Eq. (4.2) is a conformal transformation if,

$$\left(\frac{\partial w^0}{\partial x^0}\right)^2 + \left(\frac{\partial w^0}{\partial x^1}\right)^2 = \left(\frac{\partial w^1}{\partial x^0}\right)^2 + \left(\frac{\partial w^1}{\partial x^1}\right)^2 . \tag{4.3}$$

$$\frac{\partial w^0}{\partial x^0}\frac{\partial w^1}{\partial x^0} + \frac{\partial w^0}{\partial x^1}\frac{\partial w^1}{\partial x^1} = 0. \tag{4.4}$$

which arise from imposing proportionality between the original and the final metric, *i.e.*, $\tilde{g}^{00} \propto g^{00} = 1$, $\tilde{g}^{11} \propto g^{11} = 1$ and $\tilde{g}^{01} \propto g^{01} = 0$, $\tilde{g}^{10} \propto g^{10} = 0$.

These equations are equivalent to the holomorphic (+) and anti-holomorphic (−) Cauchy-Riemann equations

$$\partial_0 w_1 = \pm \partial_1 w_0, \tag{4.5}$$

$$\partial_0 w_0 = \pm \partial_1 w_1. \tag{4.6}$$

This motivates the use of complex variables z and $\bar{z}$ so we define

$$z \equiv x^0 + i x^1, \tag{4.7}$$

$$\bar{z} \equiv x^0 - i x^1, \tag{4.8}$$

$$\partial \equiv \partial_z = \frac{1}{2}\left(\partial_0 - i\partial_1\right), \tag{4.9}$$

$$\bar{\partial} \equiv \partial_{\bar{z}} = \frac{1}{2}\left(\partial_0 + i\partial_1\right). \tag{4.10}$$

The metric in the new variables takes the form

$$ds^2 = dz d\bar{z}, \tag{4.11}$$

and the Cauchy-Riemann equations can be written as

$$\bar{\partial} w(z, \bar{z}) = 0. \tag{4.12}$$

The solution to this equation is an holomorphic mapping: $z \to w(z)$. The conformal group for $D = 2$ coincides with the set of all analytic maps and it is infinite-dimensional. This is the reason why conformal symmetry is so powerful in two dimensions.

We consider now an infinitesimal transformation

$$w(z) = z + \varepsilon(z), \tag{4.13}$$

and its analogue for $\bar{z}$. Therefore,

$$ds^2 = dzd\bar{z} \to \frac{dw}{dz}\frac{d\bar{w}}{d\bar{z}}\partial z\partial\bar{z}. \tag{4.14}$$

We have infinitely many conformal infinitesimal transformations. However, in order to form a group the mapping must be invertible and map the whole plane into itself, including the point at infinity. The transformations that satisfy these conditions are called *global conformal transformations*, or Möbius transformations. *Locally conformal transformations*, on the other hand, are holomorphic mappings which need not be invertible.

If we consider the mapping $w(z)$ and we want it to be invertible, the only possible form it can take is

$$w(z) = \frac{P(z)}{Q(z)}. \tag{4.15}$$

This means the only acceptable singularities are poles. $P(z)$ and $Q(z)$ can be at most linear functions in order to avoid several distinct zeros or multiple zeros so the inverse image (of zero) is well defined,

$$w(z) = \frac{az + b}{cz + d}. \tag{4.16}$$

One more condition is needed for f to be invertible: $ad - bc \neq 0$. The conventional normalization is $ad - bc = 1$. This is called a *projective transformation*.

4.3 Witt algebra and Virasoro algebra

Let us consider an infinitesimal transformation of the form of Eq. (4.13) and take a Laurent expansion

$$\varepsilon(z) = \sum_{n\in\mathbb{Z}} c_n z^{n+1}, \tag{4.17}$$

where c_n are assumed to be infinitesimal. We can compute the action of the conformal map on functions $f(z, \bar{z})$ which leads to the generators of the conformal algebra

$$l_n = -z^{n+1}\partial_z, \tag{4.18}$$

$$\bar{l}_n = -\bar{z}^{n+1}\partial\bar{z}. \tag{4.19}$$

The commutation relations satisfied by these generators are the so called *Witt algebra* relations,

$$[l_n, l_m] = (n - m)l_{n+m}, \tag{4.20}$$

$$[\bar{l}_n, \bar{l}_m] = (n - m)\bar{l}_{n+m}, \tag{4.21}$$

$$[l_n, \bar{l}_m] = 0. \tag{4.22}$$

These generators are responsible of

- Dilations: $l_0 = -z\dfrac{\partial}{\partial z}$.
- Translations: $l_{-1} = -\dfrac{\partial}{\partial z}$.
- Special conformal transformations: $l_1 = -z^2\dfrac{\partial}{\partial z}$.

We can generate self-adjoint operators as $(l_n + \bar{l}_n)$ and $i(l_n - \bar{l}_n)$, which are the dilation and rotation operators respectively. The eigenstates of l_0 show a special relevance since it represents the scaling operator,

$$l_0 \left|\psi\right\rangle = h \left|\psi\right\rangle, \tag{4.23}$$

$$\bar{l}_0 \left|\psi\right\rangle = \bar{h} \left|\psi\right\rangle, \tag{4.24}$$

where h and $\bar{h}$ constitute the eigenvalues of the dilatation (Δ) and rotation (s) operators

$$\Delta = h + \bar{h} \rightarrow \text{Scaling dimension}, \tag{4.25}$$

$$s = h - \bar{h} \rightarrow \text{Conformal spin}. \tag{4.26}$$

4.3.1 Central extension: Virasoro algebra.

The Witt algebra leads to an incomplete description of CFT's. In terms of physics, this is due to the existence of a conformal anomaly which appears as a consequence of the regularization scales (IR and UV) in our problem. From a formal mathematical perspective, the reason of the appearance of the conformal anomaly is that the representations of the conformal group associated to field theory tend to be projective representations, *i.e.*, true representations up to a scale factor. Both physical and mathematical arguments lead us to introduce the notion of *central charge*, c, a numerical value that characterizes CFT's.

Indeed, the corresponding symmetry Lie algebra of a quantum system is, in general, a central extension of the classical symmetry algebra [84]. The symmetry algebra of a conformal field theory must be the central extension of the Witt algebra, which is the so called *Virasoro algebra* and it is given by

$$[L_m, L_n] = (m-n)L_{m+n} + \frac{c}{12}m(m^2-1)\delta_{m+n,0}. \tag{4.27}$$

The derivation of Eq. (4.27) is very interesting so a detailed calculation can be found in Appendix C.

If hermiticity conditions are imposed on Virasoro operators in order to deal with a proper quantum system, then the CFT is called unitary. This implies

$$L_n^\dagger = L_{-n}, \tag{4.28}$$

$$\bar{L}_n^\dagger = \bar{L}_n. \tag{4.29}$$

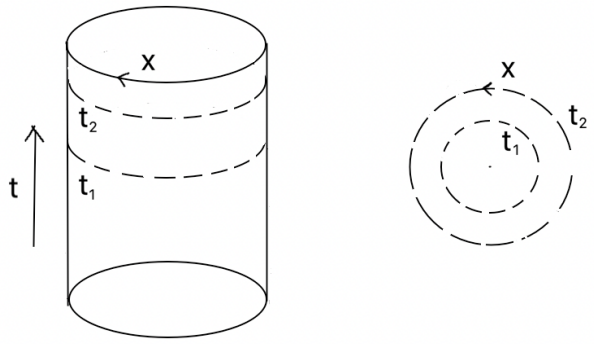

Figure 4.2: Mapping from the cylinder to the complex plane.

4.4 Radial quantization

The operator formalism of quantum mechanics implies an arbitrary choice of the time and space axis in space-time. Alternatively, in an Euclidean metric, we can choose the radial direction from the origin to be the time direction. This is what leads to *radial quantization*.

One can use spherical coordinates to express the flat metric for any Euclidean field theory on $\mathbb{R}^2$ [85]

$$d^2s = dx^\mu dx^\nu = dr^2 + r^2 d\phi^2 = r^2 \left(\frac{dr^2}{r^2} + d\phi^2 \right). \tag{4.30}$$

If we define $t = \log r$,

$$ds^2 = e^{2t} \left(dt^2 + d\phi^2 \right). \tag{4.31}$$

Performing a conformal transformation in Eq. (4.31), the factor e^{2t} is removed and the remaining metric corresponds to a two-dimensional cylinder, $\mathbb{R} \times S^1$.

Starting with a CFT on $\mathbb{R}^d$, the theory should be invariant under conformal transformations of the metric: a CFT on $\mathbb{R}^2$ should be equivalent to study the theory on $\mathbb{R} \times S^1$. This map takes circles of constant radius in $\mathbb{R}^2$ to constant t slices on the cylinder. The dilation operator on $\mathbb{R}^2$, which maps circles onto circles with different radius, corresponds to time translations on the cylinder, *i.e.*, it behaves as a Hamiltonian. Thus, this leads to the expression

$$H = L_0 + \bar{L}_0 + \text{cte.}, \tag{4.32}$$

where L_0 and $\bar{L}_0$ are the Virasoro operators responsible for dilations as was previously explained.

We start then from an infinite space-time cylinder with coordinate t going from $-\infty$ to ∞ along the direction of its axis and coordinate x going from 0 to L. In Euclidean geometry, the cylinder is described by a single complex coordinate $w = t + ix$. Now we can map the cylinder onto the complex plane, as shown in Fig. 4.2, via $z = e^{2\pi w/L}$ so $t \to -\infty$ is mapped to the origin $z = 0$ and $t \to \infty$ is sent to infinity.

4.5 Primary fields and correlation functions

The connection between a statistical mechanics and quantum field theory is made by writing the partition function and correlation functions as functional integrals,

$$Z = \frac{1}{Z}\int D\Phi \exp\left(-S[\Phi]\right), \tag{4.33}$$

$$\left\langle \phi_1(x_1)\dots\phi_k(x_k)\right\rangle = \frac{1}{Z}\int D\Phi\ \phi_1(x_1)\dots\phi_k(x_k)\exp\left(-S[\Phi]\right), \tag{4.34}$$

where $S[\Phi]$ is the Euclidean action, Φ the collection of fields and $\phi_i \in \Phi$.

Let us consider a spinless field $\phi(x)$ for simplicity. The field $\phi(x)$ is called a *quasi-primary field* if it transforms under a global conformal transformation as,

$$\phi(x) \to \tilde{\phi}(\tilde{x}) = \left|\frac{\partial\tilde{x}}{\partial x}\right|^{-\Delta/d}\phi(x), \tag{4.35}$$

where Δ is the scaling dimension. In complex coordinates for the 2D case, Eq. (4.35) can be written as

$$\tilde{\phi}\left(\omega,\bar{\omega}\right) = \left(\frac{\partial\omega}{\partial z}\right)^{-h}\left(\frac{\partial\bar{\omega}}{\partial\bar{z}}\right)^{-\bar{h}}\phi\left(z,\bar{z}\right), \tag{4.36}$$

where h and $\bar{h}$ are called conformal weights. The combinations $\Delta = h + \bar{h}$ and $s = h - \bar{h}$ are the scaling dimension and the spin of ϕ, respectively, as it was said previously. A *primary field* is a field ϕ that satisfies Eq. (4.36) for any analytic map $\omega(z)$. On the other hand, we will say the field is quasi-primary when $\omega(z)$ is a projective transformation (4.16), *i.e.*, the map is invertible. An example of a quasi-primary field which is not primary is the stress-energy tensor which will be discussed in the next section.

At the quantum level, the natural object of study are the N point correlation functions of the fields. Conformal invariance fixes completely the two-point and three-point correlation functions. For a general two-point function, the assumption of quasi-primarily fields implies

$$\left\langle \phi_1(x_1)\phi_2(x_2)\right\rangle = \left|\frac{\partial\tilde{x}}{\partial x}\right|_{x=x_1}^{\Delta_1/d}\left|\frac{\partial\tilde{x}}{\partial x}\right|_{x=x_2}^{\Delta_2/d}\left\langle \phi_1(\tilde{x}_1)\phi_2(\tilde{x}_2)\right\rangle. \tag{4.37}$$

Rotation and translation invariance added to covariance under a scale transformation leads to

$$\left\langle \phi_1(x_1)\phi_2(x_2)\right\rangle = \frac{C_{12}}{|x_1 - x_2|^{\Delta_1+\Delta_2}}, \tag{4.38}$$

for some constant C_{12} which can be conveniently set to 1. After some work, the two-point correlation function can be written as

$$\left\langle \phi_1(x_1)\phi_2(x_2)\right\rangle = \frac{\delta_{\Delta_1,\Delta_2}}{x_{12}^{2\Delta_1}}, \tag{4.39}$$

where we have set $x_{ij} = \left|x_i - x_j\right|$. The two-point function vanishes unless the two fields have the same scaling dimension.

For the three-point correlation function, covariance under rotations, translations and dilations imply that it must take the form

$$\left\langle \phi_1(x_1)\phi_2(x_2)\phi_3(x_3)\right\rangle = \frac{C_{123}}{x_{12}^{\Delta_1+\Delta_2-\Delta_3}x_{23}^{\Delta_2+\Delta_3-\Delta_1}x_{31}^{\Delta_3+\Delta_1-\Delta_2}}, \tag{4.40}$$

where the constant C_{123} is a non-trivial parameter.

The complete determination, up to a constant, of two and three-point correlation functions is a consequence of how conformal transformations are defined in two dimensions, *i.e.*, it is not possible to construct conformal invariants using only two or three points. However, for $N \geq 4$ it is possible to construct $N(N-3)/2$ independent invariants, known as anharmonic ratios or cross-ratios. Let us consider, for instance, the four-point correlation

$$\left\langle \phi_1(x_1)\phi_2(x_2)\phi_3(x_3)\phi_4(x_4)\right\rangle = f\left(\frac{x_{12}x_{34}}{x_{13}x_{24}}, \frac{x_{12}x_{34}}{x_{23}x_{14}}\right)\prod_{i<j}^{4} x_{ij}^{\Delta/3-\Delta_i-\Delta_j}, \tag{4.41}$$

with $\Delta = \sum_{i=1}^{4}\Delta_i$. The function f is not completely determined by conformal invariance.

4.6 Stress-energy tensor and Casimir energy

Under an arbitrary transformation of coordinates of the form

$$x^\mu \to x^\mu + \xi^\mu(x), \tag{4.42}$$

the change in the action is given by

$$\delta S = \int d^d x T^{\mu\nu}\partial_\mu \xi_\nu. \tag{4.43}$$

Translational invariance implies $\delta S = 0$ when we perform a coordinate change $\xi_\nu = a_\nu$, leading to

$$\partial_\mu T^{\mu\nu}(x) = 0, \tag{4.44}$$

which is equivalent to the conserved current arisen from a continuous symmetry. Rotational invariance should also make Eq. (4.43) vanish and, therefore, the stress-energy tensor must be symmetric

$$T^{\mu\nu}(x) = T^{\nu\mu}(x). \tag{4.45}$$

Finally, the dilation invariance implies that T is traceless,

$$T^\mu_\mu(x) = 0. \tag{4.46}$$

If $T^{\mu\nu}$ is assumed to be symmetric, Eq.(4.43) can be written as

$$\delta S = \frac{1}{2}\int d^d x T^{\mu\nu}\left(\partial_\mu\xi_\nu + \partial_\nu\xi_\mu\right). \tag{4.47}$$

When Eq. (4.42) is considered as an infinitesimal transformation, the corresponding change in the metric tensor to first order in ξ is

$$\begin{aligned}\tilde{g}_{\mu\nu} &= \frac{\partial x^\alpha}{\partial \tilde{x}^\mu}\frac{\partial x^\beta}{\partial \tilde{x}^\nu} g_{\alpha\beta} \\ &= \left(\delta^\alpha_\mu - \partial_\mu \xi^\alpha\right)\left(\delta^\beta_\nu - \partial_\nu \xi^\beta\right) g_{\alpha\beta} \\ &= g_{\mu\nu} - \left(\partial_\mu \xi^\nu + \partial_\nu \xi_\mu\right).\end{aligned} \tag{4.48}$$

Therefore, we can think of the stress-energy tensor as the functional derivative of the action with respect to the metric

$$\delta S = -\frac{1}{2}\int d^2x T^{\mu\nu}\delta g_{\mu\nu}. \tag{4.49}$$

Taking into account Eq. (4.1) and Eq. (4.48), we can rewrite the change in the action as

$$\delta S = \frac{1}{2}\int d^2x T^\mu_\mu \partial_\rho \xi^\rho. \tag{4.50}$$

The components of the stress-energy tensor need some rewriting when using complex coordinates. Thus, we find

$$T_{z\bar{z}} = T_{\bar{z}z} = \frac{1}{4}T^\mu_\mu = \frac{1}{4}\left(T_{00} + T_{11}\right) = 0. \tag{4.51}$$

$$T_{zz} = \frac{1}{4}\left(T_{00} - 2iT_{10} - T_{11}\right) = \frac{1}{2}\left(T_{00} - iT_{10}\right). \tag{4.52}$$

$$T_{\bar{z}\bar{z}} = \frac{1}{4}\left(T_{00} + 2iT_{10} - T_{11}\right) = \frac{1}{2}\left(T_{00} + iT_{10}\right). \tag{4.53}$$

Eq. (4.44) and the tracelessness of the stress-energy tensor lead to

$$\partial_{\bar{z}} T_{zz} = 0. \tag{4.54}$$

$$\partial_z T_{\bar{z}\bar{z}} = 0. \tag{4.55}$$

This means that $T \sim T_{zz}$ depends only on z, hence is an holomorphic function, and that $\bar{T} \sim T_{\bar{z}\bar{z}}$ depends only on $\bar{z}$, hence is an anti-holomorphic function. This is a very important element in the solvability of two-dimensional CFT. The non-vanishing components of the stress-energy tensor are chiral and anti-chiral fields, $T(z)$ and $\bar{T}(\bar{z})$, which can be written in terms of Virasoro operators

$$T(z) = \sum_{n\in\mathbb{Z}} L_n z^{-n-2}, \tag{4.56}$$

$$\bar{T}(\bar{z}) = \sum_{n\in\mathbb{Z}} \bar{L}_n \bar{z}^{-n-2}. \tag{4.57}$$

The symmetries of the stress-energy tensor lead to a very important constraint for the correlators known as the *Ward identity*. This identity is most powerful in the

case of local conformal invariance in 2D, but the starting point is a global identity valid in any dimension which is given by

$$\sum_{i=1}^{n} \left\langle \phi_1(x_1) \dots \delta\phi_i(x_i) \dots \phi_n(x_n) \right\rangle = \frac{1}{2} \int d^d x \left\langle T^{\mu\nu}(x) X \right\rangle \partial_\mu \xi_\nu(x), \tag{4.58}$$

where $\delta\phi_i(x_i)$ corresponds to the infinitesimal variation of the i-th field with respect to an infinitesimal change of coordinates, and X denotes a product of local fields $\phi_i(x_i)$ such that

$$X = \phi_1(x_1)\phi_2(x_2) \dots \phi_n(x_n). \tag{4.59}$$

If we consider operators $T(z)$ and $\bar{T}(\bar{z})$ given by Eq. (4.56) and Eq. (4.57), respectively, to be primary and the infinitesimal transformation only locally conformal, we will get a much stronger local form of the Ward identity given by

$$\left\langle T(z) X \right\rangle = \sum_{i=1}^{n} \left(\frac{h_i}{(z - z_i)^2} + \frac{\partial_i}{z - z_i} \right) \left\langle X \right\rangle . \tag{4.60}$$

The right hand side of the equation above represents the expected short-distance singularities of $T(z)$ when approaching the primary fields and it can also be expressed by

$$T(z)\phi_j(z_j, \bar{z}_j) = \frac{h_j}{(z - z_j)^2} \phi_j(z_j, \bar{z}_j) + \frac{1}{z - z_j} \partial_{z_j} \phi_j(z_j, \bar{z}_j) + ... \tag{4.61}$$

This expression is called *operator product expansion* (OPE) and two local operators inserted at nearby points can be approximated by a string of operators at on of these points.

A new characterization for primary fields arises from here as those fields whose OPE with the stress-energy tensor takes the previous form. The OPE of T with itself takes the form

$$T(z_1)T(z_2) = \frac{c/2}{(z_1 - z_2)^4} + \frac{2T(z_2)}{(z_1 - z_2)^2} + \frac{\partial_{z_2} T(z_2)}{z_1 - z_2} + ... \tag{4.62}$$

As it is observed, the stress-energy tensor is not, in general, a primary field. The only way it can be primary is if the central charge vanishes.

Since T is not primary, it cannot transform following Eq. (4.36). According to CFT, the variation of the energy-momentum tensor T under a finite conformal transformation, $z \to w(z)$, in flat space-time is given by [21]

$$T(w) = \left(\frac{dw}{dz} \right)^{-2} \left[T(z) - \frac{c}{12} \{w; z\} \right], \tag{4.63}$$

where c is the central charge of the CFT and $\{w; z\}$ is the *Schwarzian derivative*,

$$\{w; z\} = \frac{d^3 w/dz^3}{dw/dz} - \frac{3}{2} \left(\frac{d^2 w/dz^2}{dw/dz} \right)^2 . \tag{4.64}$$

The Schwarzian derivative vanishes if and only if $w(z) = \dfrac{az+b}{cz+d}$, so $T(z)$ is a quasi-primary field.

The appearance of the central charge, also called *conformal anomaly*, is related to a "soft" breaking of conformal symmetry by the introduction of a macroscopic length scale into the system, for example by boundary conditions.

Let us consider a generic conformal field theory living on the whole complex plane and map this theory on a cylinder of circumference L with periodic boundary conditions (PBC) by

$$z \to w = \frac{L}{2\pi} \ln z. \tag{4.65}$$

Using the finite transformation law of Eq. (4.63) gives

$$T_{cyl}(w) = \left(\frac{2\pi}{L}\right)^2 \left[T_{pl}(z)z^2 - \frac{c}{24}\right], \tag{4.66}$$

where T_{pl} and T_{cyl} are used to distinguish the stress tensor before and after the transformation. On the plane, scale invariance sets all one-point functions to zero so

$$\big\langle T_{pl}(z) \big\rangle = 0. \tag{4.67}$$

The expectation value of Eq. (4.66) leads to a non-zero vacuum energy density on the cylinder,

$$\big\langle T_{cyl}(w) \big\rangle = -\frac{\pi^2 c}{6L^2}. \tag{4.68}$$

The central charge c is shown to be proportional to the *Casimir energy*: the change in the vacuum energy density due to the periodicity condition on the cylinder [21]. Casimir energy goes to zero as the macroscopic scale L goes to infinity.

Moreover, we can define the change in the free energy E as

$$\delta E = \int_{L_0}^{L} \big\langle T^{00} \big\rangle \, \delta L, \tag{4.69}$$

where $T^{00} = T_{zz} + T_{\bar{z}\bar{z}}$ is obtained from Eqs. (4.51), (4.52) and (4.53). In addition, following [21], one can write a renormalized stress-ernergy tensor given by

$$T = -2\pi T_{zz}, \; \bar{T} = -2\pi T_{\bar{z}\bar{z}}. \tag{4.70}$$

Therefore,

$$\big\langle T^{00} \big\rangle = -\frac{1}{2\pi}\Big(\langle T \rangle + \big\langle \bar{T} \big\rangle\Big) = -\frac{\langle T \rangle}{\pi}. \tag{4.71}$$

Plugging Eq. (4.68) in Eq. (4.71) and then integrating as indicated in Eq. (4.69), we obtain that the free energy (up to an additive constant which only implies a shift in the energy) is

$$E_{0,cyl} = -\frac{\pi c}{6L}. \tag{4.72}$$

The same procedure can be extended to compute the free energy with an open boundary conditions configuration. However, in this case we perform the following transformation

$$z \to w = \frac{L}{\pi} \ln z, \tag{4.73}$$

which maps the upper half plane to the strip. Indeed, Eq. (4.63) now takes the form

$$T_{strip}(w) = \left(\frac{\pi}{L}\right)^2 \left[T_{pl}(z)z^2 - \frac{c}{24}\right]. \tag{4.74}$$

Assuming again that the expectation value of the stress-energy tensor vanishes on the plane as stated in Eq. (4.67), we can write the expectation value of T on the strip

$$\left\langle T_{strip}(w)\right\rangle = -\frac{\pi^2 c}{24L^2}, \tag{4.75}$$

and

$$E_{0,strip} = -\frac{\pi c}{24L}. \tag{4.76}$$

Let us define $L = Na$, where N is the number of sites in the fermionic chains and a is the lattice spacing. Then, Eq. (4.76) can be rewritten as

$$E_{0,strip} = -\frac{\pi c\,(1/a)}{24N} = -\frac{\pi c v_F}{24N}, \tag{4.77}$$

where $v_F = 1/a$ is the Fermi velocity. Indeed, we can compare this expression to Eq. (3.35) with v_F given by Eq. (3.33) and, thus, conclude that $c = 1$ for free fermions. On the other hand, the Ising model (see Section 3.6) may be described by a CFT with $c = 1/2$.

We should be aware that Eqs. (4.72) and (4.76) are universal as long as Eq. (4.67) holds. They only depend on the central charge of the corresponding theory. However, further calculations are needed when the expectation value of the stress-energy tensor does not vanish on the plane. For instance, this is the case of anti-periodic boundary conditions (APBC) for fermionic fields.

4.6.1 Fermionic fields

A CFT of a complex fermion operator with central charge $c = 1$, *i.e.*, a Dirac fermion Ψ, can be understood in terms of its decomposition in the real Majorana components ψ_1, ψ_2, with $\psi_i = \psi_i^\dagger$, conformal weights $h = \bar{h} = 1/2$ and $c = 1/2$. Thus,

$$\Psi(z,\bar{z}) = \begin{pmatrix} \chi(z,\bar{z}) \\ \bar{\chi}(z,\bar{z}) \end{pmatrix} = \frac{1}{\sqrt{2}} \begin{pmatrix} \psi_1 + i\psi_2 \\ \bar{\psi}_1 + i\bar{\psi}_2 \end{pmatrix}, \tag{4.78}$$

in Euclidean space. Therefore, to study the quantization of Ψ it is sufficient to consider the quantization of its analytic and antianalytic Majorana components, $\psi(z)$ and $\psi(\bar{z})$ [22].

There exist two choices of boundary conditions on the plane

$$\psi(e^{2\pi i}z) = -\psi(z) \to \text{Ramond (R)},\ k \in \mathbb{Z} \to \text{APBC}, \tag{4.79}$$

$$\psi(e^{2\pi i}z) = \psi(z) \rightarrow \text{Neveu-Schwarz (NS)},\ k \in \mathbb{Z} + 1/2 \rightarrow \text{PBC}\ . \tag{4.80}$$

In addition, the plane can be mapped onto the cylinder by the transformation given in Eq. (4.65) and, thus,

$$\psi_{cyl}(w) \rightarrow \psi_{cyl}(z) = \left(\frac{dz}{dw}\right)^{1/2} \psi_{pl}(z) = \sqrt{\frac{2\pi z}{L}}\psi_{pl}(z). \tag{4.81}$$

We should be aware that the factor $\sqrt{z}$ exchanges the behavior of the boundary conditions from the cylinder to the plane.

$$\psi(x + 2\pi L) = \psi(x) \rightarrow \text{Ramond (R)},\ k \in \mathbb{Z} \rightarrow \text{PBC}, \tag{4.82}$$

$$\psi(x + 2\pi L) = -\psi(x) \rightarrow \text{Neveu-Schwarz (NS)},\ k \in \mathbb{Z} + 1/2 \rightarrow \text{APBC}. \tag{4.83}$$

Since we are working on a cylinder of circumference L, we may write the mode expansion of the fermion field in terms of creation and annihilation operators with our choice of normalization as,

$$\psi(x) = \sqrt{\frac{2\pi}{L}} \sum_k b_k e^{2\pi i k x/L}, \tag{4.84}$$

where x is the space coordinate along the cylinder and the operators b_k satisfy the canonical anticommutation relations $\{b_k, b_q\} = \delta_{k+q,0}$.

PBC on the plane yield a zero expectation value of T,

$$\left\langle \psi(z)\psi(w) \right\rangle = \frac{1}{z-w} \rightarrow \left\langle T(z)_{pl} \right\rangle = 0. \tag{4.85}$$

On the other hand, APBC on the plane lead to a non-zero expectation value of T,

$$\left\langle \psi(z)\psi(w) \right\rangle = \frac{1}{2}\frac{\sqrt{z/w} + \sqrt{w/z}}{z-w} \rightarrow \left\langle T(z)_{pl} \right\rangle = \frac{1}{16z^2}. \tag{4.86}$$

Plugging the previous results in Eq. (4.66),

$$\left\langle T_{cyl}(w) \right\rangle = \begin{cases} -\dfrac{c}{24}\left(\dfrac{2\pi}{L}\right)^2 = -\dfrac{\pi^2 c}{6L^2} \rightarrow \text{NS}, \\ \\ \dfrac{c}{48}\left(\dfrac{2\pi}{L}\right)^2 = \dfrac{\pi^2 c}{12L^2} \rightarrow \text{R}. \end{cases} \tag{4.87}$$

Taking into account that the Majorana fermions have $c = 1/2$, then

$$\left\langle T_{cyl}(w) \right\rangle = \begin{cases} -\dfrac{1}{48}\left(\dfrac{2\pi}{L}\right)^2 \rightarrow \text{NS}, \\ \\ \dfrac{1}{24}\left(\dfrac{2\pi}{L}\right)^2 \rightarrow \text{R}. \end{cases} \tag{4.88}$$

4.7 Twist fields and entanglement entropy

Let us consider an infinite fermionic chain and a subsystem of it, $A = [u, v]$, with length $\ell = |u - v|$ where u and v are the endpoints of the interval. The subsystem can be described in terms of a reduced density matrix ρ_A and CFT can provide the universal behavior of the Rényi entropies $S^{(n)}(\rho_A)$ [86], as we will show in this section.

The starting point is to write the density matrix of a thermal state, ρ, as an Euclidean path integral on the imaginary time interval $(0, \beta)$ under a Hamiltonian H as

$$\rho = \frac{e^{-\beta H}}{Z}, \tag{4.89}$$

where β is the inverse temperature and $Z = \mathrm{Tr} e^{-\beta H}$ corresponds to the partition function that ensures the correct normalization. It represents a cylinder of circumference β obtained by sewing together the edges along $\tau = 0$ and $\tau = \beta$. Thus, the reduced density matrix ρ_A corresponds to the same cylinder but with an open cut in A.

The next step is to consider n copies of this cylinder sewed together along the cuts, as seen in Fig. 4.3, *i.e.*, $\mathrm{Tr}\rho_A$. These copies are also called replicas and are indexed by $k = 1, \ldots, k = n$. From this, we can define a path integral $Z_n(A)$ over an n-sheeted Riemannian surface $\mathcal{R}_n$. Then,

$$\mathrm{Tr}\rho_A^n = \frac{Z_n(A)}{Z_1(A)}, \tag{4.90}$$

and the Rényi entropies are given by

$$S^{(n)}(A) = \frac{1}{1-n} \log\big(Z_n(A)\big) + \frac{n}{1+n} \log\big(Z_1(A)\big)\,. \tag{4.91}$$

It can be shown that the partition function $Z_n(A)$ is related to the two-point correlation function of some fields that live at the cuts of A

$$Z_n(A) \propto \big\langle \mathcal{T}_n(u,0)\bar{\mathcal{T}}_n(v,0)\big\rangle\,. \tag{4.92}$$

These are the so-called *twist fields* and have been shown to behave as primary operators (see Eq. (4.36)) with dimension

$$\Delta_n = \bar{\Delta}_n = \frac{c}{24}\left(n - \frac{1}{n}\right). \tag{4.93}$$

Furthermore, the two-point correlator of primary fields is completely fixed by conformal invariance, thus

$$\big\langle \mathcal{T}_n(u,0)\bar{\mathcal{T}}(v,0)\big\rangle = \left(\frac{|u-v|}{a}\right)^{-2(\Delta_n+\bar{\Delta}_n)} = \left(\frac{\ell}{a}\right)^{-c\left(n-1/n\right)/6}, \tag{4.94}$$

where a is the lattice spacing.

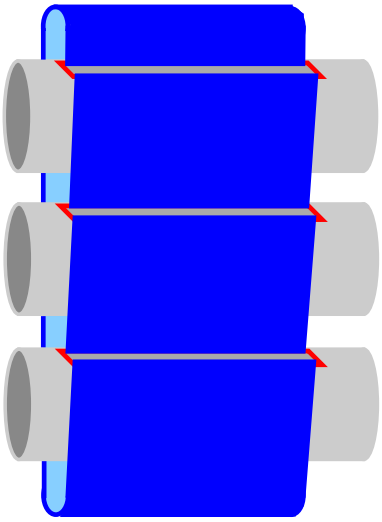

Figure 4.3: A representation of the Riemann surface formed by three copies sewed together by the open cuts.

Then, the Rényi entropies which are determined by $S_n(A) = \frac{1}{1-n}\mathrm{Tr}\rho^n$ can be written as

$$S^{(n)}(A) = S(\ell) = \frac{1}{1-n}\log\left(\frac{\ell}{a}\right)^{-c\left(n-1/n\right)/6} + c'_n = \frac{c}{6}\left(1+\frac{1}{n}\right)\log\left(\frac{\ell}{a}\right) + c'_n, \quad (4.95)$$

where c'_n is a non-universal constant.

From the previous result, one can also compute the entanglement entropy [86]

$$S(\ell) = \frac{c}{3}\log\left(\frac{\ell}{a}\right) + c'_1. \quad (4.96)$$

Let us now consider a system of size N with PBC, and a subsystem A of length ℓ. Then, the Rényi entropies are given by

$$S^{(n)}(\ell) = \frac{c}{6}\left(1+\frac{1}{n}\right)\log\left(\frac{N}{\pi a}\sin\left(\frac{\pi\ell}{N}\right)\right) + c'_n, \quad (4.97)$$

where c'_n is also a non-universal constant and the quantity inside the logarithm is the chord length, which tends to ℓ when $N \gg 1$.

On the other side, for an open chain we consider a subsystem $A = [0, \ell]$ of length ℓ. In this case, one of the boundaries of the interval under consideration corresponds to the physical boundary of the system. As a consequence, it was shown that the Rényi entropies can be expressed as

$$S^{(n)}(\ell) = \frac{c}{12}\left(1+\frac{1}{n}\right)\log\left(\frac{N}{\pi a}\sin\left(\frac{\pi\ell}{N}\right)\right) + \tilde{c}'_n, \quad (4.98)$$

where $\tilde{c}'_n$ is a non-universal constant. Therefore, the entanglement entropy for an open chain is given by [69]

$$S(\ell) = \frac{c}{6} \log \left(\frac{N}{\pi a} \sin \left(\frac{\pi \ell}{N} \right) \right) + \tilde{c}'_1. \tag{4.99}$$

Summary

This summary provides a brief overview of the most important points from Part I, and intends to facilitate the reading of the following chapters.

- Given a quantum system $\mathcal{S} = A \cup B$ with finite dimensional Hilbert spaces $\mathcal{H}_A$ and $\mathcal{H}_B$, respectively, a pure state is given by the vector $|\psi\rangle \in \mathcal{H}_{AB}$. If $|\psi\rangle = |\phi\rangle \otimes |\varphi\rangle$ with $|\phi\rangle \in \mathcal{H}_A$ and $|\varphi\rangle \in \mathcal{H}_B$, it is said to be factorized. Otherwise, $|\psi\rangle$ is entangled. Mixed states are statistical ensembles of pure states and may be described in terms of density matrices.

- Given a many-body system $\mathcal{S} = A \cup B$ in a pure state $\rho = |\psi\rangle\langle\psi|$, the state that describes A is given by the reduced density matrix ρ_A,

$$\rho_A = \mathrm{Tr}_B \rho. \tag{4.100}$$

  The spectrum of ρ_A codifies the entanglement properties of A. Moreover, quantum correlations between A and B, *i.e.*, the entanglement, can be measured by the von Neumann entanglement entropy (EE),

$$S(A) = -\mathrm{Tr}\left(\rho_A \log \rho_A\right). \tag{4.101}$$

  The EE, $S(A)$, measures the amount of information associated to the fact that the state ρ_A is not pure.

- Quantum many-body systems are difficult to describe due to the exponential growth of the underlying Hilbert space, which hosts all possible quantum states, with the number of particles in the system. Nevertheless, the EE for ground states (GS) of gapped local Hamiltonians obey an area law and, thus, can be distinguished from randomly chosen quantum states in $\mathcal{H}$. However, there also exist GS that violate the area law such as GS of some fermionic chains with position-dependent, *i.e* inhomogeneous, hopping amplitudes.

- Free fermionic chains have been shown to be of great relevance since they can be described by a Hamiltonian H, which can be solved in terms of single-body modes and single-body energies, added to the fact that some spin models can be mapped to free fermion systems. For that aim, in the homogeneous case,

it is possible to diagonalize the corresponding hopping matrix in order to find the eigenstates and the spectrum of H, which is given by

$$\varepsilon_k = -2\cos k, \tag{4.102}$$

where k stands for all the allowed modes and depends on the boundary configurations. From Eq. (4.102), it is feasible to compute the energy of the GS

$$E = \sum_{k=1}^{N/2} \varepsilon_k. \tag{4.103}$$

Since the corresponding Hamiltonian presents particle-hole symmetry, the GS is given by filling up all the modes with negative energy, *i.e.*, half-filling: $N/2$. The result shows that the energy contains a non-universal contribution proportional to the system size N, plus finite-size corrections of order $O(1/N)$.

- Finite-size corrections, of order $O(1/N)$, to the energy are fixed by a 2D conformal field theory (CFT) when the system is subject to conformal invariance and they are shown to be proportional to the central charge c. The central charge arises naturally when the central extension of the algebra of conformal transformations, *i.e.*, those which preserve angles, is performed.

- It has been proved that the EE entropy for a block of size ℓ of an open chain of size N can be written as

$$S(\ell) = \frac{c}{6}\log\left(\frac{N}{\pi a}\sin\left(\frac{\pi\ell}{N}\right)\right) + S_{\text{non-univ}}, \tag{4.104}$$

where a is the lattice spacing parameter and $S_{\text{non-univ}}$ is a non-universal contribution.

Part II

Novel Results

Chapter 5

Casimir forces on deformed fermionic chains

This chapter is based on the following article:

- B. Mula, S.N. Santalla, J. Rodríguez-Laguna, *Casimir forces on deformed fermionic chains*, Phys. Rev. Research **3**, 013062 (2021).

We characterize the Casimir forces for the Dirac vacuum on free-fermionic chains with smoothly varying hopping amplitudes, which correspond to (1+1)D curved space-times with a static metric in the continuum limit. The first-order energy potential for an obstacle on that lattice corresponds to the Newtonian potential associated to the metric, while the finite-size corrections are described by a curved extension of the conformal field theory predictions, including a suitable boundary term. We show that, for weak deformations of the Minkowski metric, Casimir forces measured by a local observer at the boundary are universal. We provide numerical evidence for our results on a variety of (1+1)D deformations: Minkowski, Rindler, anti-de Sitter (the so-called rainbow system) and sinusoidal metrics. Moreover, we show that interactions do not preclude our conclusions, exemplifying with the deformed Heisenberg chain.

5.1 Introduction and context

As we already discussed in Section 1.1, the quantum vacuum on a static space-time is nothing but the ground state (GS) of a certain Hamiltonian. Therefore, it is subject to quantum fluctuations which help minimize its energy. Yet, these fluctuations are clamped near the boundaries, giving rise to the celebrated *Casimir effect* [8], see [87] for experimental confirmations. Its relevance extends away from the quantum realm, with applications to thermal fluctuations in fluids [88]. Its initial description required two infinite parallel plates, giving rise to an attractive force between them as was also explained in Section 1.1. In fact, this attraction was rigorously proved for identical plates by Kenneth and Klich [9], yet the force can become repulsive or even cancel out when the boundary conditions do not match [89]. The special features of fermionic 1D systems have also been considered [90, 91].

For fields subject to conformal invariance, the Casimir force is associated to the *conformal anomaly*, measured by the central charge in 2D conformal field theory (CFT), c, as it was seen in Chapter 4. For further details see [19–22]. In Section **??**, we showed that the expression for the energy contains a non-universal contribution proportional to the system size N, plus finite-size corrections of order $O(1/N)$. These finite-size corrections depend on the boundary conditions, as shown in Eqs. (3.35), (3.36) and (3.37), which are fixed by conformal invariance (see Section 4.6). Moreover, conformal invariance is strong enough to yield an analytical expression for the Casimir forces in presence of arbitrarily shaped boundaries [23].

The peculiarities of Casimir forces in curved space-times have been considered by several authors [24]. The problem is already difficult for static space-times and weak gravitational fields [25–28]. The Casimir force takes the same form on weak static gravitational fields at first-order, when coordinate differences are substituted by actual distances, although with non-trivial second-order corrections. Interestingly, the Casimir effect has been put forward as a possible explanation of the cosmological constant, making use of Lifshitz theory [92, 93].

Even if our technological abilities do not allow us to access direct measurements of the Casimir effect in curved space-times, we are aware of possible strategies to develop quantum simulators using current technologies, such as ultracold atoms in optical lattices [7]. Concretely, it has been shown that the Dirac vacuum on certain static space-times can be characterized in such a quantum simulator [5], and an application has been devised to measure the Unruh radiation (see Section 1.3), including its non-trivial dimensional dependence [6, 94, 95]. The key insight is the use of *curved optical lattices*, in which fermionic atoms are distributed on a flat optical lattice with inhomogeneous hopping amplitudes, thus simulating a position-dependence index of refraction or, in other terms, an *optical metric*.

Dirac vacuum in such curved optical lattices present quite novel properties. When the background metric is negatively curved, i.e.: (1+1)D anti-de Sitter (AdS), the entanglement entropy (EE) may violate maximally the area law [96] (see Section 1.2.6), forming the so-called *rainbow state* [97–99]. Interestingly, the EE of blocks within the GS of a (1+1)D system with conformal invariance is fixed by CFT [13, 69, 86, 100, 101]. Such conformal arguments can be extended to a statically deformed (1+1)D system, and the EE of the rainbow system was successfully predicted [102], along with other interesting magnitudes, such as the entanglement spectrum, entanglement contour and entanglement Hamiltonian [103, 104].

The aim of this chapter is to extend the aforementioned (1+1)D CFT predictions on curved backgrounds to characterize the Casimir force for the fermionic vacuum on curved optical lattices. This article is organized as follows. In Section 5.2 we describe our physical system and summarize the CFT techniques employed to evaluate the EE on curved backgrounds, providing some examples. Section 5.3 characterizes the Casimir forces on curved optical lattices, using the same example backgrounds, emphasizing the role of universality in the finite-size corrections. In Section 5.4 we extend our results to the inhomogeneous Heisenberg chain. The article closes with a series of conclusions and proposals for further work.

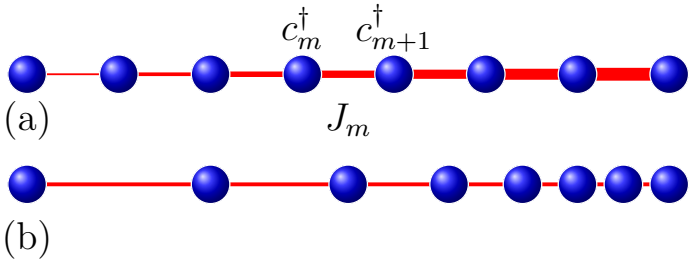

Figure 5.1: (a) Illustration of an inhomogeneous chain with $N = 8$ sites. (b) Corresponding positions after the deformed coordinates $\tilde{x}$.

5.2 Fermions on curved optical lattices

Let us consider an open fermionic chain with (even) N sites, whose Hilbert space is spanned by creation operators $c_m^\dagger$, $m \in \{1, \cdots, N\}$ following standard anticommutation relations. We can define an inhomogeneous hopping Hamiltonian as in Eq. (3.1),

$$H(\mathbf{J})_N = -\sum_{m=1}^{N-1} J_m c_m^\dagger c_{m+1} + \text{h.c.}, \tag{5.1}$$

where $\mathbf{J} = \{J_m\}_{m=1}^{N-1}$ are the *hopping amplitudes*, $J_m \in \mathbb{R}^+$ referring to the link between sites m and $m+1$ as in Fig. 5.1 (a). In order to obtain some physical intuition, let us remember that the set of $\{J_m\}$ constitutes a position-dependent Fermi velocity, i.e.: a signal takes a time of order J_m^{-1} to travel between sites m and $m+1$. If the $\{J_m\}$ are *smooth enough*, we can assume $J_m = J(x_m)$ for a certain smooth function $J(x)$, with $x_m = m\Delta x$. Unless otherwise specified, we will use $\Delta x = 1$.

It can be proved that Eq. (5.1) is a discretized version of the Hamiltonian for a Dirac fermion on a curved (1+1)D space-time with a static metric of the form [5, 99, 102]

$$ds^2 = -J^2(x)dt^2 + dx^2, \tag{5.2}$$

i.e. a space-time metric with a position dependent speed of light or, equivalently, a modulated *index of refraction*. Defining $\tilde{x}(x)$ such that

$$d\tilde{x} = \frac{dx}{J(x)}, \tag{5.3}$$

we have

$$ds^2 = J^2(x)(-dt^2 + d\tilde{x}^2), \tag{5.4}$$

which is conformally equivalent to the Minkowski metric. This deformation is illustrated in Fig. 5.1 (b): sites get closer when the J_m associated to their link is large, giving rise to an homogeneous effective hopping amplitude.

Conformal equivalence between metrics (5.4) and the Minkowski metric suggests that conformal field theory (CFT) techniques might describe the universal properties of low-energy eigenstates of Hamiltonian (5.1). Indeed, we will show that this is the case, once those universal properties have been ascertained.

Some interesting metrics fall into this category. If $J(x) = J_0$ is a constant, we recover Minkowski space-time on a finite spatial interval. The Rindler metric, which is the space-time structure perceived by an observer moving with constant acceleration a in a Minkowski metric, is described by

$$J(x) = J_0 + ax. \tag{5.5}$$

Notice that it presents an *horizon* at $x_h = -J_0/a$, where the local speed of light vanishes. Information can not cross this point, thus separating space-time into two *Rindler wedges* [105]. We will consider some other choices for the hopping amplitudes, such as the *sine metric*,

$$J(x) = J_0 + A\sin(kx), \tag{5.6}$$

or a rainbow metric given by

$$J(x) = J_0 \exp\left(-h\left|x - \frac{N}{2}\right|\right), \tag{5.7}$$

for $h \geq 0$, with $h = 0$ corresponding to the Minkowski case. This metric has constant negative curvature except at the center, $x = N/2$, thus resembling an anti-de Sitter (AdS) space, and has been considered recently because its vacuum presents volumetric entanglement [97–99, 102–104]. Unless otherwise stated, we will always assume $J_0 = 1$.

5.2.1 Free fermions on the lattice

The exact diagonalization of Hamiltonian (5.1) is a straightforward procedure which only involves the solution of the associated single-body problem as we showed in Section 3.1. Let us define the hopping matrix, $T_{ij} = T_{ji} = -J_i\delta_{i,j+1}$, such that

$$H(\mathbf{J})_N = \sum_{i,j} T_{ij} c_i^\dagger c_j, \tag{5.8}$$

then we can diagonlize the hopping matrix, $T_{ij} = \sum_k U_{i,k}\epsilon_k \bar{U}_{j,k}$, where ϵ_k are the single-body energies and the columns of $U_{i,k}$ represent the single-body modes. The GS of Hamiltonian (5.1) can be written as $|\Psi\rangle = \prod_{k=1}^{N/2} b_k^\dagger |0\rangle$, where $|0\rangle$ is the Fock vacuum and $b_k^\dagger = \sum_i U_{i,k} c_i^\dagger$.

As we already mentioned in Section 3.1, the system presents particle-hole symmetry, $\epsilon_k = -\epsilon_{N+1-k}$, with $U_{i,k} = (-1)^i U_{i,N+1-k}$. At half-filling the local density is always homogeneous, $\left\langle c_n^\dagger c_n \right\rangle = 1/2$ for all n, independently of the metric. For the Minkowski metric,

$$\left\langle c_n^\dagger c_{n+1} \right\rangle = \sum_{k=1}^{N/2} \bar{U}_{nk} U_{n+1,k} \approx \frac{c_0}{2} \equiv \frac{1}{\pi}, \tag{5.9}$$

plus a correction term presenting parity oscillations, related to the fact that the Fermi momentum is $k_F = \pi/2$.

5.2.2 CFT and entanglement for curved lattice fermions

Let us provide a cursory summary of the application of CFT techniques to the characterization of the entanglement structure of the fermionic vacuum on curved optical lattices.

The von Neumann entanglement entropy of a block A of a pure state $|\Psi\rangle$, discussed in Section 1.2.3, is defined as

$$S_A = -\mathrm{Tr}\left[\rho_A \log \rho_A\right], \tag{5.10}$$

where $\rho_A = \mathrm{Tr}_{\bar{A}} |\Psi\rangle \langle\Psi|$ is the reduced density matrix for block A, and $\bar{A}$ is its complement. In the case of Gaussian states, which follow Wick's theorem, this magnitude can be determined from the two-point correlation function with low computational effort [106]. Following [69, 101], the EE of a lateral block $A = \{1, \cdots, \ell\}$ of the GS of a conformal system with central charge c on a chain with N sites can be written as in Eq. (4.99)

$$S(\ell) = \frac{c}{6} \log\left(\frac{N}{\pi \Delta x} \sin\left(\frac{\pi \ell}{N}\right)\right) + S_{\text{non-univ}}. \tag{5.11}$$

where $c = 1$ for free fermions (see Section 4.6), Δx is the UV cutoff and $S_{\text{non-univ}}$ is a non-universal contribution containing a constant term and parity oscillations which has been explicitly computed for the free-fermionic case [107, 108].

Expression (5.11) has been successfully extended to evaluate entanglement entropies on the GS of Hamiltonian (5.1) [102, 103]. When Dirac fermions are inserted in a smooth static optical metric of the type (5.2), the EE deforms appropriately, i.e. the block lengths must be transformed via Eq. (5.3),

$$\ell \to \tilde{\ell} = \tilde{x}(\ell \Delta x) = \int_{x_0}^{\ell \Delta x} \frac{dx}{J(x)} \approx \sum_{p=1}^{\ell-1} \frac{\Delta x}{J_p}, \tag{5.12}$$

while $\tilde{N} = \tilde{x}(N \Delta x)$. We must also take into account the transformation of the UV cutoff,

$$\Delta x \;\to\; \Delta \tilde{x}(\ell) = \frac{\Delta x}{J(\ell)}. \tag{5.13}$$

Thus, we obtain

$$S(\ell) = \frac{c}{6} \log\left(\frac{\tilde{N}}{\pi \Delta \tilde{x}} \sin\left(\frac{\pi \tilde{\ell}}{\tilde{N}}\right)\right) + S_{\text{non-univ}}. \tag{5.14}$$

Concretely, in [102, 103] the EE for lateral blocks within the GS of the rainbow Hamiltonian (5.1) using (5.7) was obtained using

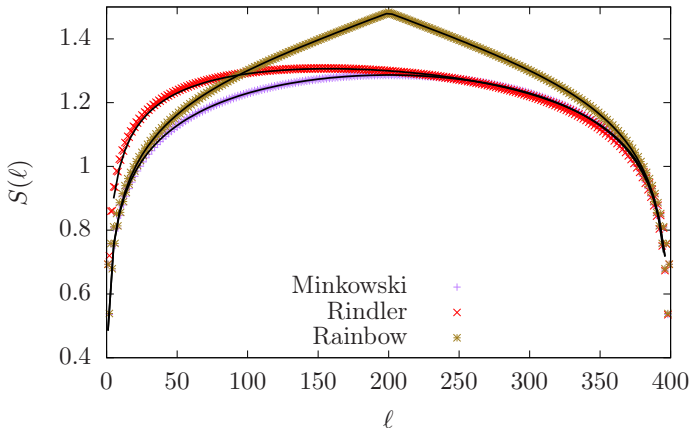

Figure 5.2: Entanglement entropy of the GS of free fermionic systems on a optical chain with $N = 400$ for three different metrics: Minkowski, rainbow (Eq. (5.7) with $h = 0.01$) and Rindler (Eq. (5.5) with $a = 2$), using the procedures of [106] The continuous lines are the CFT prediction, given by Eq. (5.14), with a non-universal constant term added.

$$\Delta\tilde{x} = e^{-h|N/2-\ell|}\Delta x, \tag{5.15}$$

$$h\tilde{N} = 2(e^{hN/2} - 1)\Delta x, \tag{5.16}$$

$$h\tilde{\ell} = \begin{cases} \left(e^{hN/2} - e^{h(N/2-\ell)}\right)\Delta x, & \text{if } \ell \leq N/2, \\ \left(e^{hN/2} + e^{h(\ell-N/2)}\right)\Delta x, & \text{if } \ell \geq N/2. \end{cases} \tag{5.17}$$

In the limit $h\ell \gg 1$, the EE of a block of size $\ell \leq N/2$ becomes

$$S(\ell) \approx \frac{ch}{6}\ell + S_{\text{non-univ}}, \tag{5.18}$$

i.e. it yields a volume law for entanglement [103], violating maximally the so-called area law of entanglement [96]. We can also apply Eq. (5.14) to the case of the Rindler metric, where we find

$$S(\ell) = \frac{1}{6}\log\left(\frac{\ell\log N}{\pi\Delta x}\sin\left(\frac{\pi\log(N/\ell)}{\log N}\right)\right) + S_{\text{non-univ}}. \tag{5.19}$$

The validity of these expressions can be checked in Fig. 5.2, where we have plotted the entropy $S(\ell)$ as a function of the block size ℓ for three systems using $N = 400$: the Minkowski case, Eq. (5.11), the rainbow case with $h = 0.01$, Eq. (5.14) with (5.17), and the Rindler case with $a = 2$, via Eq. (5.19). Indeed, the non-universal terms are present, which also carry parity oscillations, but they are a small correction to the entanglement entropy as predicted by the CFT.

The accuracy of the CFT prediction allows us to conjecture that free Dirac fermions on curved optical lattices can be characterized by a suitable deformation

of a conformal field theory, expecting that the non-universal terms will be small enough. We will put this conjecture to the test in the next section.

5.3 Casimir forces on curved optical lattices

Let us characterize the Casimir forces on curved optical lattices in successive approximations. First of all, we will show that the GS energy of Hamiltonian (5.1) is proportional to the sum of the hoppings in first-order perturbation theory. This will lead us to show that the force felt by a classical obstacle immerse in that state will be similar to the Newtonian gravitational force in the corresponding metric. Then, we will reach the main result of this work: the finite-size corrections to the Casimir energy are universal, and the corresponding expressions are a deformed variant of the general CFT form.

5.3.1 Potential energy and correlator rigidity

Let us consider a free fermionic chain of N sites on a deformed metric, following Eq. (5.1). The exact vacuum energy can be written as

$$E_N = -2 \sum_{p=1}^{N-1} J_p \, \mathrm{Re}\langle c_p^\dagger c_{p+1} \rangle. \tag{5.20}$$

We can estimate this expression via perturbation theory, if we assume that $J_p = J_0 + \delta J_p$ and make use of Eq. (5.9). The result at first-order is

$$E_0 \approx -c_0 S_N, \qquad \text{where } S_N \equiv \sum_{p=1}^{N-1} J_p. \tag{5.21}$$

The validity of this approximation can be checked in panel (a) of Fig. 5.3, for four different metrics: Minkowski, Rindler, Sine and Rainbow. The accuracy of our conjecture suggests that the local correlators in the deformed vacuum are still homogeneous. In fact, we will make the further claim that the *local correlators are rigid*, i.e. $\langle c_p^\dagger c_{p+1} \rangle \approx c_0/2$ for a weakly deformed metric. This claim has been checked independently in the panel (b) of Fig. 5.3, where the local correlators are shown for different deformations. Indeed, their average values are still very close to $c_0 = 2/\pi$, and the only substantial deviation is provided by the expected parity oscillations which are well known in the Minkowski case.

A heuristic argument to understand correlator rigidity may be as follows. For fermionic fields in Minkowski space-time we have $\langle \psi(x)\psi(x+\Delta x) \rangle \sim \Delta x^{-1}$. After a deformation, $\Delta x \to \Delta \tilde{x} = \Delta x / J(x)$. Yet, the fields transform also as $\tilde{\psi}(x) = J^{1/2}(x)\psi(x)$, and the local correlator remains invariant.

Let us consider a classical particle standing between sites p and $p+1$, which acts like an obstacle inhibiting the local hopping by a factor $\gamma < 1$, $J_p \to \gamma J_p$. Let us now evaluate the excess energy of the deformed GS as a function of p, $V(p) = E_0(p) - E_0$, which acts as a *potential energy function* for the obstacle. The results are shown in Fig. 5.4, where we plot $V(p)$ for the same four different situations, using $N = 100$

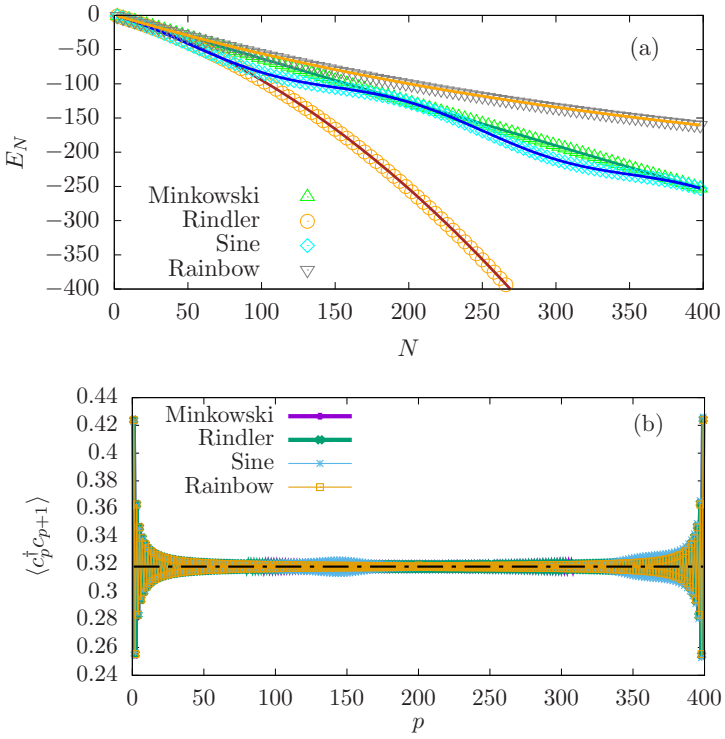

Figure 5.3: (a) Check of the bulk prediction for the energy, $E_0 \approx -c_0 S_N$ for four metrics: Minkowski, Rindler ($a = 0.01$), Sine ($A = 0.5$, $k = \pi/100$) and Rainbow ($h = 5 \cdot 10^{-3}$. Numerical values are given in dots, while the theoretical prediction is provided in the full line. (b) Illustration of the correlator rigidity. Local correlators, $\langle c_p^\dagger c_{p+1} \rangle$ as a function of the position p for the same four metrics.

and both $\gamma = 0.01$ and $\gamma = 0.75$. As γ approaches 1 the trivial case is recovered, i.e. the potential energy is equivalent to E_0.

The first salient feature of Fig. 5.4 is that the potential energy $V(p)$ resembles the hopping function $J(x)$, with some strong parity oscillations. We are thus led to conjecture that a classical particle moving on a static metric in (1+1)D would be dragged by a force similar to the gravitational pull. Making use of Hellmann-Feynman's theorem, we see that

$$V(p) \approx -2J_p \mathrm{Re} \left\langle c_p^\dagger c_{p+1} \right\rangle \approx -2J_p c_0. \tag{5.22}$$

5.3.2 Finite-size corrections

The GS of a finite open chain of N sites in Minkowski space-time is given by Cardy's expression [19–22] (see also Section 3.5, Eq. 3.35),

$$E_N = -c_0(N-1) - c_B - \frac{c\pi v_F}{24N} + O(N^{-2}), \tag{5.23}$$

where c is the associated central charge, v_F is the Fermi velocity and c_0 and c_B are non-universal constants, which correspond to the bulk energy per link and the

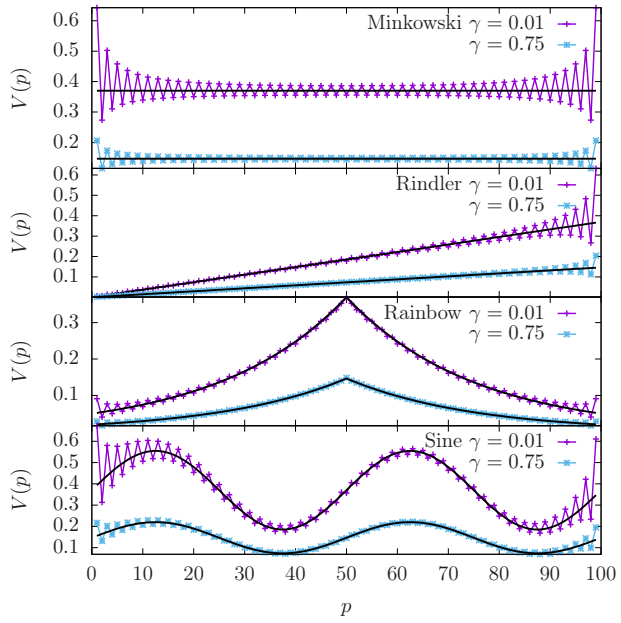

Figure 5.4: Potential energy $V(p)$ obtained by inhibiting the p-th hopping by a factor γ, $J_p \to \gamma J_p$, for four different metrics: Minkowski, Rindler ($a = 0.01$), rainbow ($h = 0.04$) and sinusoidal ($A = 0.5$ and $k = 2\pi/50$), always using $N = 100$ and two values of $\gamma = 0.01$ and 0.75. In continuous line, we plot $J(x)$ multiplied by a factor which only depends on γ.

boundary energy. Notice that the last term is *universal*, since its form is fixed by conformal invariance [19–22] (see Section 4.6), but the bulk and boundary terms are not. The GS energy of Hamiltonian (5.1) with $J_n = 1$ follows Eq. (5.23) very accurately, using $c = 1$ for Dirac fermions, $v_F = 2$, $c_0 = 2/\pi$ and $c_B = 4/\pi - 1$.

Our main target is to generalize expression (5.23) to the case of deformed backgrounds. Indeed, we may follow the guidelines of Section 5.2.2 and attempt a substitution $x \to \tilde{x}$, such that $d\tilde{x}/dx = J(x)^{-1}$, but *it will not work* for the bulk and boundary terms. In that case, the bulk energy would become proportional to $\tilde{N}$. Thus, in the rainbow case we should obtain an energy term which grows exponentially with N for any fixed $h > 0$, which is not found. Indeed, as we will show, that transformation is only relevant for the universal term.

Let us propose an extension of Eq. (5.23) to curved backgrounds based on physical arguments, term by term.

- The term $c_0(N-1)$ stands for the bulk energy, which should be replaced by $c_0 S_N$, i.e. the sum of the $N-1$ first hopping amplitudes, multiplied by the local correlator term.
- The boundary term, c_B should be proportional to the terminal hoppings, thus generalizing to $c_B(J_1 + J_{N-1})/2$.
- The conformal correction is universal. Thus, it must be naturally deformed, changing N^{-1} into $\tilde{N}^{-1}$, where $\tilde{N}$ is the effective length in deformed coordinates, given by $\tilde{N} = \sum_{i=1}^{N-1} J_i^{-1}$ (we let $\Delta x = 1$).

Thus, we claim that the correct generalization of Eq. (5.23) to curved optical lattices is given by

$$E_N = -c_0 S_N - \frac{c_B}{2}\left(J_1 + J_{N-1}\right) - \frac{c\pi v_F}{24\tilde{N}} + O(N^{-2}). \tag{5.24}$$

This expression can be more rigorously justified through a careful analysis of the conformal field theory origin of Eq. (5.23), and this is discussed in Appendix D.1.

The inverse of the deformed length $\tilde{N}^{-1}$ can be given an interesting physical interpretation. Indeed, it is easy to recognize $(N-1)\tilde{N}^{-1}$ as the *harmonic average* of the local speeds of light, which can be understood as an *effective* Fermi velocity, $\bar{v}_F$. Yet, for small deformations, the harmonic average is similar (and lower than) the arithmetical average. Thus, for the sake of simplicity, we approximate $\bar{v}_F \approx 2S_N/(N-1)$. Thus, we may provide an approximate version of Eq. (5.24) for a weakly deformed (1+1)D lattice,

$$E_N \approx -c_0 S_N - \frac{c_B}{2}(J_1 + J_{N-1}) - \frac{\pi S_N}{12N^2}. \tag{5.25}$$

5.3.3 Universality of Casimir forces in curved backgrounds

Numerical checks of Eqs. (5.24) or (5.25) must be subtle, because the finite-size correction is typically much smaller than the bulk energy term. Let us consider an alternative observable: the Casimir force measured by a local observer located at the boundary. Since energy is associated to a frequency, local energy measurements at site x will be given by

$$E(x) = \frac{E_N}{g_{00}^{1/2}(x)} = \frac{E_N}{J_N}. \tag{5.26}$$

Such an observer will measure a force given by the covariant spatial derivative of $F = -D_x E(x)$, taking the lattice spacing $\Delta x = 1$ (see Appendix D.2 for details) and changing the sign for convenience, we define

$$F_N \equiv \frac{E_N - E_{N-2}}{J_{N-1} + J_{N-2}}. \tag{5.27}$$

Assuming smoothly varying hopping amplitudes we obtain

$$F_N \equiv -c_0 - \frac{c_B}{2}\left(\frac{J_N'}{J_N}\right) - \frac{\pi}{12N^2} + \frac{\pi S_N}{6J_N N^3}. \tag{5.28}$$

Let us consider the terms individually. The first, $c_0 = 2/\pi$, is simply associated to the bulk energy. The second is a *boundary force*, which is absent from the homogeneous case, and will take a leading role in some cases. For very weak deformations, $J_N \approx J_0 + \delta J_N$ is a small deformation, we can assume that $S_N \approx N J_N$, and we obtain

$$F_N \approx -c_0 - \frac{c_B}{2}\left(\frac{J_N'}{J_N}\right) + \frac{\pi}{12N^2}. \tag{5.29}$$

Thus, we are led to the following claim: *Casimir forces on a weakly curved background are metric-independent when measured by a local observer at the boundary.*

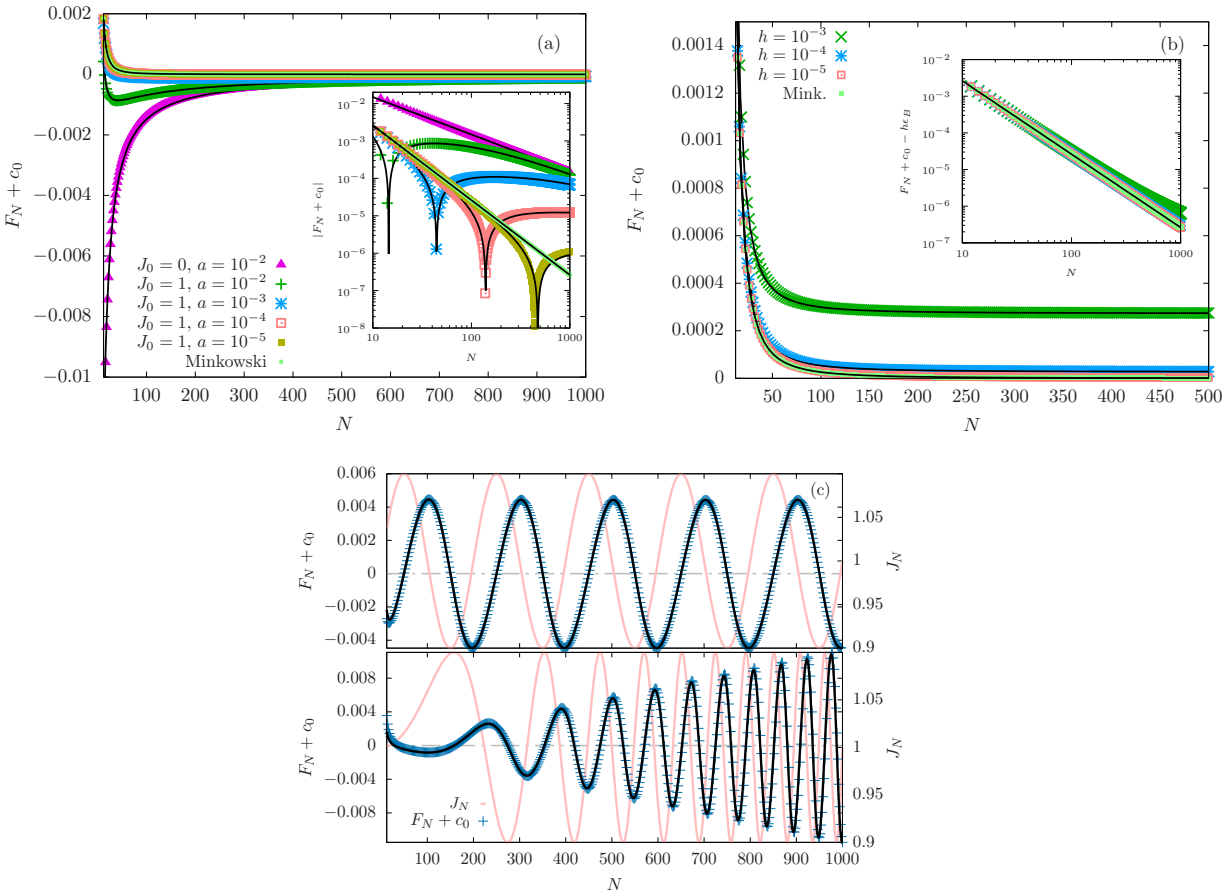

Figure 5.5: Casimir forces, $F_N + c_0$, for different metrics. (a) Rindler metric. Inset, log-log plot of $|F_N + c_0|$ as a function of N, in log-log scale. Notice most small systems are dominated by the CFT correction, while for larger sizes the boundary term N^{-1} dominates. (b) Rainbow metric, we observe that $F + c_0$ tends to $\epsilon_B h$. Inset: log-log plot of $F_N + c_0 - \epsilon_B h$. (c) Sinusoidal metric (top) and modulated frequency metric (bottom).

Indeed, consider an observer on a classical obstacle located at site p. It will be subject both to a left and a right Casimir forces. The bulk and boundary parts will cancel out, and only the universal finite-size correction will survive, yielding

$$F(p) = F_{N-p} - F_p = \frac{\pi}{12}\left(\frac{1}{(N-p)^2} - \frac{1}{p^2}\right). \tag{5.30}$$

The validity of expression (5.29) can be checked in Fig. 5.5. In all cases, the black continuous line is the theoretical prediction, Eq. (5.29). Fig. 5.5 (a) shows the forces $F_N + c_0$ as a function of N for Rindler metrics of different sizes, varying both J_0 and the acceleration a. We have included the Minkowski case, which corresponds to $J_0 = 1$ and $a = 0$, as one of the limits. We notice that $F_N + c_0$ can be both positive and negative, depending on the values of J_0 and the acceleration a. This behavior is explained through our expression (5.29): the boundary term scales like N^{-1} and it is always negative. Meanwhile, the universal conformal term scales like N^{-2} and is always positive. Thus, the prevalence of one or the other explains the global behavior, but for large enough N the boundary term is always dominant. This trade-off can be visualized in the inset of Fig. 5.5 (a), where we plot the absolute value $|F_N + c_0|$ as a function of N in log-log scale. For Minkowski, $J_0 = 1$ and $a = 0$, the $1/N^2$ behavior extends for all sizes, but as soon as $a > 0$ we observe a small-N behavior like N^{-2} which performs a crossover into the dominant N^{-1} term beyond a finite size which scales as $(J_0/a)^{1/2}$.

Fig. 5.5 (b) shows the case of the Casimir forces in the rainbow state, for which the boundary term is constant: $J'_N/J_N = -h$ for all N. Thus, the behavior of $F_N + c_0$ corresponds merely to the CFT term, Eq. (5.23) with a constant additive correction. This behavior is further clarified when this constant is removed, and we observe the nearly perfect collapse of all the forces in the inset of Fig. 5.5 (b).

We have also considered is the sinusoidal metric, Eq. (5.6), where the boundary term dominates the force for large N, while the CFT term dominates for low N, as we can see in the top panel of Fig. 5.5 (c). There, we can observe the behavior of the hoppings (in pale pink), along with the forces and their fit to expression (5.29). Indeed, the force behaves like the derivative of the hopping function. In order to highlight this behavior, we have considered yet another metric, given by

$$J_N = 1 + A\sin(kN^2), \tag{5.31}$$

i.e. a modulated frequency sinusoidal. The results are shown in the bottom panel of Fig. 5.5 (c), showing again an excellent agreement between the theory and the numerical experiments.

5.4 Casimir force in the inhomogeneous Heisenberg model

We may wonder whether these results are only valid for free fermions or if, instead, they can be applied to other CFT. Thus, we have considered one of the

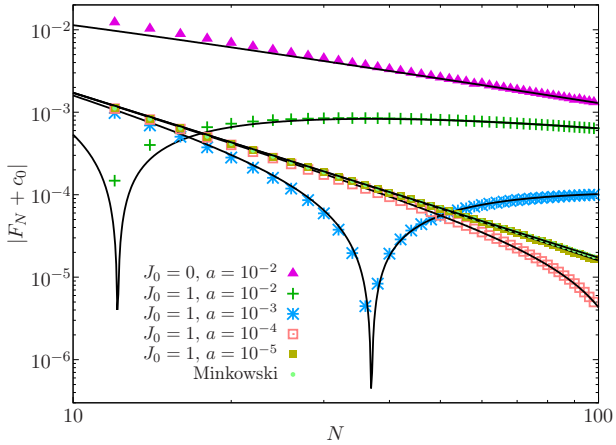

Figure 5.6: Casimir forces for the spin-1/2 Heisenberg chain with Rindler couplings. The black lines correspond to the theoretical prediction, given by Eq. (5.34). Compare to the inset of Fig. 5.5 (a).

simplest critical interacting systems, described in Section 3.6.4, the (inhomogenous) spin-1/2 Heisenberg model in 1D, defined by

$$H = -\sum_{i=1}^{L-1} J_i \, \vec{S}_i \cdot \vec{S}_{i+1}, \tag{5.32}$$

Using the Jordan-Wigner transformation we may rewrite it in fermionic language as

$$H = -\sum_{i=1}^{L-1} J_i \left(c_i^\dagger c_{i+1} + \text{h.c.} \right) + 2 \sum_{i=1}^{L} J_i \, n_i n_{i+1}, \tag{5.33}$$

where we can see that fermionic particles at nearby sites repel each other, making it impossible to use free-fermion techniques. Yet, the GS energy of this Hamiltonian can be accurately obtained using the density matrix renormalization group (DMRG) algorithm [49,50]. The results for the Rindler couplings, Eq. (5.5) are shown in Fig. 5.6. The maximal size that we have reached is lower than in the previous case, $N = 100$, because the numerical computation is more demanding. Yet, the results show that a straightforward extension of Eq. (5.29) predicts the force values with a remarkable accuracy using $c_0 = 0.4431$, $c_B = 0.2618$ and $v_F = 1.319$, through

$$F_N \approx -c_0 - \frac{c_B}{2} \left(\frac{J'_N}{J_N} \right) + \frac{\pi v_F}{24 N^2}. \tag{5.34}$$

Fig. 5.6 shows $|F_N + c_0|$ in logarithmic scale as a function of N for different Rindler deformations of the Heisenberg Hamiltonian, along with the theoretical prediction, Eq. (5.29). These plots can be compared with the inset of Fig. 5.5 (a).

5.5 Conclusions and further work

We have derived an expression for the ground-state energy of the discretized version of the Dirac equation in a deformed (1+1)D medium, which corresponds to the vacuum state in static curved metrics. We can model a classical particle navigating through the system depressing a local hopping, and then it can be readily checked that the classical particle moves approximately in a potential which corresponds to the classical gravitational potential associated with the metric. The quantum corrections to this semi-classical result can be obtained by suitably deforming the predictions of conformal field theory (CFT). Indeed, we have checked that the finite-size corrections are dominated by two terms: a boundary term related to the derivative of the local hopping amplitude at the edge of the system, and a naturally deformed version of the CFT force, where the central charge is preserved. The conformal correction can be interpreted in two complementary ways: either the Fermi velocity is substituted by the (harmonic) average value of the hopping terms, or the system size is transformed by its deformed value.

In any case, we should emphasize that the finite-size corrections to the vacuum energy are, indeed, *universal*. Moroever, we have shown that an observer at a boundary measuring the Casimir forces will obtain a metric-independent value.

It is relevant to ask whether our results extend to other conformal field theories, both interacting, such as Heisenberg, or non-interacting, such as the Ising model in a transverse field. Even more challenging will be to extend these results to (2+1)D field theories and to consider non-static metrics, where the dynamical effects will be relevant, linking them to the dynamical Casimir effect [109]. Even if the energy is not defined in those cases, a force can still be found acting on classical particles. It is also interesting to consider chains under strong inhomogeneity or randomness [110–113].

As a natural next step, we intend also to develop protocols in order to confirm these results in the laboratory employing ultra-cold atoms in optical lattices, where similar curved-metric problems have been addressed in the past, such as the measurement of the Unruh effect [5, 6].

Chapter 6

Depletion in fermionic chains with inhomogeneous hoppings

This chapter is based on the following article:

- B. Mula, N. Samos Sáenz de Buruaga, G. Sierra, S.N. Santalla, J. Rodríguez-Laguna, *Depletion in fermionic chains with inhomogeneous hoppings*, Phys. Rev. B **106**, 224204 (2022).

The ground state of a free-fermionic chain with inhomogeneous hoppings at half-filling can be mapped into the Dirac vacuum on a static curved space-time, which presents exactly homogeneous occupations due to particle-hole symmetry. Yet, far from half-filling we observe density modulations and depletion effects. The system can be described by a 1D Schrödinger equation on a different static space-time, with an effective potential which accounts for the depleted regions. We provide a semiclassical expression for the single-particle modes and the density profiles associated to different hopping patterns and filling fractions. Moreover, we show that the depletion effects can be compensated for all filling fractions by adding a chemical potential proportional to the hoppings. Interestingly, we can obtain exactly the same density profiles on a homogeneous chain if we introduce a chemical potential which is inverse to the hopping intensities, even though the ground state is different from the original one.

6.1 Introduction and context

As we already said, fermionic chains have been put forward to simulate the Dirac vacuum in curved space-times, which would lead us to perform experiments on the Unruh effect (see Section 1.3) or Casimir forces on a background gravitational field (see Chapter 5) [5, 6, 114]. Such quantum simulators can be built using ultracold fermionic atoms on an optical lattice, employing modulated laser beams to provide inhomogeneous hopping amplitudes between neighboring cells [7]. The key insight is that an inhomogeneity in the hoppings will give rise to an effective space-time metric in the thermodynamic limit, under some mild conditions.

In the aforementioned examples the Dirac vacuum is obtained as the ground state (GS) of the lattice Hamiltonian at half-filling, which was discussed in Section 3.1. Interestingly, when the underlying lattice is bipartite the system presents particle-hole symmetry and the occupation numbers become exactly homogeneous. Moreover, its large scale physical properties can be accounted for using conformal invariance arguments on the appropriately deformed metric [21, 22, 102–104]. Yet, as the filling fraction is lowered (or raised) the density will vary from point to point. Morever, it may become negligible in the region containing the lowest hopping amplitudes, a phenomenon which we have termed *depletion*. This result can be readily understood in the strong inhomogeneity regime, employing a strong-disorder renormalization group (SDRG) scheme [115], because the orbitals with the lowest energies are localized upon the lowest hopping amplitudes, which may correspond sometimes to effective long-distance renormalized bonds. An illustration of this situation can be seen in Fig. 6.1. Yet, in the weak inhomogeneity limit the mathematical description of the depletion effects faces some technical challenges: second-order derivatives of the fields must be considered in the gradient expansion of the Hamiltonian, thus breaking explicitly the conformal symmetry which characterizes the half-filling case.

This depletion has already been observed by other authors. For example, it has been reported that the entanglement entropies of inhomogeneous fermionic chains away from half-filling can be interpreted as those corresponding to an effective shorter chain, corresponding to the non-depleted region [116]. Moreover, the effect of a finite density fermion field in entanglement has been studied both in the relativistic [117] and non-relativistic frameworks [118].

This work addresses the emergence of depletion in inhomogeneous pure-hopping free fermionic chains away from half-filling, and it is divided as follows. In Section 6.2 we describe our physical model, while Section 6.3 describes the depletion phenomenon in the strong disorder limit. Section 6.4 describes our continuum approximation for all filling fractions, and the effective Schrödinger equation on a different space-time metric. Section 6.5 describes our theoretical approach to the density profiles and the depleted areas. Section 6.6 shows the depletion for the entanglement entropy and the entanglement contour. The question of the effective potential is addressed in Section 6.7, showing that it can be either proportional to the hopping amplitudes or inversely proportional to them, depending on our precise definition. Finally, Section 6.8 summarizes our findings and discusses our suggestions for further work.

6.2 Model

Let us consider an open fermionic chain with N (even) sites, whose Hilbert space is spanned by creation operators $c_i^\dagger$, $i \in \{1, \cdots, N\}$ following standard anticommutation relations. $\{c_i^\dagger, c_j\} = \delta_{i,j}$. The Hamiltonian is the same as in Eq. (5.1),

$$H(\mathbf{J})_N = -\sum_{i=1}^{N-1} J_i \, c_i^\dagger c_{i+1} + \text{h.c.}, \tag{6.1}$$

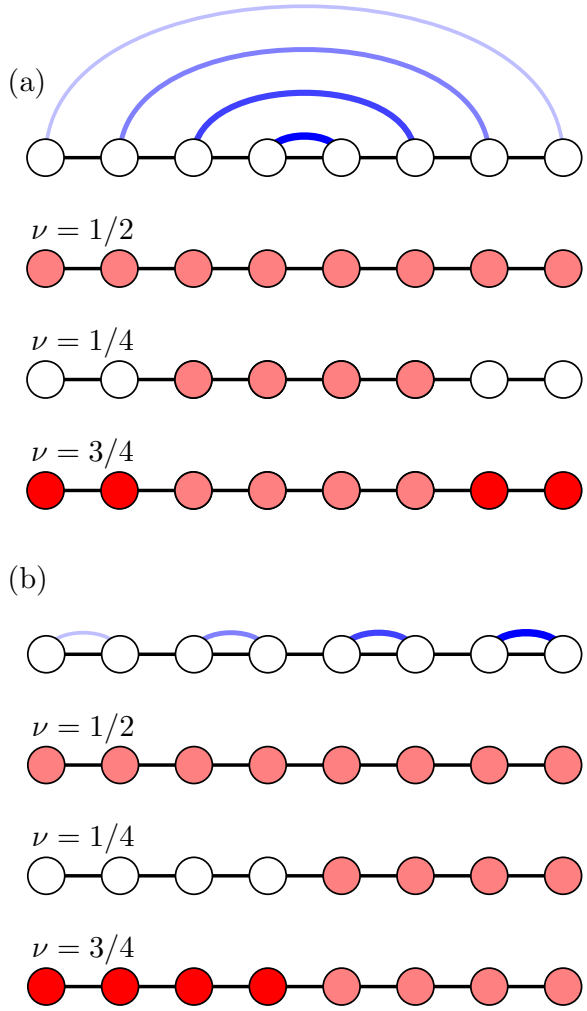

Figure 6.1: Depletion in free-fermionic chains with inhomogeneous hoppings, explained using the SDRG for different values of the filling fraction ν. In (a) we have a rainbow chain whose single-particle orbitals are bonds between symmetrically placed sites. For $\nu = 1/2$, all the bonds get single occupation (light red) and the density is exactly homogeneous. For $\nu = 1/4$ we only occupy the two strongest bonds, leaving a depleted area near the borders. For $\nu = 3/4$ the weakest bonds get double occupation (bright red), while the strongest remain with single occupation. In (b) we have a dimerized chain such that the energy associated to each bond grows rightwards. For $\nu = 1/2$ we obtain the same homogeneous density. For $\nu = 1/4$ only the rightmost bonds are occupied, and the left half is depleted. For $\nu = 3/4$ the leftmost bonds obtain double occupation, and the rightmost ones still get one particle.

where $\mathbf{J} = \{J_i\}_{i=1}^{N-1}$ are the *hopping amplitudes*, $J_i \in \mathbb{R}^+$ referring to the link between sites i and $i+1$. The Hamiltonian given by Eq. (6.1) has been fully described in Section 5.2.

In all cases, we will assume that the sequence of hopping amplitudes presents a proper thermodynamic limit. Let $\mathbf{J}_N = \{J_{i,N}\}_{i=1}^{N-1}$ be a family of hopping amplitudes for all possible chain lengths N. Then, we assume that there exists a continuous function $J : [0,1] \mapsto \mathbb{R}^+$ such that $J_{i,N} = J(i/N)$. For concreteness, let us consider three different examples as we did in Chapter 5. The *Rindler metric* is the space-time structure perceived by an observer moving with constant acceleration in a Minkowski metric, described by

$$J(x) = J_0 x. \tag{6.2}$$

Another natural choice is the *sine metric*,

$$J(x) = J_0 + J_1 \cos(2\pi x), \tag{6.3}$$

or the *rainbow metric* [97–99, 102–104, 110, 112, 119, 120], given by

$$J(x) = J_0 \exp\left(-\hat{h}\left|x - \frac{1}{2}\right|\right), \tag{6.4}$$

where we define $h = \hat{h}N$ for convenience. Eq. 6.4 is valid for $h \geq 0$, with $h = 0$ corresponding to the Minkowski case. This metric presents a constant negative curvature except at the center [99, 102], $x = 1/2$, thus resembling an anti-de Sitter (adS) space [104], and has been extensively discussed because it presents a maximal apparent violation of the area law of the entanglement entropy. Notice that the J_0 parameter is irrelevant in all cases, since it just fixes the global energy scale, and we will take it as one.

6.2.1 Density and particle-hole symmetry

The correlation matrix can be easily computed for the GS of Hamiltonian (6.1),

$$C_{ij} \equiv \langle \psi_m | \, c_i^\dagger c_j \, | \psi_m \rangle = \sum_{k=1}^{m} \bar{U}_{ki} U_{kj}, \tag{6.5}$$

and, concretely, the local occupation or density is found as $\langle n_i \rangle = C_{ii}$. Since our system is bipartite, let us define an operator P acting on the single-particle wave-functions that flips the sign of all components within one of the sublattices. It is easy to prove that $JP = -PJ$. In other terms, if U_k is an eigenstate of J with energy ε_k, then PU_k will be another eigenstate of J with energy $-\varepsilon_k$. Every negative energy orbital has a positive energy partner related through a P operation, thus proving the particle-hole symmetry of the spectrum, as it was mentioned in Section 3.1. Since U is a unitary matrix, $\sum_{k=1}^{N} |U_{ki}|^2 = 1$, for all i. We may decompose the sum into two,

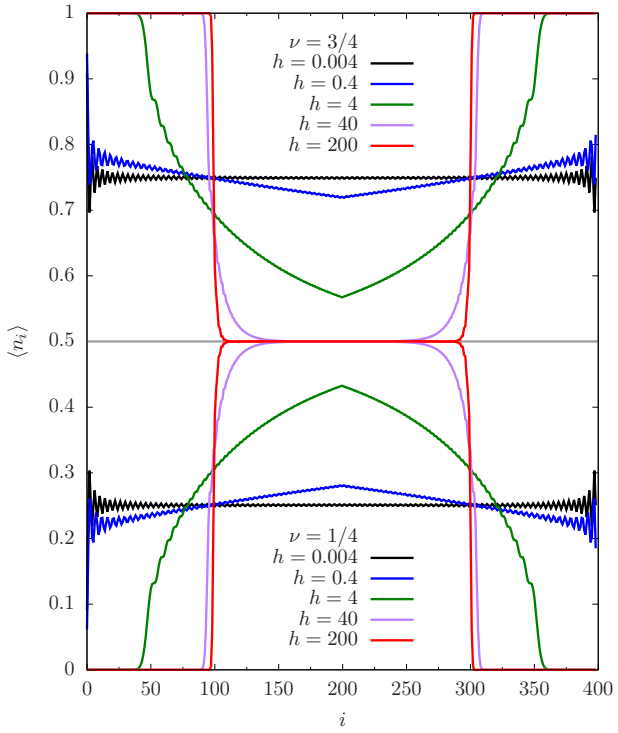

Figure 6.2: Density profiles for the rainbow chain with $N = 400$ sites and two filling fractions, $\nu = 1/4$ and $\nu = 3/4$, for different values of the inhomogeneity parameter h. Notice that for low inhomogeneities we always have a nearly flat profile, which gets more modulated as the inhomogeneity increases, converging towards the SDRG prediction as the inhomogeneity becomes large. As predicted by particle-hole symmetry, the $\nu = 1/4$ and $\nu = 3/4$ cases present mirror symmetry for all the values of the inhomogeneity.

$$1 = \sum_{k=1}^{N/2} |U_{ki}|^2 + \sum_{k=N/2+1}^{N} |U_{ki}|^2, \tag{6.6}$$

but the second sum must be exactly the same as the first, because $|U_{ki}|^2 = |U_{N+1-k,i}|^2$. Therefore, each sum must add up to $1/2$, thus proving that the eigenstate $\left|\psi_{N/2}\right\rangle$ at half-filling must have homogeneous occupation, $n_i = 1/2$ for all sites, independently of the hopping amplitudes.

6.3 Depletion at strong inhomogeneity

Let us consider the strong inhomogeneity regime, in which the values of the hopping amplitudes differ largely between different links. In this situation, the strong-disorder renormalization group (SDRG) approach developed by Dasgupta and Ma describes the low-energy states very effectively [113, 115, 121–123]. Indeed, the SDRG algorithm instructs us to select the most energetic link, J_i, and to establish a bonding or anti-bonding orbital over the corresponding couple of sites, depending on the hopping sign, which are afterwards removed from the system. Let us stress

that the particle occupying such a bond has the same probability of being found on each site. The neighboring sites to this new bond are then linked among themselves by an effective hopping amplitude, which is obtained via second-order perturbation theory,

$$\tilde{J}_i = -\frac{J_L J_R}{J_i}, \tag{6.7}$$

where J_L and J_R are the left and right neighboring hopping amplitudes, and the minus sign is due to the fermionic nature of the particles. Notice that this new effective link can be selected in the next iteration, if it happens to be the strongest one, thus yielding a long-distance bond. Some interesting synthetic states, such as the rainbow state, are built in such a way that all bonds (except the first one) are long-distance [97, 98].

When the SDRG algorithm is performed at half-filling we fill up $m = N/2$ bonds, each of which delocalizes a particle between a different pair of (perhaps not neighboring) sites. Thus, each site has an occupation probability of $1/2$, in accordance with the theorem of Section 6.2.1. Yet, if we place $m < N/2$ particles, they will always occupy the region with highest hopping amplitudes, even if the renormalization procedure yields long-distance bonds. Fig. 6.2 shows indeed that, in the strong inhomogeneity regime, we can observe two different density regions for $m < N/2$: half-occupied and empty. For $m > N/2$, due to particle-hole symmetry, we occupy the same bonds but in reversed order. Each site within a doubly occupied bond gets maximal occupation, $\langle n_i \rangle = 1$. Therefore, as we increase the filling fraction above $\nu = 1/2$ we fill up completely the regions with the lowest hopping amplitudes, mirroring the previous process.

This filling sequence is illustrated in Fig. 6.1 (a) for a rainbow chain and (b) a dimerized chain for filling fractions $\nu = 1/2$, $\nu < 1/2$ and $\nu > 1/2$ with a small size. In Fig. 6.2, on the other hand, we can see the actual densities numerically obtained for a larger chain, with $N = 400$, using $\nu = 1/4$ and $\nu = 3/4$, as a function of the parameter h which controls the level of inhomogeneity. As h grows, we move from a nearly uniform density profile towards the square profile of the SDRG prediction, which differs in the cases of $\nu = 1/4$ and $\nu = 3/4$. Indeed, in both cases we have $\langle n_i \rangle = 1/2$ at the central half of the chain, while the lateral regions are depleted for $\nu = 1/4$ or full for $\nu = 3/4$.

6.4 Depletion at weak inhomogeneity

In this section we establish a continuum approximation to Hamiltonian (6.1) for all possible filling fractions obtained through a gradient expansion. At half-filling our model is known to map into the Dirac Hamiltonian in the continuum limit,

$$i\not{D}_x \psi(x) = 0, \tag{6.8}$$

where D_x is the covariant derivative on a given space-time metric given by the hopping function $J(x)$ [99, 102]. In this work we will consider the situation away from half-filling, showing that the gradient expansion should be taken to second

order in the derivatives of the field, giving rise to a continuum approximation based on the Schrödinger equation on a curved background metric,

$$-\nabla_x^2\psi(x) + V(x)\psi(x) = E\psi(x), \tag{6.9}$$

where ∇_x^2 stands for the *Laplace-Beltrami* operator on a different manifold [124], whose metric is also given by the hopping function $J(x)$.

6.4.1 Dirac Hamiltonian

Let us assume that the local creation and annihilation operators can be approximated in terms of two slowly varying fermionic fields, $\psi_L(x)$ and $\psi_R(x)$, which makes reference to the right and left parts of the wavefunction,

$$\begin{aligned} c_m &= \sqrt{a}\left(e^{ik_F x}\psi_L(x) + e^{-ik_F x}\psi_R(x)\right), \\ c_m^\dagger &= \sqrt{a}\left(e^{-ik_F x}\psi_L^\dagger(x) + e^{ik_F x}\psi_R^\dagger(x)\right), \end{aligned} \tag{6.10}$$

where a is the lattice spacing, $x = ma$, and k_F the Fermi momentum, giving rise to the Hamiltonian

$$\begin{aligned} H(x) = -\int_0^{\mathcal{N}} dx\ J(x) \Big[& e^{-ik_F a}\psi_L^\dagger(x+a)\psi_L(x) + e^{ik_F a}\psi_R^\dagger(x+a)\psi_R(x) \\ & -e^{-ik_F a}e^{-2ik_F x}\psi_L^\dagger(x+a)\psi_R(x) + e^{ik_F a}e^{2ik_F x}\psi_R^\dagger(x+a)\psi_L(x)\Big], \end{aligned} \tag{6.11}$$

with $\mathcal{N} = Na$.

We should remark that the crossed terms, such as $\psi_L^\dagger(x+a)\psi_R(x)$, have strongly oscillating prefactors $e^{-2ik_F x}$, and thus their integral becomes negligible. As an initial approach, we may expand the fields to first order in a, $\psi(x+a) \approx \psi(x) + a\partial_x\psi(x)$, thus yielding the effective Hamiltonian

$$\begin{aligned} H(x) = -\int_0^{\mathcal{N}} dx J(x) \Bigg[& \left(2\cos(k_F a) - ae^{-ik_F a}\frac{J'(x)}{J(x)}\right)\psi_L^\dagger(x)\psi_L(x) \\ & + \left(2\cos(k_F a) - ae^{ik_F a}\frac{J'(x)}{J(x)}\right)\psi_R^\dagger(x)\psi_R(x) \\ & +2ai\sin(k_F a)\left(\psi_L^\dagger(x)\partial_x\psi_L(x) - \psi_R^\dagger(x)\partial_x\psi_R(x)\right)\Bigg]. \end{aligned} \tag{6.12}$$

Let us perform a generic coordinate transformation, $x \to \tilde{x}$, such that

$$\frac{d\tilde{x}}{dx} = \tilde{G}(\tilde{x}), \tag{6.13}$$

so that $\partial_x = \tilde{G}(\tilde{x})\partial_{\tilde{x}}$, $\partial_x^2 = \tilde{G}(\tilde{x})\tilde{G}'(\tilde{x})\partial_{\tilde{x}} + \tilde{G}^2(\tilde{x})\partial_{\tilde{x}}^2$ and $\psi(x) = \tilde{\psi}(\tilde{x})\tilde{G}^{1/2}(\tilde{x})$. We will choose $\tilde{G}(\tilde{x})$ so as to make the coefficient of the first derivative homogeneous. Therefore, $\tilde{G}(\tilde{x}) = \tilde{J}(\tilde{x})$ and Eq. (6.12) can be written as

$$H(\tilde{x}) = -\int_0^{\mathcal{N}} d\tilde{x} \left[2ai \sin(k_F a) \left(\tilde{\psi}_L^\dagger \partial_{\tilde{x}} \tilde{\psi}_L(\tilde{x}) - \tilde{\psi}_R^\dagger(\tilde{x}) \partial_{\tilde{x}} \tilde{\psi}_R(\tilde{x}) \right) \right.$$
$$\left. + \cos(k_F a) \left(2\tilde{J}(\tilde{x}) - a \frac{\tilde{J}'(\tilde{x})}{\tilde{J}(\tilde{x})} \right) \left(\tilde{\psi}_L^\dagger(\tilde{x}) \tilde{\psi}_L(\tilde{x}) + \tilde{\psi}_R^\dagger(\tilde{x}) \tilde{\psi}_R(\tilde{x}) \right) \right], \tag{6.14}$$

which in the case of half-filling, i.e. $k_F a \to \pi/2$, reduces to

$$H_D(\tilde{x}) = -\int_0^{\mathcal{N}} d\tilde{x}\ 2ai\ \sin(k_F a) \left(\tilde{\psi}_L^\dagger(\tilde{x}) \partial_{\tilde{x}} \tilde{\psi}_L(\tilde{x}) - \tilde{\psi}_R^\dagger(\tilde{x}) \partial_{\tilde{x}} \psi_R(\tilde{x}) \right). \tag{6.15}$$

Yet, we observe that for $k_F a < \pi/2$ the Dirac equation acquires a potential term, which may seem at first sight to be responsible for the depletion effect, but is not. Indeed, the eigenstates of (6.14) can be obtained in a closed form (equivalently for $\tilde{\psi}_R$),

$$\tilde{\psi}_L(\tilde{x}) = \exp\left[\frac{-i}{2a \sin(k_F a)} \left(\omega \tilde{x} - \int \cos(k_F a) \left(2\tilde{J}(\tilde{x}) - a \frac{\tilde{J}'(\tilde{x})}{\tilde{J}(\tilde{x})} \right) d\tilde{x} \right) \right], \tag{6.16}$$

where ω is an integration constant. In other words, the wavefunctions are modulated planes wave in $\tilde{x}$ and they will not decay exponentially. See Appendix E for more details.

6.4.2 Second order approximation

In order to reproduce the observed depletion effects we should expand the fields to second order in the lattice parameter a,

$$\psi(x+a) \approx \psi(x) + a\partial_x \psi(x) + \frac{a^2}{2} \partial_x^2 \psi(x), \tag{6.17}$$

thus yielding a Hamiltonian of the form

$$
\begin{aligned}
H(x) = -\int_0^{\mathcal{N}} dx J(x) \Bigg[& \left(2\cos(k_F a) - a e^{-ik_F x} \frac{J'(x)}{J(x)} + \frac{a^2}{2} e^{-ik_F x} \frac{J''(x)}{J(x)} \right) \psi_L^\dagger(x)\psi_L(x) \\
& + \left(2\cos(k_F a) - a e^{ik_F x} \frac{J'(x)}{J(x)} + \frac{a^2}{2} e^{ik_F x} \frac{J''(x)}{J(x)} \right) \psi_R^\dagger(x)\psi_R(x) \\
& + 2ai \sin(k_F a) \left(\psi_L^\dagger(x)\partial_x\psi_L(x) - \psi_R^\dagger(x)\partial_x\psi_R(x) \right) \\
& + a^2 e^{ik_F x} \frac{J'(x)}{J(x)} \psi_R^\dagger(x)\partial_x\psi_R(x) + a^2 e^{-ik_F x} \frac{J'(x)}{J(x)} \psi_L^\dagger(x)\partial_x\psi_L(x) \\
& + a^2 \cos(k_F a) \left(\psi_L^\dagger(x)\partial_x^2\psi_L(x) + \psi_R^\dagger(x)\partial_x^2\psi_R(x) \right) \Bigg],
\end{aligned}
\tag{6.18}
$$

which gives rise to the following equations of motion,

$$
\begin{aligned}
E\psi(x)_{R/L} = -J(x) \Bigg[& \left(2\cos(k_F a) - a e^{\pm ik_F a} \frac{J'(x)}{J(x)} + \frac{a^2}{2} e^{\pm ik_F a} \frac{J''(x)}{J(x)} \right) \psi(x)_{R/L} \\
& \mp 2ai \sin(k_F a)\partial_x\psi(x)_{R/L} + a^2 e^{\pm ik_F a} \frac{J'(x)}{J(x)} \partial_x\psi(x)_{R/L} \\
& + a^2 \cos(k_F a)\partial_x^2\psi(x)_{R/L} \Big],
\end{aligned}
\tag{6.19}
$$

where the R/L notation makes reference to the right and left parts of the wavefunction, and the corresponding sign should be chosen in each case. We would like to notice that a second-order discrete version of Eq. (6.19) with lattice spacing a yields our original single-body Hamiltonian (6.1), thus proving the direct equivalence between both systems.

In the rest of the section we will transform this equation into a Schrödinger equation, making use of two transformations: (a) a coordinate transformation following Eq. (6.13), which is equivalent to embedding our system in a non-trivial space-time metric, and (b) a gauge transformation in order to get rid of the first derivative term.

Our next purpose is then to make the coefficient of the second derivative homogeneous through a suitable change of variable $\tilde{x}$. Making a slight abuse of notation, we let $\tilde{J}(\tilde{x})\tilde{G}^2(\tilde{x}) = 1 \to \tilde{G}(\tilde{x}) = \tilde{J}^{-1/2}(\tilde{x})$. Notice the difference with Eq. (6.12), in which we had $\tilde{G}(\tilde{x}) = \tilde{J}(\tilde{x})$ once the appropriate transformation of coordinates was performed in order to obtain a homogeneous first-derivative term. The equation of motion in these new transformed coordinates reads

$$
\begin{aligned}
E\tilde{\psi}(\tilde{x})_{R/L} = & -a^2\cos(k_F a)\partial_{\tilde{x}}^2\tilde{\psi}(\tilde{x})_{R/L} \pm 2i\sin(k_F a)\left(a\tilde{J}^{1/2}(\tilde{x}) - \frac{a^2}{2}\frac{\tilde{J}'(\tilde{x})}{\tilde{J}(\tilde{x})}\right)\partial_{\tilde{x}}\tilde{\psi}(\tilde{x})_{R/L} \\
& - 2\cos(k_F a)\left(\tilde{J}(\tilde{x}) - \frac{a}{4}\frac{\tilde{J}'(\tilde{x})}{\tilde{J}^{1/2}(\tilde{x})} + \frac{7a^2}{32}\frac{\tilde{J}'^2(\tilde{x})}{\tilde{J}^2(\tilde{x})} - \frac{a^2}{8}\frac{\tilde{J}''(\tilde{x})}{\tilde{J}(\tilde{x})}\right)\tilde{\psi}(\tilde{x})_{R/L} \\
& - \frac{e^{\pm ik_F a}}{2}\left(-a\frac{\tilde{J}'(\tilde{x})}{\tilde{J}^{1/2}(\tilde{x})} - a^2\frac{\tilde{J}'^2(\tilde{x})}{\tilde{J}^2(\tilde{x})} + a^2\frac{\tilde{J}''(\tilde{x})}{\tilde{J}(\tilde{x})}\right)\tilde{\psi}(\tilde{x})_{R/L}. \qquad (6.20)
\end{aligned}
$$

This equation can be rewritten so as to make the single-body operator manifestly hermitian,

$$
\begin{aligned}
& E\tilde{\psi}(\tilde{x})_{R/L} = -a^2\cos(k_F a)\partial_{\tilde{x}}^2\tilde{\psi}(\tilde{x})_{R/L} \\
& \pm 2i\sin(k_F a)\left(a\tilde{J}^{1/4}(\tilde{x})\partial_{\tilde{x}}\left(\tilde{J}^{1/4}(\tilde{x})\tilde{\psi}(\tilde{x})_{R/L}\right) - \frac{a^2}{2}\left(\frac{\tilde{J}'(\tilde{x})}{\tilde{J}(\tilde{x})}\right)^{1/2}\partial_{\tilde{x}}\left(\frac{\tilde{J}'(\tilde{x})}{\tilde{J}(\tilde{x})}\right)^{1/2}\tilde{\psi}(\tilde{x})_{R/L}\right) \\
& - 2\cos(k_F a)\left(\tilde{J}(\tilde{x}) - \frac{a}{2}\frac{\tilde{J}'(\tilde{x})}{\tilde{J}^{1/2}(\tilde{x})} - \frac{a^2}{32}\frac{\tilde{J}'^2(\tilde{x})}{\tilde{J}^2(\tilde{x})} + \frac{a^2}{8}\frac{\tilde{J}''(\tilde{x})}{\tilde{J}(\tilde{x})}\right)\tilde{\psi}(\tilde{x})_{R/L}. \qquad (6.21)
\end{aligned}
$$

In order to transform our equation of motion into a Schrödinger equation, our next task is to get rid of the first derivative term using a gauge transformation,

$$
\tilde{\psi}(\tilde{x})_{R/L} = e^{i\beta_{R/L}(\tilde{x})}\tilde{\Psi}(\tilde{x})_{R/L}, \qquad (6.22)
$$

which implies that

$$
\begin{aligned}
\partial_{\tilde{x}}\tilde{\psi}(\tilde{x})_{R/L} &= i\beta'_{R/L}(\tilde{x})e^{i\beta_{R/L}(\tilde{x})}\tilde{\Psi}(\tilde{x})_{R/L} + e^{i\beta_{R/L}(\tilde{x})}\partial_{\tilde{x}}\tilde{\Psi}(\tilde{x})_{R/L}, \\
\partial_{\tilde{x}}^2\tilde{\psi}(\tilde{x})_{R/L} &= i\beta''_{R/L}(\tilde{x})e^{i\beta_{R/L}(\tilde{x})}\tilde{\Psi}(\tilde{x})_{R/L} \qquad (6.23) \\
&\quad - \beta'^2_{R/L}(\tilde{x})e^{i\beta_{R/L}(\tilde{x})}\tilde{\Psi}(\tilde{x})_{R/L} 2i\beta'_{R/L}(\tilde{x})e^{i\beta_{R/L}(\tilde{x})}\partial_{\tilde{x}}\tilde{\Psi}(\tilde{x})_{R/L} \\
&\quad + e^{i\beta_{R/L}(\tilde{x})}\partial_{\tilde{x}}^2\tilde{\Psi}(\tilde{x})_{R/L}. \qquad (6.24)
\end{aligned}
$$

The condition that we have to impose so that the first-derivative terms cancel out is

$$
\beta'_{R/L}(\tilde{x}) = \mp\tan(k_F a)\left(\frac{1}{2}\frac{\tilde{J}'(\tilde{x})}{\tilde{J}(\tilde{x})} - \frac{1}{a}\tilde{J}^{1/2}(\tilde{x})\right). \qquad (6.25)
$$

Applying this transformation we obtain

$$
\begin{aligned}
E\tilde{\Psi}(\tilde{x})_{R/L} = & -\frac{1+\cos(k_F a)^2}{\cos(k_F a)}\tilde{J}(\tilde{x})\tilde{\Psi}(\tilde{x})_{R/L} \\
& + a\frac{1}{\cos(k_F a)}\frac{\tilde{J}'(\tilde{x})}{\tilde{J}^{1/2}(\tilde{x})}\tilde{\Psi}(\tilde{x})_{R/L} \\
& - \frac{a^2}{4}\left(\frac{\sin(k_F a)^2}{\cos(k_F a)}\frac{\tilde{J}'^2(\tilde{x})}{\tilde{J}^2(\tilde{x})} - \frac{\cos(k_F a)}{4}\frac{\tilde{J}'^2(\tilde{x})}{\tilde{J}^2(\tilde{x})} + \cos(k_F a)\frac{\tilde{J}''(\tilde{x})}{\tilde{J}(\tilde{x})}\right)\tilde{\Psi}(\tilde{x})_{R/L} \\
& - a^2\cos(k_F a)\partial_{\tilde{x}}^2\tilde{\Psi}(\tilde{x})_{R/L}. \qquad (6.26)
\end{aligned}
$$

Eq. (6.26) has the form of a Schrödinger equation in $\tilde{x}$ with a mass $M = 2/\cos(k_F a)$ that tends to zero as $k_F a \to \pi/2$, thus rendering the approximation invalid in that limit. The effective potential, to zero order in a, becomes

$$
V(\tilde{x}) \approx -\frac{1+\cos(k_F a)^2}{\cos(k_F a)}\tilde{J}(\tilde{x}). \qquad (6.27)
$$

Notice that, for $k_F a \ll 1$ we have to a very good approximation $V(\tilde{x}) \approx -2\tilde{J}(\tilde{x})$ or, equivalently, $V(x) = -2J(x)$, while for larger values of $k_F a$ the different modes of our system correspond to different Schrödinger equations. The reason is that the prefactors of Eq. (6.26) present explicit dependence on $k_F a$. The next corrections, corresponding to higher orders in a, can be shown to be small or constant for the hopping amplitudes employed in this work. We would also like to stress that our system is now embedded on a manifold with metric $ds^2 = dt^2 - d\tilde{x}^2$, and all geometrical measurements should be transformed back before further comparisons with our original discrete model.

Let us discuss the numerical validity of Eq. (6.26), which is familiar to us due to its Schrödinger form. For highly excited states we are allowed to perform a Wentzel-Kramers-Brillouin (WKB) approximation, which leads to a form

$$
\tilde{\Psi}(\tilde{x})_{R/L} \sim \frac{1}{\sqrt{\tilde{p}(\tilde{x})}}e^{\pm i\tilde{p}(\tilde{x})\tilde{x}}, \qquad (6.28)
$$

in the new coordinate $\tilde{x}$, where $\tilde{p}(\tilde{x})$ is the momentum of a particle in that position according to classical mechanics, i.e. $p(x) = \pm\sqrt{2M(E - V(x))}$

$$
\tilde{p}(\tilde{x}) = \sqrt{\frac{1}{\cos(k_F a)^2}\left(\frac{1+\cos(k_F a)^2}{\cos(k_F a)}\tilde{J}(\tilde{x}) + E\right)}, \qquad (6.29)
$$

Yet, we should transform this solution back to our original coordinate system in order to check its numerical validity, making use of the change of coordinates for a probability distribution, $|\tilde{\Psi}(\tilde{x})|^2 d\tilde{x} = |\Psi(x)|^2 dx$, which leads to

$$
|\Psi(x)_{R/L}| = \frac{|\tilde{\Psi}(\tilde{x})_{R/L}|}{J^{1/4}(\tilde{x})} \sim \frac{1}{\sqrt{\tilde{p}(\tilde{x})}}\frac{1}{J^{1/4}(\tilde{x})}. \qquad (6.30)
$$

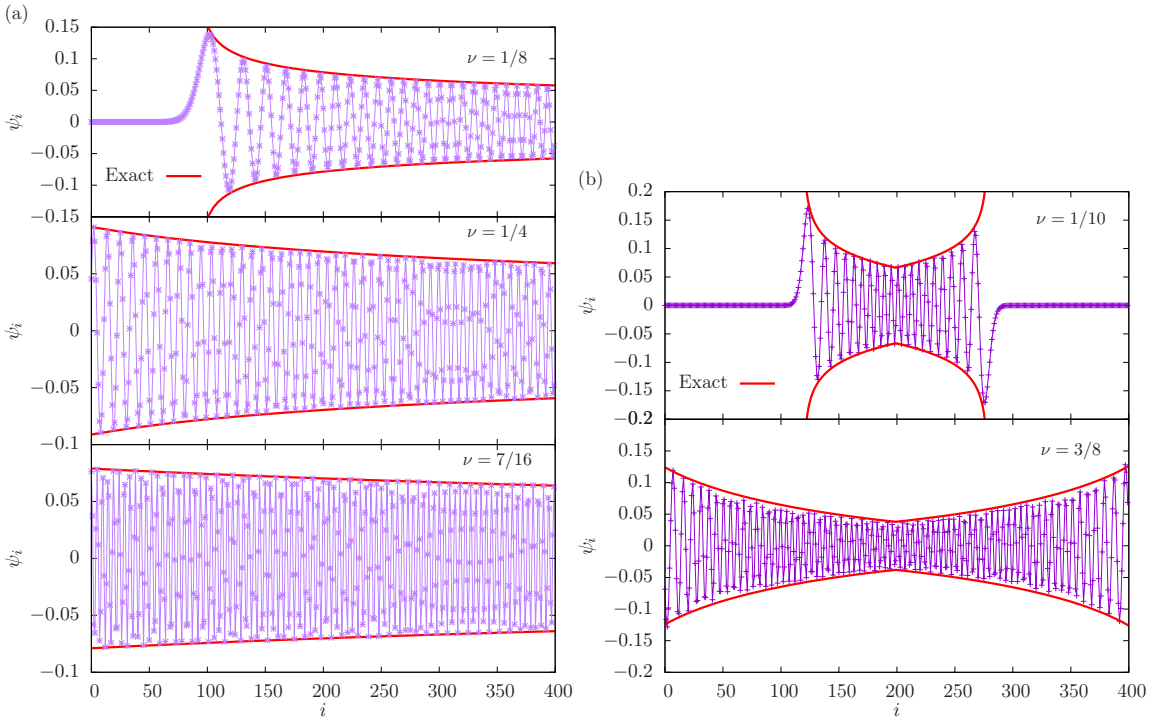

Figure 6.3: Comparing the modes obtained from Hamiltonian (6.1) using $N = 400$ for Rindler and Rainbow chains with the WKB approximation given in Eq. (6.30), considering different filling fractions ν. The continuous red line represents the semiclassical approximation Eq. (6.30) to the continuous approximation given in Eq. (6.26). Panel (a): Rindler chain, from top to bottom, $m = 50$, 100 and 175. Panel (b): rainbow chain, top to bottom $m = 40$ and $m = 150$.

We have checked the validity of Eq. (6.30) in Fig. 6.3. In panel (a) we have chosen a Rindler system with $J(x) = \frac{1}{4} + x$ with $N = 400$ and shown the modes $m = 50$, 100 and 175. The continuous red curve in each case corresponds to the approximation (6.30), suitably normalized. We can see that the decay is nearly perfect. Panel (b) shows the same situation for the rainbow chain, using $h = 4$, $N = 400$, with the modes $m = 40$ and $m = 150$. We can see that the decay is nearly perfect in all the cases.

We should stress that our continuum approximation, Eq. (6.19) can not be employed to obtain a continuum limit of our original model. Indeed, for $a \to 0$, all terms containing derivatives of the field $\psi(x)$ vanish, thus rendering the equation useless. In order to make sense of Eq. (6.19) we must keep a finite and this implies that we should preserve all derivatives of the gradient expansion. Alternatively, we may define a new physical variable $u = x/a$, in such a way that any derivative with respect to x multiplied by a becomes a derivative with respect to u: $\partial_u = a\partial_x$.

6.5 Density profiles

Our next aim will be to provide a continuum approximation to the density profiles observed for free-fermionic chains with inhomogeneous hopping amplitudes away from half-filling, based on the validity of the Schrödinger equation on a different manifold, Eq. (6.26), using a certain effective potential $V(x)$. If we fill all orbitals up to a certain energy E, we will observe depletion in the classically forbidden regions, defined by $V(x) > E$, and bounded by the turning points, defined by $V(x_*) = E$. To order zero in a, from (6.27), we may estimate these turning points as

$$E = -\frac{1+\cos(k_F a)^2}{\cos(k_F a)} J(x_*). \tag{6.31}$$

This result can also be obtained in a heuristic way, starting from a simplified version of Eq. (6.19),

$$\begin{aligned} E\psi(x)_{R/L} = -J(x) \big(& 2\cos(k_F a)\psi(x)_{R/L} \\ & \mp 2ai \sin(k_F a)\partial_x \psi(x)_{R/L} \\ & + a^2 \cos(k_F a)\partial_x^2 \psi(x)_{R/L} \big) . \end{aligned} \tag{6.32}$$

Now, we suppose that the wavefunction is locally a plane wave with a certain position dependent momentum $q(x)$, i.e. $\psi(x)_{R/L} \sim e^{\pm iq(x)x}$. Then,

$$\begin{aligned} E = & -J(x)(2\cos(k_F a) + 2a\sin(k_F a)q(x) \\ & - a^2 \cos(k_F a) q(x)^2), \end{aligned} \tag{6.33}$$

and we can then obtain $q(x)$ solving a quadratic equation. If $q(x)$ is not real, then x belongs to the classically forbidden region. Thus, by making the discriminant zero we reach Eq. (6.31).

We can obtain an approximation to the local density $\rho(x)$ of a Schrödinger equation by considering a particle with energy E traveling through a small segment of size Δx around position x, where the potential energy is $V(x)$. Its momentum will be given by

$$q(x) = \sqrt{2m(E - V(x))}. \tag{6.34}$$

Within a semiclassical approximation we may estimate the number of orbitals with presence on that segment assuming that the momenta are discretized as $q(x) \approx n\pi/N \approx \pi\rho(x)$. Thus, we have

$$\rho(x) \approx \frac{1}{\pi}\sqrt{2m\left(E - V(x)\right)}. \tag{6.35}$$

In our case, for low values of $k_F a$ we also build the density by filling up the modes of a Schrödinger equation, and thus we may write

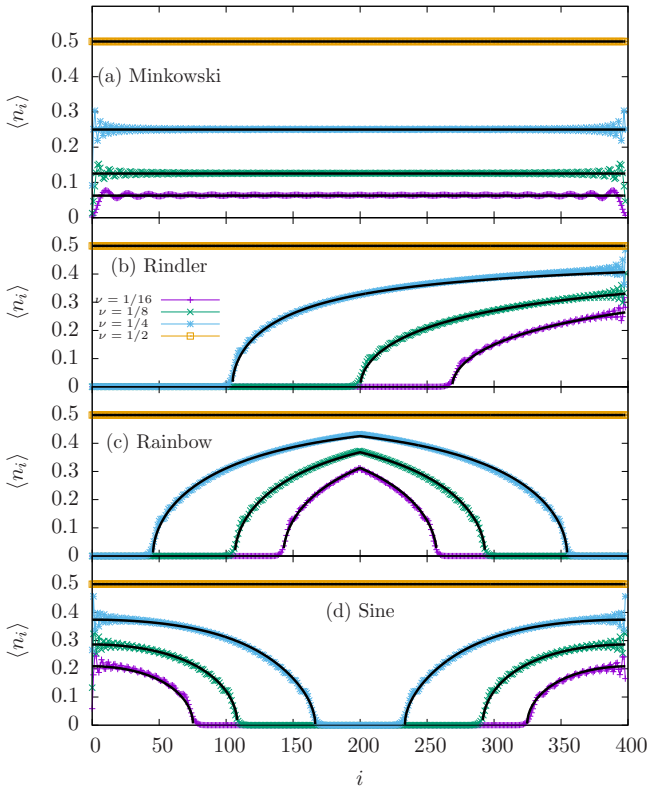

Figure 6.4: Fermionic density for a chain of $N = 400$ sites with different filling fractions 1/2, 1/4, 1/8 and 1/16 and four different inhomogeneities: (a) Minkowski, (b) Rindler, $J(x) = x$, (c) Rainbow, $J(x) = \exp(-\hat{h}|x - 1/2|)$ with $h = 4$ ($h = \hat{h}N$) and (d) Sine, $J(x) = 1 + 0.5\cos(2\pi x)$. The black curves correspond to the theoretical curves, given by Eq. (6.37).

$$\tilde{\rho}(\tilde{x}) \approx \frac{1}{\pi}\sqrt{\frac{2}{a^2}\left(E - 2\tilde{J}(\tilde{x})\right)}. \tag{6.36}$$

Yet, this expression is designed for the transformed coordinate $\tilde{x}$. We should express it in our original coordinate in order to make useful predictions, using $\tilde{\rho}(\tilde{x})d\tilde{x} = \rho(x)dx$, we have $\rho(x) = \tilde{\rho}(\tilde{x})\tilde{J}^{-1/2}(\tilde{x})$, and therefore

$$\rho(x)a \approx A\sqrt{\frac{E}{J(x)} - 2}, \tag{6.37}$$

where A is a normalization constant. Indeed, $\rho(x)a$ can be interpreted as the local occupation, which can be directly compared to $\langle c_i^\dagger c_i \rangle$ for $i = x/a$. Interestingly, the density is directly related to the *inverse* of the hopping function $J(x)$. Notice that Eq. (6.37) is not necessarily valid for larger values of $k_F a$, since the modes that we are filling up do not correspond to the same Schrödinger equation.

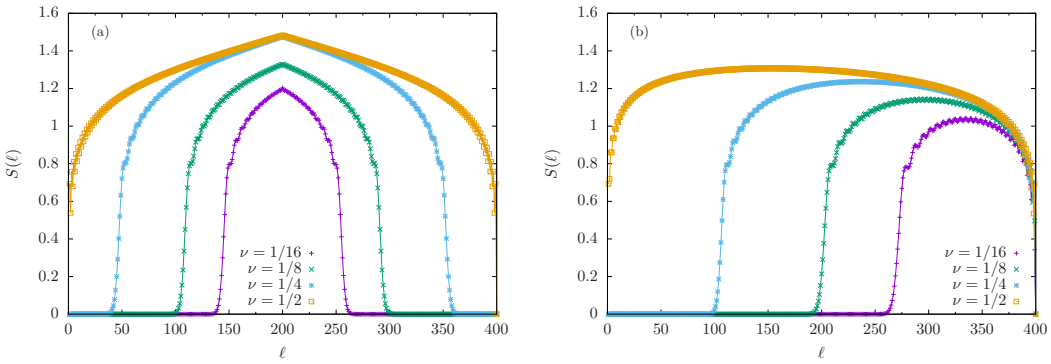

Figure 6.5: EE of free fermionic systems on an optical chain with $N = 400$ for two different metrics. (a) Rainbow (Eq. (6.4) with $h = 4$), (b) Rindler (Eq. (6.2) with $J_0 = 1$.

We have computed numerically the fermionic density for different hopping functions, and observed depletion in all the considered cases, except for the Minkowski space-time, as we can see in Fig. 6.4. As expected, the depleted regions decrease their size as the filling fraction grows. Moreover, Eq. (6.37) predicts very well the density profiles for all $\nu \leq 1/4$. Surprisingly, for all values of the filling fraction the functional form

$$\rho(x)a = A\sqrt{\frac{1}{J(x)} - B}, \tag{6.38}$$

fits extremely well the numerical density profiles, as we can check in Fig. 6.4.

6.6 Entanglement entropy and entanglement contour

We already saw in Chapter 5 that the entanglement entropy for deformed systems at half-filling is given by a CFT extension of Eq. (5.11), written in Eq. (5.14)

$$S(\ell) = \frac{c}{6}\log\left(\frac{\tilde{N}}{\pi\Delta\tilde{x}}\sin\left(\frac{\pi\tilde{\ell}}{\tilde{N}}\right)\right) + S_{\text{non-univ}}, \tag{6.39}$$

where ℓ is the size of the block we are considering.

However, for filling-fractions $\nu \neq 1/2$ the EE also shows depleted areas which are shown in Fig. 6.5: (a) rainbow and (b) Rindler. As it was expected, these empty regions coincide with the depleted areas in the fermionic density, for the corresponding filling-factor, represented in Fig. 6.4: there can not be entanglement in empty regions.

Moreover, it has been conjectured in previous works [116] that the region where the particles can be placed must be a CFT and, thus, CFT predictions can be used. With that aim, one may think that Eq. (6.39) should be able to reproduce the EE outside of the depleted areas that appear when we are away from half-filling.

However, we have not be able to obtained successful results in this direction yet although we expect it to be true.

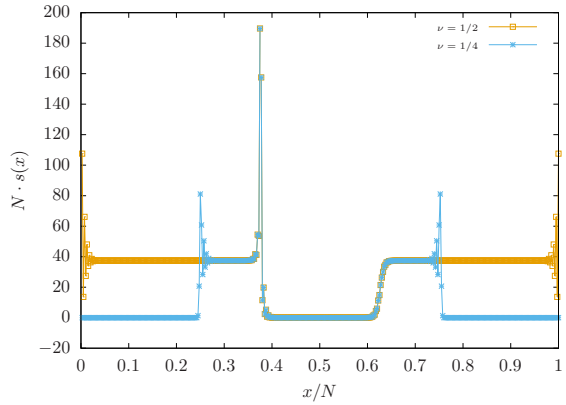

Figure 6.6: Contour functions for the entanglement entropy of the rainbow case (Eq. (6.4)), $L \times s_A(x)$ and $L \times_B (x)$ in terms of x/L, with $h = 4$ and $L = 400$. We have considered two complementary blocks $A = (0, x_0)$ and $B = (x_0, L)$, separated by one entangling point at $x_0 = 150$. Two filling fractions have been brought into play: $\nu = 1/2$ (orange) and $\nu = 1/4$ (blue). The depleted regions can be observed away from half-filling. A linear divergence is observed in the neighborhood of the entangling point, explained in [103], while finite parity oscillations occur close to the boundaries of the segment.

Furthermore, one can also look at the entanglement contour (see Section 2.8) for a deformed system away from half-filling. We have consider the rainbow case for two different filling-fractions shown in Fig. 6.6: $\nu = 1/2$ and $\nu = 1/4$.

Indeed, there are several analytical results for the entanglement contour of the inhomogeneous chain with rainbow hopping amplitudes [103], which explain the linear divergence observed in the neighborhood of the entangling point in Fig. 6.6, while finite parity oscillations occur close to the boundaries of the segment. On the other side, the depleted areas appear to be exactly the same as in the fermionic density and in the entanglement entropy for each appropriate filling-factor.

6.7 Compensating and mimicking potentials

As we have discussed above, our continuum approximation led to an effective Schrödinger equation with a potential whose classically forbidden areas correspond to the depletion regions of the particle density.

Let us extend our original model, Eq. (6.1), introducing an inhomogeneous chemical potential $\boldsymbol{\mu} = \{\mu_i\}_{i=1}^N$,

$$H(\mathbf{J}, \boldsymbol{\mu})_N = -\sum_{i=1}^{N-1} J_i \left(c_i^\dagger c_{i+1} + \text{h.c.} \right) + \sum_{i=1}^{N} \mu_i c_i^\dagger c_i. \tag{6.40}$$

We may introduce a *compensating potential*, defined by

$$\mu_i = \mu_0 J_i, \tag{6.41}$$

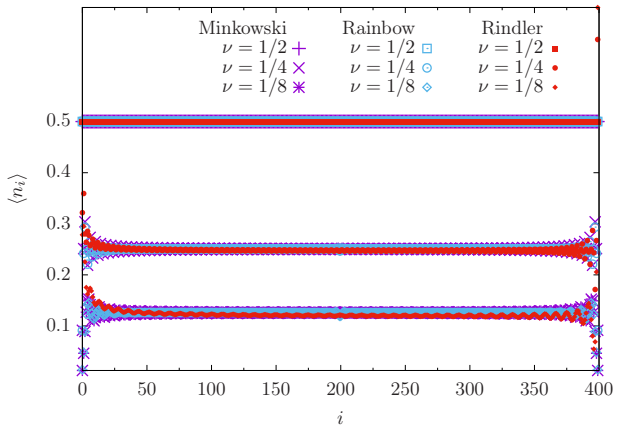

Figure 6.7: Density profile for the GS of Hamiltonian (6.40) with a compensating potential, using three types of hopping functions: Minkowski, Rindler and rainbow, and different filling fractions, $\nu = 1/2$, $1/4$ and $1/8$.

where we implicitly assume that the chemical potential at site i is given by the average of its two neighboring hopping constants. With such choice, the GS of Hamiltonian (6.40) always presents a flat density profile, for all filling fractions, whenever $\mu_0 = 2\cos(k_F a)$, as it can be checked in Fig. 6.7. In mathematical terms, the reason is that the added chemical potential cancels out the potential energy term in Eq. (6.19). In this case the Hamiltonian does not present any terms which are independent of the lattice spacing, a, and thus we are allowed to renormalize the hopping function, $J(x) \to \infty$, $a \to 0$, while $J(x)a \to \hat{J}(x)$, thus yielding a proper continuum limit.

The physical meaning of this compensating effect is also interesting. Let us start out with the GS of Hamiltonian (6.40) using $J_i = 1$ and $\mu_i = 0$, filled up with νN fermions. We notice that the energy cost of introducing a new particle does not decay to zero as the system size increases, and instead is bounded by $-2\cos(k_F a)$, with $k_F a = \pi\nu$. Thus, the system can not be conformally invariant. We can change that by introducing a chemical potential, $\mu_i = 2\cos(k_F a)$. In that case, the energy cost of introducing extra particles becomes zero. This new system can be set in any different static 1+1D metric by introducing an appropriate Weyl factor, thus yielding the compensating potential system [102, 119].

Now we may ask a complementary question. Let us keep a flat hopping function, $J(x) = 1$, i.e. $J_i = 1$. Can we find a chemical potential $\{\mu_i\}$ which *mimics* the density profiles obtained from the inhomogeneous hopping function without chemical potential, for the same filling fraction? Interestingly, the answer is yes.

Let us consider the bulk equations to obtain the eigenstates of the original hopping matrix. Let $(\psi_1 \cdots \psi_N)^T$ be the eigenvector of the hopping matrix with eigenvalue E. Then,

$$J_{n-1}\psi_{n-1} + J_n\psi_{n+1} = E\psi_n, \tag{6.42}$$

which can be rewritten for very smooth $\mathbf{J}$ as

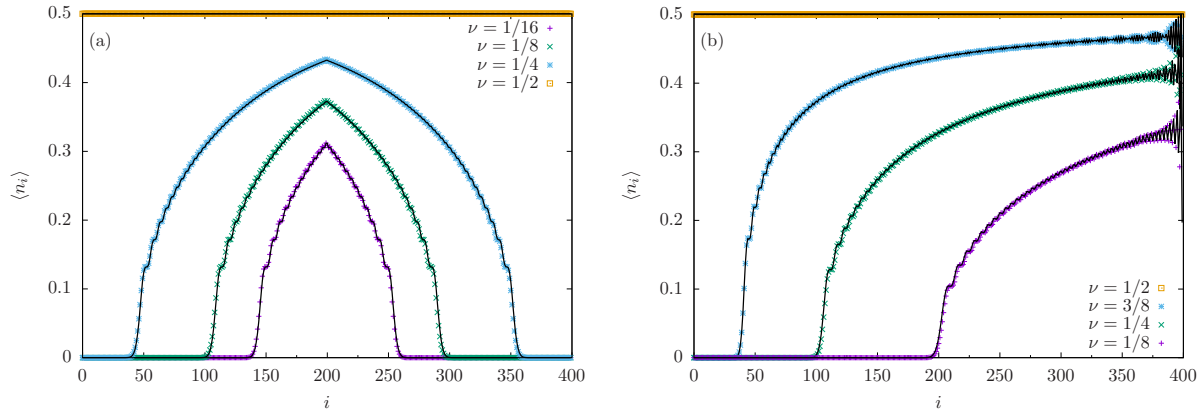

Figure 6.8: Density profiles of the GS of Hamiltonian (6.40) using homogeneous hoppings, $J_i = 1$, and the corresponding mimicking potential, Eq. (6.46), for (a) a rainbow chain with $N = 400$ and $h = 4$ and (b) a Rindler system with $J(x) = x$, using the filling fractions shown in the key, along with the original density profiles using inhomogeneous hoppings and without chemical potential.

$$J_n(\psi_{n-1} + \psi_{n+1}) \approx E\psi_n. \tag{6.43}$$

Now we can take the hopping amplitude to the RHS, assuming that it is non-zero,

$$\psi_{n-1} + \psi_{n+1} - \left(\frac{E}{J_n} - E\right)\psi_n \approx E\psi_n, \tag{6.44}$$

which can be read as a homogeneous hopping Hamiltonian with a chemical potential μ_n of the form

$$\mu_n = E\left(\frac{1}{J_n} - 1\right), \tag{6.45}$$

i.e. the chemical potential depends on the energy itself, and thus the secular equation becomes non-linear. This reasoning motivates the following *mimicking* chemical potential

$$\mu_i = \frac{\mu_0}{J_i} \tag{6.46}$$

In Fig. 6.8 we plot the density profiles associated to the ground states of Eq. (6.40) with the above chemical potential Eq. (6.46), along with the original density profiles obtained for inhomogeneous hoppings and without chemical potential. The coincidence between them both is extremely remarkable, given that Eq. (6.46) only ensures the similarity between the highest energy filled mode in both cases.

Thus, we are led to ask whether the two GS are the same or not. Fig. 6.9 provides a negative answer to that question. In it we have shown the entanglement entropies (EE) of blocks $A = [1, \cdots, \ell]$ as a function of ℓ for both states in the rainbow case (6.39), defined as $S(\ell) = -\mathrm{Tr}_A(\rho_A \log \rho_A)$ with $\rho_A = \mathrm{Tr}_{\bar{A}} |\Psi\rangle \langle\Psi|$. As it was shown in [116], the EE of our states is approximately equal to the EE of blocks of a shorter

system bounded by the turning points at half-filling [102, 119]. Yet, the EE of the GS of the mimicking system are different, presenting strong similarities to the EE of homogeneous chains [69].

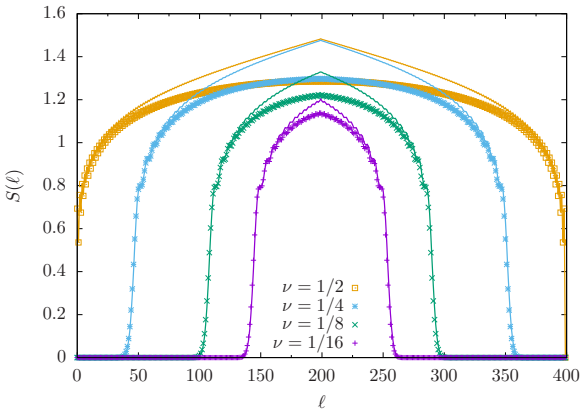

Figure 6.9: Entanglement entropy $S(\ell)$ of blocks of the form $[1, \cdots, \ell]$ of the mimicking GS (points) and the original GS (lines), with the same filling fractions for rainbow chains with $h = 0.01$ and $N = 400$.

6.8 Conclusions and further work

A free-fermionic chain without chemical potential and with inhomogeneous hoppings at half-filling will present an exactly homogeneous density profile. In the continuum limit, this system represents a Dirac fermion on a static curved background, with the lapse function of the metric given by the hopping amplitudes. Yet, if we move away from half-filling we will notice that the particles concentrate at the regions with higher hopping amplitudes, and leave the regions with lower hopping amplitudes empty, a phenomenon that we have called *depletion*.

In the strong inhomogeneity regime, the Dasgupta-Ma renormalization scheme allows to prove that this should be the case, since the particles will establish bonds on top of the larger hoppings, either original or renormalized. Thus, the depletion is exact.

In the weak inhomogeneity regime, we have shown that the associated single-particle problem is equivalent to a Schrödinger equation on a different static curved manifold, with the lapse function given by the *square root* of the hopping amplitudes, and a potential determined by the hopping amplitudes and the filling fraction. Notice that this shows that the effective system does not show conformal invariance. Naturally, the laplacian operator must be substituted with the Laplace-Beltrami operator corresponding to the associated metric, and the depleted regions correspond to the classically forbidden areas of this Schrödinger equation. The wavefunctions and the density profiles can be accurately obtained using a semiclassical approximation.

It is interesting to ask how this model breaks the conformal symmetry which is known to hold at half-filling. Indeed, a second order expansion of the fields is

required to find a continuum approximation to our lattice model, instead of the first-order expansion at half-filling. The second-order derivative term, which maps into a laplacian, breaks explicitly the conformal invariance introducing a length scale, which is inversely proportional to the effective mass.

We may introduce a *compensating potential* in our system, through a chemical potential proportional to the hopping amplitudes, which exactly cancels the depletion effect and provides exactly homogeneous density profiles. In this case, the continuous approximation allows us to conjecture that the system recovers its full conformal invariance.

We have also introduced a *mimicking potential*, which provides exactly the same density profiles away from half filling on a fermionic chain with homogeneous hoppings. Interestingly, this mimicking potential is inversely proportional to the hopping amplitudes. Yet, the associated ground state is not the same as in the original case, as we have been able to show checking the entanglement entropies of lateral blocks. The ground states of the compensating and mimicking systems present interesting challenges which should be considered in further work.

Chapter 7

Ergotropy and entanglement in critical spin chains

This chapter is based in the following article:

- B. Mula, E.M. Fernández, J.E. Alvarellos, J.J. Fernández, D. García-Aldea, S.N. Santalla, J. Rodríguez-Laguna, *Ergotropy and entanglement in critical spin chains*, Phys. Rev. B **107**, 075116 (2023).

A subsystem of an entangled ground state is in a mixed state. Thus, if we isolate this subsystem from its surroundings we may be able to extract work applying unitary transformations, up to a maximal amount which is called ergotropy. Once this work has been extracted, the subsystem will still contain some bound energy above its local ground state, which can provide valuable information about the entanglement structure. We show that the bound energy for half a free fermionic chain decays as the square of the entanglement entropy divided by the chain length, thus approaching zero for large system sizes, and we conjecture that this relation holds for all 1D critical states.

7.1 Introduction and context

Quantum thermodynamics applies the core concepts of quantum information theory [125–127] to design optimal nanoscale devices, such as quantum thermal machines [128–130]. A very fruitful concept is that of *ergotropy* [131, 132], i.e. the maximal work that can be reversibly extracted from a mixed state, which is a crucial tool in order to build efficient quantum batteries [133–135]. Indeed, ergotropy is known to be strongly influenced by the presence of quantum correlations of different types [136–140]. Of course, if we lift the reversibility constraint, we may use quantum measurements to extract work in an optimal way [141, 142].

Yet, the connection works in both directions, and we may employ quantum thermodynamics to characterize the entanglement structure of a quantum system. As it is well known and it was explained in Chapter 2, a subsystem of a ground state (GS) is usually not in its local ground state. Instead, it must be described by

a reduced density matrix, which can be expressed as a thermal density matrix under a certain entanglement Hamiltonian (EH), which need not coincide with the local one [143, 144]. Notice that the EH allows us to describe the entanglement structure of complex quantum states in thermal terms. Both the EH and its eigenvalues, which define the entanglement spectrum (ES) [68], have provided invaluable insight to characterize the entanglement structure of the low energy states of quantum many-body systems [106, 112, 145–151], in some cases exploiting their conformal invariance [103, 119, 152].

In this work we introduce the notion of *subsystem ergotropy* within a GS in order to characterize its entanglement structure through the analysis of the energetic relations between a subsystem A and its environment B. The expected value of the local energy of any subsystem will typically exceed its own GS energy, and the subsystem ergotropy is defined as the part that can be extracted in the form of work. Our analysis will focus on a few simple quantum many-body systems, starting with a detailed analysis of free fermionic chains, and extending our study to other critical spin chains. In all the considered cases, we benefit from the constraints imposed by conformal invariance on the reduced density matrix. We show that, once the maximal work has been extracted, the remaining bound energy presents universal scaling as the square of the entanglement entropy of the block divided by the system size, thus approaching zero for large system sizes.

This chapter is organized as follows. Section 7.2 develops the basic theoretical background, combining tools from quantum thermodynamics and quantum information theory. Then we show our analytical and numerical calculations for a free fermionic chain in Section 7.3. Other critical spin chains, such as the Ising model in a transverse field or the Heisenberg model, are briefly considered in 7.4.

7.2 Theoretical background

7.2.1 Ergotropy of generic mixed states

The *ergotropy* W of a mixed state ρ with respect to a Hamiltonian H can be defined as the maximal amount of work that can be extracted from the state by applying unitary operations [131, 132], i.e.

$$W \equiv \max_{U} \Big(\mathrm{Tr}(\rho\, H) - \mathrm{Tr}(U \rho U^{\dagger}\, H) \Big) , \tag{7.1}$$

where U is any unitary transformation. Alternatively, it can be shown [131] that the ergotropy corresponds to the maximal work that can be reversibly extracted from the system, but the former characterization suits our purposes better. A state defined by a density matrix ρ is called *passive* with respect to H when its ergotropy is zero, i.e. when we can not extract any work from it by performing unitary operations. In that case, the eigenstates of H and ρ must be *aligned* such that the highest probability state of ρ will correspond to the lowest eigenstate of H, and so on. Thermal states built on H, written as $\rho = Z^{-1} \exp(-\beta H)$ with $\beta = 1/T$ the inverse temperature (we assume $k_B = 1$) and Z the normalization factor, are always passive with respect to their Hamiltonian, but the converse is not true. In other words: all thermal states

are passive, but not all passive states are thermal.

Let $\lambda_0 \geq \lambda_1 \geq \cdots \geq \lambda_{N-1}$ be the eigenvalues of ρ, where N is the dimension of the Hilbert space. Similarly, let $E_0 \leq E_1 \leq \cdots \leq E_{N-1}$ denote the eigenvalues of H in ascending order, and let $E = \mathrm{Tr}(\rho H)$ be the expected value of the energy of the system. Now, let us define the passivized state,

$$\tilde{\rho} \equiv U \rho U^\dagger, \tag{7.2}$$

with U the unitary operator implicitly defined in Eq. (7.1). Naturally, the spectra of both density matrices must coincide,

$$\mathrm{Sp}(\rho) = \mathrm{Sp}(\tilde{\rho}) = \{\lambda_k\}_{k=0}^{N-1}, \tag{7.3}$$

Since the passive energy $\widetilde{E} \equiv \mathrm{Tr}(\tilde{\rho} H)$ must be minimal among all density matrices with the same spectrum, we deduce that the maximal probability, λ_0, must share eigenstate with the the GS energy of H, E_0; the second probability, λ_1, with the first excited state, E_1, and so on. Therefore,

$$\widetilde{E} = \sum_{k=0}^{N-1} \lambda_k E_k, \tag{7.4}$$

and degeneracies do not pose any complications. The ergotropy is given by

$$W \equiv E - \widetilde{E} \leq E - E_0. \tag{7.5}$$

Notice that since we have chosen a common basis of eigenvectors of H and $\tilde{\rho}$, the two operators must commute, $[H, \tilde{\rho}] = 0$. In general, this density matrix $\tilde{\rho}$ need not be *thermal* for H, i.e. it may not be written as $\tilde{\rho} \approx Z^{-1} \exp(-\beta H)$ for any value of β.

7.2.2 Subsystem ergotropy

Let us consider a quantum system on a composite Hilbert space $\mathcal{H} = \mathcal{H}_A \otimes \mathcal{H}_B$, with Hamiltonian H,

$$H = H_A \otimes I_B + I_A \otimes H_B + H_{AB} \equiv H_0 + H_{AB}, \tag{7.6}$$

where $H_{\{A,B\}}$ acts on $\mathcal{H}_{\{A,B\}}$ respectively, and H_{AB} will be called the *interaction Hamiltonian*. Of course, this decomposition is not unique, and we will assume that H_{AB} has been chosen *as small as possible* in some norm. Let $|\Psi\rangle$ be the (non-degenerate) GS energy of H, which can always be written as a Schmidt decomposition given by Eq. (2.16)

$$|\Psi\rangle = \sum_{k=1}^{n_S} \lambda_k^{1/2} |\alpha_k\rangle \otimes |\beta_k\rangle , \tag{7.7}$$

where $|\alpha_k\rangle \in \mathcal{H}_A$, $|\beta_k\rangle \in \mathcal{H}_B$ are two orthornormal sets, $\lambda_k \geq 0$ (also in non-increasing order) and $n_S \leq \min(\dim(\mathcal{H}_A), \dim(\mathcal{H}_B))$ is the Schmidt number. The reduced density matrix for part A can be written as in Eq. (2.17)

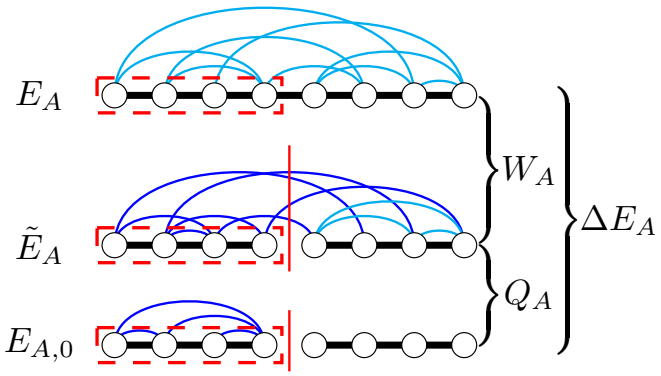

Figure 7.1: Illustrating the energies involved in our discussion of the subsystem ergotropy and their differences. Indeed, E_A denotes the expected value of the H_A within the global GS of H, $\tilde{E}_A$ is the minimal energy achieved through unitary operations on $\mathcal{H}_A$ and $E_{A,0}$ is the GS of H_A. Moreover, $\Delta E_A = E_A - E_{A,0}$ is the *excess energy*, $W_A = E_A - \tilde{E}_A$ is the subsystem ergotropy and $Q_A = \tilde{E}_A - E_{A,0}$ is the subsystem bound energy. The blue archs denote entanglement, as it is explained in the text. Notice that, in order to define these energies, block A must be physically separated from its environment.

$$\rho_A = \sum_{k=1}^{n_S} \lambda_k \left|\alpha_k\right\rangle \left\langle\alpha_k\right| . \tag{7.8}$$

Being positive definite, this matrix can always be written as a thermal density matrix,

$$\rho_A = \exp(-K_A), \tag{7.9}$$

where K_A is called the *entanglement Hamiltonian* (EH) associated to part A. Of course, K_A need not be equal to H_A, the local Hamiltonian, and this difference will be crucial in what follows. Also, let us introduce the entanglement spectrum (ES) as the spectrum of the EH [68].

Now let us physically separate subsystem A from its environment, i.e. subsystem B, by suddenly quenching H_{AB} to zero. The subsequent behavior of our subsystem will be described by H_A, with spectrum $\{E_{A,k}\}$, which we may assume to be non-degenerate. We define the three energies involved in our problem:

- $E_A = \left\langle\Psi|H_A \otimes I_B|\Psi\right\rangle$, the expected value of H_A in the global GS.
- $\widetilde{E}_A = \sum_k \lambda_k E_{A,k}$, the passive energy of the system, obtained through unitary transformations.
- $E_{A,0}$, the GS of H_A.

These three energies must be in descending order, $E_A \geq \tilde{E}_A \geq E_{A,0}$. We define the *excess energy* as $\Delta E_A \equiv E_A - E_{A,0}$. The subsystem ergotropy can be computed as

$$W_A = E_A - \tilde{E}_A, \tag{7.10}$$

while

$$Q_A \equiv \tilde{E}_A - E_{A,0}, \tag{7.11}$$

denotes the amount of energy which is unavailable, which we will call the *subsystem bound energy* [127]. See Fig. 7.1 for an illustration. The top panel represents the GS of H, and E_A is the energy associated to block A. The light blue archs represent the entanglement links [153,154] which characterize the entanglement structure. We reach the middle panel applying a suitable unitary operator on block A, maximally reducing its energy to $\widetilde{E}_A$ while preserving the entanglement spectrum and, *a fortiori*, the amount of entanglement with the rest of the system, which in this figure is represented by the number of links leaving A. The newly established links are now denoted in dark blue. Finally, the lowest panel denotes the GS of H_A, which is now disentangled from the environment, with energy $E_{A,0}$.

7.2.3 Ergotropy and time evolution

Once we have split the subsystem A from its environment, it will evolve under the action of its local Hamiltonian, H_A, following von Neumann's equation,

$$i\hbar\, \partial_t \rho_A = [H_A, \rho_A]. \tag{7.12}$$

Remarkably, this time evolution preserves both the expected value of the energy, E_A, and the full spectrum of the density matrix, even though the subsequent dynamics can be complex [155–157]. It is relevant to ask how much work we can obtain from this time-evolved density matrix employing unitary transformations, i.e. how the ergotropy evolves after the split quench. The answer is that the ergotropy is exactly preserved along the time evolution. A proof of this fact is straightforward. The time-evolved density matrix for the subsystem after the split can be written as $\rho_A(t) = V(t)\rho_A(0)V^\dagger(t)$ for some unitary transformation $V(t)$. The ergotropy of this matrix, defined in Eq. (7.1), is exactly the same, because the associated passivized state, given in Eq. (7.2), is exactly the same, if we just use the identity

$$\tilde{\rho}_A = U\rho_A(0)U^\dagger = UV^\dagger(t)\rho_A(t)V(t)U^\dagger, \tag{7.13}$$

allowing us to define a new unitary transformation, $\tilde{U} = UV^\dagger(t)$, such that $\tilde{\rho}_A = \tilde{U}\rho_A\tilde{U}^\dagger$. This result implies that the work extraction procedure need not start immediately after the disconnection between the subsystem and its environment, as long as the subsequent evolution is unitary.

7.2.4 Interaction energy inequality

Thus, we can extract work from a subsystem of a composite quantum state in its GS. Yet, this work should always be less than the corresponding increase in the energy of the system induced by our interaction, because otherwise the current system energy would be lower than the GS energy, E. We can prove this result

easily. After the unitary transformation on subsystem A the global system will be $\left|\tilde{\Psi}\right\rangle$, such that

$$\left\langle\tilde{\Psi}\right| H \left|\tilde{\Psi}\right\rangle = \widetilde{E} = \widetilde{E}_A + \widetilde{E}_B + \widetilde{E}_{AB}, \tag{7.14}$$

where each term on the rhs corresponds to the expectation value of one of the three operators, H_A, H_B and H_{AB} on $\left|\tilde{\Psi}\right\rangle$, and we notice that $\widetilde{E}_B = E_B$. This energy $\widetilde{E} \geq E$, the GS energy, which can be decomposed equally, $E = E_A + E_B + E_{AB}$. Taking into account that $E_A - \widetilde{E}_A = W_A$, we obtain

$$\widetilde{E}_{AB} - E_{AB} \geq W_A \geq 0. \tag{7.15}$$

which implies that the gain through ergotropy must be less or equal than the loss in the interaction term.

7.3 Ergotropy of a free fermionic chain

We now particularize the previous calculation to the case of a free fermionic chain, before extending our results to other critical spin chains. As we will show, the ergotropy and bound energy of free fermionic chains can be explicitly computed and present universal features associated to conformal invariance, in similarity to the Casimir energy [19, 20, 114]. For simplicity, we will restrict ourselves to the case in which the block A corresponds to the left half of the chain.

7.3.1 Free fermionic chains

Let us consider a fermionic chain of N (even) sites with open boundaries, described by the Hamiltonian

$$H_N = -\sum_{i,j=1}^{N} T_{ij}\, c_i^\dagger c_j, \tag{7.16}$$

where $c_i^\dagger$ and c_i denote the fermionic creation and annihilation operators on site i and $T_{ij} = \bar{T}_{ji}$ denotes the *hopping matrix*. We will focus on the homogeneous chain with open boundaries, whose hopping amplitudes are given by $T_{ij} = \delta_{i,j\pm1}$. In this case, the low energy behavior of the chain can be accurately represented by a conformal field theory (CFT) [21, 22].

In Section 3.1 we discussed that the GS of Hamiltonian (7.16) can be obtained through the eigenvalues $\{\varepsilon_k\}$ (in increasing order) and eigenmodes $\{U_{ki}\}$ of the hopping matrix T_{ij}, which are usually called single-body energies and modes, respectively. The spectrum presents particle-hole symmetry, $\varepsilon_k = -\varepsilon_{N+1-k}$, and the GS is obtained by filling up the $N/2$ negative energy modes, such that

$$E = \sum_{k=1}^{N/2} \varepsilon_k, \tag{7.17}$$

while the corresponding eigenstate is a Slater determinant determined by its correlator matrix (see Section 3.2), defined as

$$C_{ij} \equiv \left\langle c_i^\dagger c_j \right\rangle = \sum_{k=1}^{N/2} \bar{U}_{ki} U_{kj}. \tag{7.18}$$

All the entanglement properties can be determined from matrix C. Indeed, the reduced density matrix of any block A of size ℓ can be obtained diagonalizing the corresponding $\ell \times \ell$ submatrix, C_A. The set $\{\nu_k^A\}$ of eigenvalues of C_A, where each $\nu_k^A \in [0,1]$ determines uniquely the full ES, will be called *entanglement occupations*. The von Neumann entropy of block A, as we showed in Section 3.3, can be expressed as [106]

$$S_A = -\sum_{k=1}^{\ell} \left(\nu_k^A \log(\nu_k^A) + (1-\nu_k^A) \log(1-\nu_k^A) \right). \tag{7.19}$$

In Section 4.7 we discussed that conformal symmetry fixes the universal part of the entanglement entropy of a lateral block $A = \{1, \cdots, \ell\}$ of a critical chain with N sites, [13, 100, 101]

$$S_A \approx \frac{c}{6} \log\left(\frac{N}{\pi} \sin\left(\frac{\pi \ell}{N} \right) \right) + S_{\text{non-univ}}, \tag{7.20}$$

where $c = 1$ is the central charge of the associated CFT [21, 22] and $S_{\text{non-univ}}$ is a non-universal constant. Moreover, the EH of a free fermionic chain must also present a free fermionic form, Eq. (7.16), with a different hopping matrix [143, 144],

$$\rho_A = \frac{1}{Z} \exp(-K_A) = \frac{1}{Z} \exp\left(-\sum_{i,j=1}^{\ell} K_{ij}^A c_i^\dagger c_j \right). \tag{7.21}$$

The single-body energies of the EH, $\mathcal{E}_k^A$, can be obtained from the entanglement occupations through the Fermi-Dirac expression,

$$\nu_k^A = \frac{1}{1 + \exp(\mathcal{E}_k^A)}, \tag{7.22}$$

and they are (approximately) equally spaced, with a level separation given by the so-called *entanglement gap*, $\mathcal{E}_A \approx \mathcal{E}_{k+1}^A - \mathcal{E}_k^A$, which is known to behave like [103]

$$\mathcal{E}_A \approx \frac{2\pi^2}{\log(\gamma N)}, \tag{7.23}$$

where $\log \gamma \approx 2.3$ is a non-universal constant [103]. Moreover, an approximate inverse relation has been proposed between the entanglement gap and the entanglement entropy,

$$\mathcal{E}_A S_A \approx \frac{\pi^2}{3}. \tag{7.24}$$

7.3.2 Casimir energy and free fermions

Our next aim is to compute the three energies involved in our calculations: E_A, $\widetilde{E}_A$ and $E_{A,0}$. Let us start with $E_{A,0}$ for convenience. We proceed to build H_A, the hopping matrix for the block A, and obtain its eigenvalues, $\{\varepsilon_k^A\}_{k=1}^{N/2}$, in increasing order. The GS energy of A is given by

$$E_{A,0} = \sum_{k=1}^{N/4} \varepsilon_k^A. \tag{7.25}$$

An approximate expression for $E_{A,0}$ as a function of N can be provided [19,20,114]

$$E_0(N) = -c_0(N-1) - c_B - \frac{c\pi v_F}{24N} + O(N^{-2}), \tag{7.26}$$

where we distinguish three terms as explained in Chapter 5. The first one, $-c_0(N-1)$, with $c_0 = 2/\pi$, is the *bulk energy*. The second term, $-c_B = -(4/\pi - 1)$, is the *boundary term*. The third one provides the finite-size correction and is fixed by conformal invariance. Indeed, $c = 1$ is the central charge associated to our theory and $v_F = 2$ is the Fermi velocity given by Eq. (3.33). Thus, we have

$$E_{A,0} \approx -c_0 \left(\frac{N}{2} - 1\right) - c_B - \frac{\pi}{6N}. \tag{7.27}$$

We can use a similar strategy to estimate E_A, but we should proceed with care. Indeed, we can obtain E_A numerically from the GS of the whole chain, subtracting the energy associated to the central link and dividing by two,

$$E_A = \frac{E_0(N)}{2} - C_{N/2,N/2+1}. \tag{7.28}$$

The first term can be easily estimated from (7.27),

$$\frac{E_0(N)}{2} \approx -c_0 \left(\frac{N}{2} - 1\right) + \frac{c_0}{2} - \frac{c_B}{2} - \frac{\pi}{24N}, \tag{7.29}$$

and the second one can be found making use of (7.18), giving rise to an alternating behavior (see Appendix F),

$$C_{n,n+1} \approx -\frac{c_0}{2} - \frac{\pi}{24(N+1)^2} + \frac{(-1)^n}{2(N+1)\sin\left(\frac{\pi(n+1/2)}{N+1}\right)}, \tag{7.30}$$

which, since $N/2$ is even, reduces for the central link to

$$C_{N/2,N/2+1} \approx -\frac{c_0}{2} - \frac{\pi}{24(N+1)^2} + \frac{1}{2(N+1)}, \tag{7.31}$$

yielding

$$E_A \approx -c_0 \left(\frac{N}{2} - 1\right) - \frac{c_B}{2} - \left(\frac{\pi}{24} + \frac{1}{2}\right)\frac{1}{N}. \tag{7.32}$$

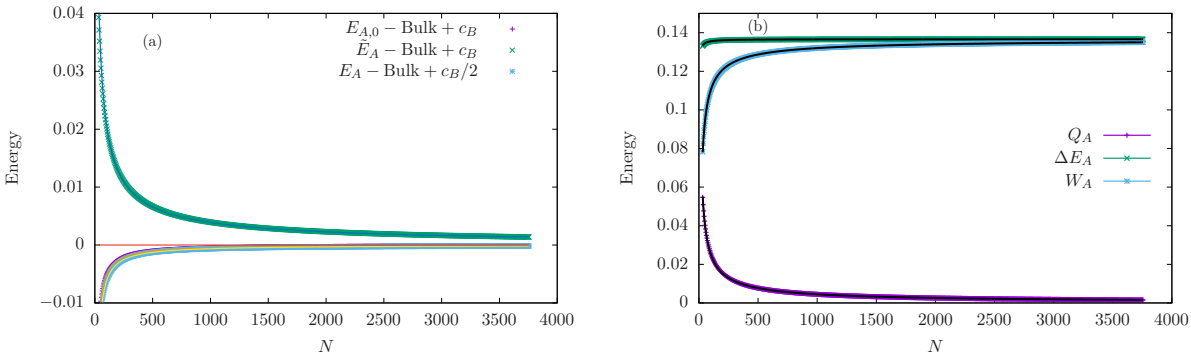

Figure 7.2: (a) The three energies involved, E_A, $\widetilde{E}$ and $E_{A,0}$, for a free fermionic chain, with A the left half, as a function of the system size, along with the theoretical asymptotic expressions, Eqs. (7.27), (7.32) and (7.39). (b) The three energy differences, $\Delta E_A = E_A - E_{A,0}$, $W_A = E_A - \widetilde{E}$, $Q_A = \widetilde{E} - E_{A,0}$, and their expected theoretical values according to Eqs. (7.33), (7.40) and (7.41).

We notice that the bulk term is exactly the same as for $E_{A,0}$, and the boundary term is exactly half, as we would expect intuitively, since this subsystem only possesses one boundary instead of two. We should stress that a naive calculation would yield a Casimir correction $\pi/(24N)$, but we obtain an additional contribution from the energy associated to the central link. The validity of the approximations to these two energies, $E_{A,0}$ and E_A, can be checked in Fig. 7.2 (a).

Therefore, the excess energy, $\Delta E_A = E_A - E_{A,0}$, is given by

$$\Delta E_A \approx \frac{c_B}{2} + \left(\frac{\pi}{8} - \frac{1}{2}\right)\frac{1}{N}. \tag{7.33}$$

7.3.3 Bound energy and entanglement

Extracting the maximal amount of work through unitary operators reversibly is equivalent to minimizing the block energy while preserving the full spectrum of the reduced density matrix. Thus, we proceed to *align* the occupation eigenvectors with the eigenstates of H_A, whose eigenvalues will be denoted by $\{\varepsilon_k^A\}$. The passive energy $\widetilde{E}_A$ can be written as

$$\widetilde{E}_A = \sum_{k=1}^{\ell} \nu_k \varepsilon_k^A. \tag{7.34}$$

Since $E_A \leq \widetilde{E}_A \leq E_{A,0}$, it is reasonable to consider that the passive energy $\widetilde{E}_A$ will also present the same bulk term as in Eq. (7.27), but with different corrections. Let us provide a similar asymptotic expansion to its value.

The eigenvalues of H_A can be found exactly as it shown in Section 3.4 (see Eq. (3.28)),

$$\varepsilon_p^A = -2\cos\left(\frac{p\pi}{N/2+1}\right), \tag{7.35}$$

with $p \in \{1 \cdots N/2\}$, and those of the correlation matrix C_A can also be approximated as

$$\nu_p^A \approx \frac{1}{1 + \exp\Big(-\beta\left(p - N/4\right)\Big)}, \tag{7.36}$$

where β corresponds to the entanglement gap, given in Eq. (7.23) [103]. Thus, the passive energy is given by

$$\widetilde{E}_A = \sum_{p=1}^{N/2} \varepsilon_p^A \nu_p^A \approx \sum_{p=1}^{N/2} \frac{-2\cos(2\pi p/N)}{1 + e^{-\beta(p-N/4)}}. \tag{7.37}$$

If we take the continuum limit, making use of the Sommerfeld expansion [158] and the Euler-Maclaurin formula, we arrive at

$$\widetilde{E}_A \approx -c_0\left(\frac{N}{2} - 1\right) - c_B - \frac{c\pi v_F}{12N} + \frac{2\pi^3}{3N\beta^2}, \tag{7.38}$$

so we obtain the final form

$$\widetilde{E}_A \approx -c_0\left(\frac{N}{2} - 1\right) - c_B - \frac{\pi}{6N} + \frac{\log^2(\gamma N)}{6\pi N}. \tag{7.39}$$

The reader can find the detailed calculation in Appendix G.

We may now find the analytic expression for the ergotropy,

$$W_A = E_A - \widetilde{E}_A \approx \frac{c_B}{2} + \left(\frac{\pi}{8} - \frac{1}{2}\right)\frac{1}{N} - \frac{\log^2(\gamma N)}{6\pi N}, \tag{7.40}$$

where the requirement $W_A \geq 0$ demands that $c_B > 0$. This expression can be checked in panel (a) of Fig. 7.2. Furthermore, we can estimate the bound energy,

$$Q_A = \widetilde{E}_A - E_{A,0} \approx \frac{\log^2(\gamma N)}{6\pi N} \geq 0, \tag{7.41}$$

which is unconditionally positive, and can also be checked in panel (b) of Fig. 7.2. Notice that Eq. (7.41) implies that the bound energy is directly related to the inverse squared of the entanglement gap of the system, or the square of the entanglement entropy. Using Eq. (7.20) and Eq. (7.23), we obtain an approximate relation

$$Q_A\, N \approx \frac{6}{\pi} S_A^2, \tag{7.42}$$

which provides a relation between the entanglement entropy of a block of a free fermionic chain and the bound energy associated. Eq. (7.42) is the main prediction of this work, and we conjecture that its validity extends beyond the case of free fermionic chains, to any critical state in 1D described by a conformal field theory. The validity of this expression can be numerically checked in Fig. 7.3.

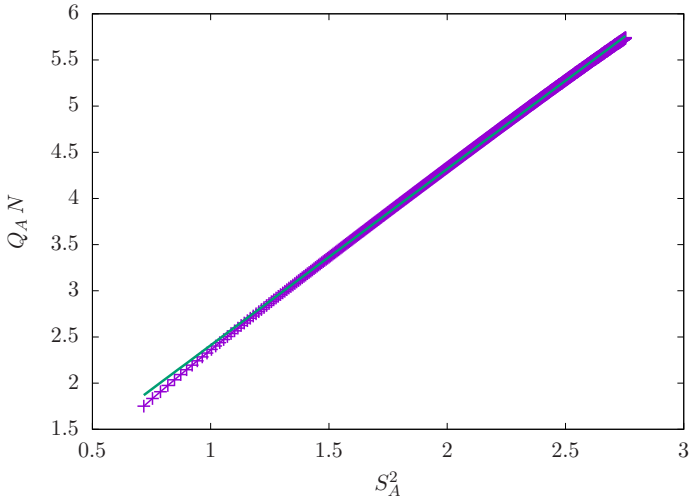

Figure 7.3: Numerical check of the linear relation between the bound energy multiplied by the system size, $Q_A N$, and the entanglement entropy squared, S_A^2 for the free fermionic chains, Eq. (7.42), for sizes N in the same range as in Fig. 7.2. The slope of the straight line, as expected, is $6/\pi \approx 1.9$.

.

We may define an ergotropy fraction $w_A = W_A/\Delta E_A$ and a bound fraction, $q_A = Q_A/\Delta E_A$, as the ratios between the ergotropy or the bound energy to the excess energy. We can see that $w_A \to 1$ and $q_A \to 0$ as $N \to \infty$, implying that for larger systems we can extract most of the excess energy in the form of work using unitary transformations.

7.4 Preliminary results on other critical models

We have considered two other spin chains, the critical Ising model in a transverse field (ITF) and the Heisenberg model, both introduced in Section 3.6, and performed numerical explorations using a combination of Lanczos and exact diagonalization for small systems which provide preliminary numerical evidence of the validity of Eqs. (7.41) and (7.42) for these systems.

The Hamiltonian of the ITF model that we have considered is given by

$$H_{\rm ITF} = -\sum_{i=1}^{N-1} \sigma_i^z \sigma_{i+1}^z - \Gamma \sum_{i=1}^{N} \sigma_i^x, \tag{7.43}$$

for $\Gamma = 1$. The low energy eigenstates of $H_{\rm ITF}$ are known to follow a conformal field theory with central charge $c = 1/2$ [21, 22]. Therefore, the entanglement entropy of the left half can be written as a linear function of $\log(N)$. We have obtained preliminary numerical results employing exact diagonalization up to size $N = 14$, which are shown in Fig. 7.4. In panel (a) we show with points the energy decomposition, ΔE_A, W_A and Q_A, for the left-half chain of the even sized systems, along with their fits with continuous lines to theoretical curves suggested by the generalization of Eqs. (7.33), (7.40) and (7.41), i.e.

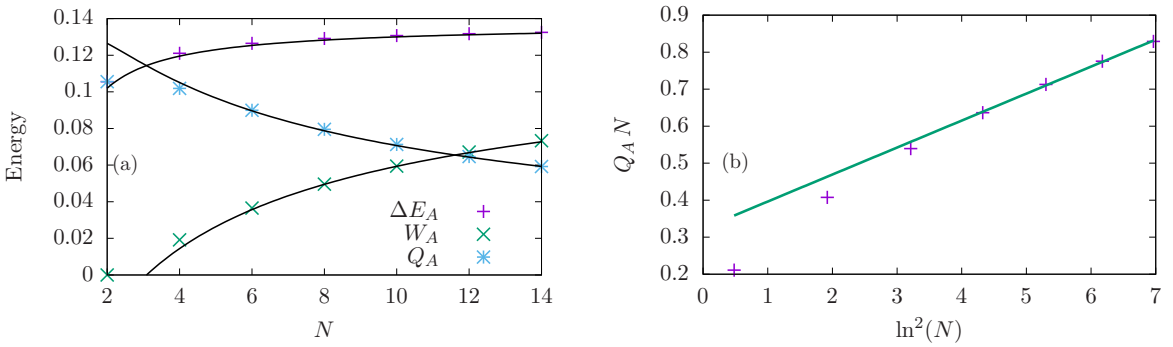

Figure 7.4: Subsystem energy decomposition for small Ising critical chains, with N up to 14. (a) Energies ΔE_A, W_A and Q_A for the left-half chain as a function of the system size, along with the expected theoretical fits. (b) Approximate linear relation between $Q_A N$ and $\log^2(N)$, showing the expected relation between Q_A and S_A, Eq. (7.42), along with a linear fit to the last five points.

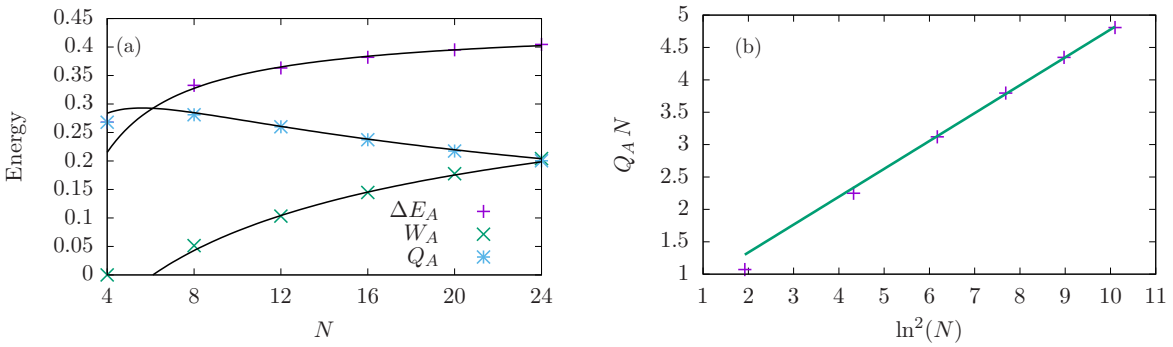

Figure 7.5: Subsystem energy decomposition for small Heisenberg chains, with N up to 24, using only multiples of four. (a) Energies ΔE_A, W_A and Q_A for the left-half chain, along with the expected theoretical fits. (b) Approximate linear relation between $Q_A N$ and $\log^2(N)$, showing the expected relation between Q_A and S_A, Eq. (7.42), along with a linear fit to the last five points.

$$\begin{aligned} \Delta E_A &\approx \alpha_1 - \frac{\alpha_2}{N}, \\ W_A &\approx \alpha_1 - \frac{\alpha_2}{N} - \alpha_3 \frac{\log^2(\alpha_4 N)}{N}, \\ Q_A &\approx \alpha_3 \frac{\log^2(\alpha_4 N)}{N}. \end{aligned} \tag{7.44}$$

In our case the optimal values of the parameters are $\alpha_1 \approx 0.137$, $\alpha_2 \approx 0.07$, $\alpha_3 \approx 0.044$ and $\alpha_4 \approx 5.5$. We would like to stress that we fit the 21 points of the three curves using the same values for the α_i parameters. In Fig. 7.4 (b) we observe an approximate linear relation between NQ_A and $\log^2(N)$, as expected, along with a linear fit obtained from the larger systems. Even though the functional form is shown to be approximately correct, we should use these fitting parameters with care, due to the small system size.

On the other hand, we have considered the antiferromagnetic spin 1/2 Heisenberg chain with open boundaries, given by the Hamiltonian

$$H_{\text{Heisenberg}} = \sum_{i=1}^{N-1} \vec{S}_i \cdot \vec{S}_{i+1}, \tag{7.45}$$

which also corresponds to a conformal field theory for low energies, with $c = 1$ in this case, and can be mapped to an interacting fermion Hamiltonian using the Jordan-Wigner transformation [21, 22]. As it was mentioned above, the GS can be analytically obtained using the Bethe Ansatz, but we have chosen to obtain it using the Lanczos algorithm up to $N = 24$, taking into account the full SU(2) symmetry of the model. Panel (a) of Fig. 7.5 shows the energy decomposition for the left-half of the chain, using only values of N which are multiples of four. Again, we plot along a fit of these 18 points to the form (7.44), obtaining approximate parameters $\alpha_1 \approx 0.44$, $\alpha_2 \approx 0.9$, $\alpha_3 \approx 0.41$ and $\alpha_4 \approx 1.32$. Panel (b) of Fig. 7.5 shows the linear relation between $Q_A N$ and $\log^2(N)$, highlighting the validity of Eq. (7.42), again comparing to a linear fit for the largest sizes.

The approximate validity of Eq. (7.42) in all three models is related to the fact that it only depends on the following facts:

- The Casimir expression for the energy of the GS.
- The affine relation between the entanglement entropy and $\log(N)$.
- The approximate inverse relation between the entanglement entropy and the entanglement gap.

All these relations stem from conformal invariance, a property shared by all three models discussed in this work.

It would be interesting to check the validity of our preliminary results for larger system sizes in the ITF and Heisenberg cases. The ITF case can be evaluated using

a combination of Jordan-Wigner and Bogoliubov transformations. The Heisenberg case is more involved, since e.g. the density matrix renormalization group (DMRG) can not be used in a straightforward manner [159], because we need to use both the entanglement spectrum and the full energy spectrum of the subsystem.

7.5 Conclusions and further work

In this work we have considered the excess energy possessed by a subsystem of a ground state. Part of this excess energy can be extracted via unitary operations, which we call *subsystem ergotropy*, and part of it can not be extracted in this way, which we call *subsystem bound energy*. For concreteness, we have considered one-dimensional systems which present conformal invariance, and we have done the calculations in detail for free fermionic chains, combining numerical calculations with a detailed analysis of the Casimir corrections to the GS energy. The most relevant relation found is a linear functional dependence between the subsystem bound energy and the square of its entanglement entropy divided by the system size. We have shown that this relation is likely to apply to other critical spin chains, thus allowing us to conjecture that its validity will extend to all 1D conformal field theories.

We would like to stress that, as the system size grows, the fraction of excess energy which can be extracted as work approaches one. In other words: almost all the subsystem energy becomes available in the thermodynamic limit. This result is non-trivial, although it responds to our intuition that for larger systems we have a larger freedom to manipulate the local mixed state. It is relevant to ask how general this result is. For instance, we may wonder about the behavior of the subsystem ergotropy away from criticality, i.e. for dimerized spin chains or for the Ising model with a non-critical value of the transverse field Γ, or how to extend it to higher dimensional systems.

Our results encourage further exploration of the application of quantum thermodynamics to the analysis and characterization of entanglement. Beyond the quantitative study of the ergotropy and bound energies, it is relevant to ask about the passive state which we obtain when all the ergotropy has been obtained. Indeed, it must be a thermal state under the entanglement Hamiltonian, but it is also relevant to ask about its properties under its own local Hamiltonian, and how do these two Hamiltonians relate. Given the relation between the entanglement Hamiltonian and the Unruh effect [94, 102, 160], this research programme may bear fruits also to the interplay between gravity, entanglement and thermodynamics.

Chapter 8

Conclusions

This last chapter provides a brief summary of the conclusions and the work done in this thesis.

In Chapter 5 we have considered critical chains, specially free fermionic chains, with inhomogeneous hopping amplitudes, *i.e.*, position-dependent couplings between sites along the chain. Inhomogeneous chains can be interpreted as deformed systems: the geometry of the system changes and must be described in terms of a Riemann metric. In particular, we can say we are in Minkowski flat space-time when dealing with the homogeneous case.

Furthermore, it has been proved that the Hamiltonian on the lattice is a discretized version of the Hamiltonian for a Dirac fermion on a curved $(1+1)$D space-time where the associated metric presents a position-dependent speed of light or, equivalently, a modulated index of refraction. Under the appropriate transformation of coordinates, this metric can be rewritten as conformally equivalent to the Minkowski metric. Indeed, conformal equivalence between the curved metrics due to inhomogeneity and the Minkowski metric suggests that CFT techniques may be employed to describe the properties of low-energy states. However, conformal equivalence between these metrics only holds when dealing with the ground state of the system, *at half-filling*, which constitutes the scenario of the results obtained in this work:

- Finite-size corrections to the Casimir energy are universal and the corresponding expressions are a deformed variant of the general CFT form. Indeed, we have found a theoretical description of the energy of the GS of a finite open chain with inhomogeneous hopping amplitudes. However, since numerical checks must be subtle because the finite-size correction is typically much smaller than the bulk energy term, we have considered an alternative observable: the Casimir force measured by a local observer located at the boundary of the system. As a consequence, we show that Casimir forces measured by an observer on the boundary on a weakly curved background are metric-independent followed by numerical evidence. Furthermore, these results have been extended to the inhomogeneous Heisenberg model.

- The GS energy of the lattice Hamiltonian corresponding to an open fermionic

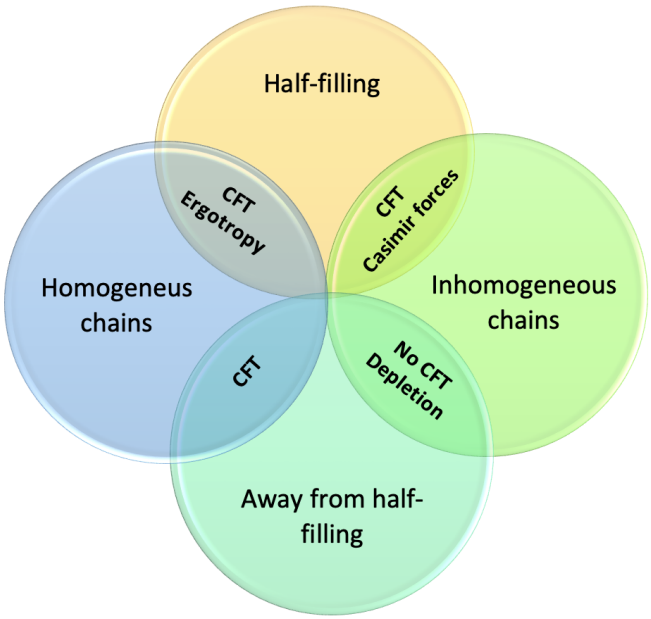

Figure 8.1: Overview of the topics addressed along this thesis.

chain with position-dependent hopping amplitudes is proportional to the sum of the hoppings in first-order perturbation theory. This leads us to claim that the force felt by a classical obstacle immerse in that state will be similar to the Newtonian gravitational force in the corresponding metric. Moreover, this conjecture suggests that the local correlators in the deformed vacuum are still homogeneous, *i.e.*, local correlators are rigid, which has been checked analytically and numerically.

In Chapter 6 we have worked with inhomogeneous free fermionic chains away from half-filling. In this case, conformal invariance is lost and new physics arises. The main result of this work is the following:

- The fermionic density for curved backgrounds shows completely empty regions away from half-filling, contrary to the homogeneous occupation found for all filling-fractions in Minkowski flat space-time and at half-filling in the inhomogeneous case. These depleted areas can be explained using a continuum approximation of the lattice Hamiltonian. With that aim, fermionic fields must be expanded to second order in the lattice spacing parameter. Indeed, we show that their appearance is due to an effective potential coming from a Schrödinger-like equation for curved backgrounds.

In Chapter 7 we show how quantum thermodynamics can be employed to characterize the entanglement structure of a quantum system. In particular, we consider a subsystem of the GS of a critical chain. The expected energy of any subregion will typically exceed its own GS energy and the subsystem ergotropy is defined as the

part of this energy that can be extracted in the form of work. The most relevant results of this work can be summarized as follows:

- Once the maximal work has been extracted, the remaining bound energy presents universal scaling as the square of the entanglement entropy of the block divided by the system size, thus approaching zero for large systems. This has been shown for open fermionic chains and extended to other critical systems in 1D, allowing us to conjecture that it may be applied to all 1D conformal field theories.

- The expected energy of a subsystem of the GS of a critical chain yields a Casimir correction plus an additional term coming from the energy associated to the central link of the chain, when the subsystem under consideration corresponds to half of the chain.

- The fraction of the excess energy which can be extracted as work approaches one as the system size grows.

Although the topics addressed throughout this work may look disconnected, they actually show important relations among them as it is shown in Fig. 8.1. We have considered homogeneous and inhomogeneous critical chains in two different scenarios: half-filling and away from half-filling.

Homogeneous chains show conformal invariance for any filling-fraction so CFT techniques have long been applied giving rise to well known analytical results, such as the energy of the GS for an open chain and EE predictions at half-filling. Thus, we have used homogeneous critical chains at their GS as the perfect scenario to study ergotropy. If we remain at half-filling but move towards inhomogeneous systems, conformal invariance is still preserved. Therefore, the study of Casimir forces on curved backgrounds has been developed in this scenario as an extension of the CFT predictions on flat space-times. However, inhomogeneous chains away from half-filling do not hold conformal invariance and new physics arises: depletion. In conclusion, in this thesis we have made use of CFT techniques when available and developed new theory when needed in order to explore low-energy states of both homogeneous and inhomogeneous critical chains.

Conclusiones

Este último capítulo constituye un breve resumen de las conclusiones generales y el trabajo realizado en esta tesis.

En el Capítulo 5 hemos considerado cadenas críticas, en especial cadenas de fermiones libres, con amplitudes de salto inhomogéneas, es decir, con acoplos dependientes de la posición entre los distintos sitios del sistema. Las cadenas inhomogéneas pueden ser interpretadas como sistemas deformados: la geometría del sistema varía y debe ser descrita en términos de una métrica de Riemann. En concreto, podemos decir que trabajamos en el espacio-tiempo plano de Minkowski cuando la cadena es homogénea.

Se ha demostrado que el Hamiltoniano en la red es una versión discretizada del Hamiltoniano de un fermión de Dirac en un espacio-tiempo curvo (1+1)D donde la métrica asociada presenta una velocidad de la luz dependiente de la posición o, de manera equivalente, un índice de refracción modulado. Bajo un cambio de coordenadas apropiado, esta métrica puede escribirse como equivalente conforme a la métrica de Minkowski. Esta equivalencia conforme entre métricas nos sugiere que las técnicas de CFT pueden ser utilizadas para describir las propiedades de los estados de baja energía. Sin embargo, la equivalencia conforme entre las métricas curvas y el espacio-tiempo plano solo ocurre cuando el sistema se encuentra en su estado fundamental, es decir, a llenado mitad, el cual constituye el escenario de los resultados obtenidos en este capítulo:

- Las correcciones de tamaño finito a la energía de Casimir son universales y sus expresiones correspondientes son una versión deformada de la predicción de la CFT. Hemos encontrado una descripción teórica del estado fundamental de una cadena infinita, con condiciones de contorno abiertas, en espacio-tiempos curvos. La comprobación numérica de estas correcciones no es sencilla debido a que son mucho más pequeñas que el término central. Por este motivo, definimos un nuevo observable: la fuerza de Casimir medida por un observador local situado en un extremo. En consecuencia, las fuerzas de Casimir, medidas por un observador que se encuentra en el borde del sistema, en espacio-tiempos ligeramente deformados, no dependen de la métrica. Este resultado se extiende, además, al modelo de Heisenberg inhomogéneo.

- El estado fundamental del Hamiltoniano discreto correspondiente a una cadena fermiónica con condiciones de contorno abiertas y amplitudes de salto

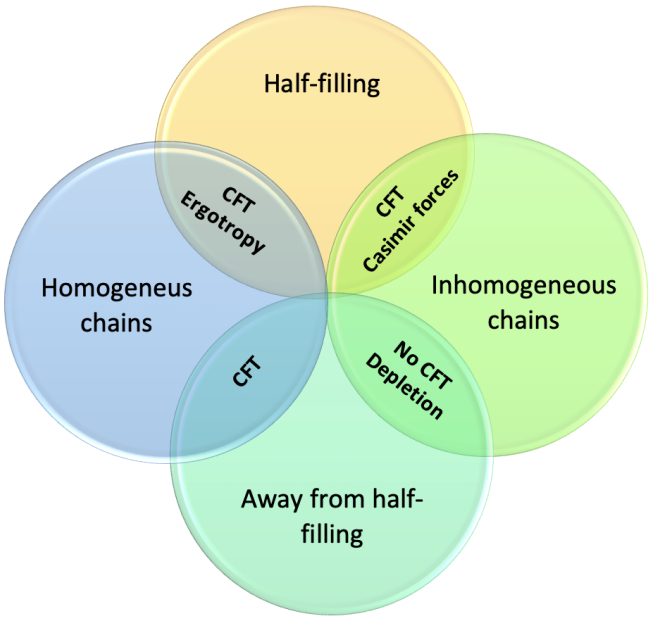

Figure 8.2: Visión general de los temas tratados en esta tesis.

inhomogéneas, es proporcional a la suma de estas amplitudes en teoría de perturbaciones a primer orden. Por tanto, la fuerza que experimienta un obstáculo clásico inmerso en este estado es similar al potencial gravitatorio en la métrica correspondiente. Además, esta conjetura sugiere que los correladores locales en el vacío deformado son los mismos que en el caso homogéneo, es decir, los correladores locales son rígidos, lo cual se ha comprobado tanto de manera analítica como numérica.

En el Capítulo 6 hemos considerado cadenas inhomogéneas de fermiones libres fuera del llenado-mitad. En este caso, no hay invariancia conforme y aparece nueva física. El resultado principal de este capítulo es el siguiente:

- La densidad fermiónica en sistemas deformados muestra zonas complematemnte vacías cuando nos encontramos fuera del llenado mitad. Por el contrario, la ocupación es homogénea para cualquier fracción de llenado en el caso homogéneo y para llenado mitad en el caso inhomogéneo, que es donde hay invariancia conforme. Las regiones de depleción pueden ser explicadas mediante una aprocimación continua del Hamiltoniano en la red. Para ello, los campos fermiónicos han de ser expandidos a segundo orden en el parámetro de espaciado de la red. Estas regiones de depleción aparecen debido a la existencia de un potencial efectivo procedente de una ecuación de tipo Schrödinger en espacio-tiempos curvos.

En el Capítulo 7 mostramos cómo la termodinámica cuántica puede ser utilizada para caracterizar la estructura de entrelazamiento de un sistema cuántico. Para ello, consideramos un subsistema del estado fundamental de una cadena crítica. La

energía esperada de cualquier subregión excede, en general, la energía de su propio estado fundamental. La parte de este exceso de energía que se puede extraer en forma de trabajo es lo que denominamos ergotropía del subsistema. Los resultados más relevantes de este capítulo son los siguientes:

- Una vez se ha extraido el máximo trabajo del subsistema, la energía que queda presenta un comportamiento universal que viene determinado por el cuadrado de la entropía de entrelazamiento del bloque dividida entre el tamaño total del sistema. Por tanto, tiende a cero para sistemas grandes. Este resultado ha sido comprobado para cadenas de fermiones libres y ha sido extendido a otras cadenas críticas, dando lugar a la conjetura de que es aplicable a todas las teorías conformes en una dimension.

- La energía esperada de un subsistema del estado fundamental de una cadena crítica presenta una correción de Casimir más un término adicional que proviene de la energía asociada al enlace central, cuando el subsistema que estamos considerando es la mitad de la cadena.

- La fracción de exceso de energía que puede extraerse del sistema en forma de trabajo tiende a uno cuando el sistema aumenta de tamaño.

Aunque los temas tratados en esta tesis parecen presentar poca relación entre sí, estos están estrechamente conectados tal y como se puede ver en la Fig. 8.2. Hemos considerado cadenas homogéneas e inhomogénas en dos escenarios diferentes: a llenado mitad y fuera del llenado mitad.

Las cadenas homogéneas presentan invariancia conforme para cualquier fracción de llenado, por lo que las técnicas de CFT pueden ser utilizadas. Los estados fundamentales de los sistemas homogéneos a llenado mitad han constituido el escenario para el estudio de la ergotropía. Si nos mantenemos a llenado mitad pero consideramos cadenas inhomogéneas, la invariancia conforme se mantiene. Por tanto, el estudio de las fuerzas de Casimir en espacio-tiempos curvos se ha llevado a cabo en este marco como una extensión de las predicciones de la CFT en la métrica de Minkowski. Sin embargo, la simetría conforme se rompe en cadenas inhomogéneas fuera del llenado mitad y nueva física aparece: la depleción. En resumen, en esta tesis hemos utlizado las predicciones de CFT en los casos con invariancia conforme y hemos desarrollado nueva teoría para los casos contrarios, con el objetivo de estudiar los estados de baja energía de sistemas homogéneos e inhomogéneos.

Appendix A

Schmidt decomposition

Let us consider the pure state given by Eq. (2.12)

$$|\Psi\rangle = \sum_{ij} C_{ij} \left|a_i b_j\right\rangle, \tag{A.1}$$

where $\{|a\rangle\}$ and $\{|b\rangle\}$ are orthonormal basis of the Hilbert spaces $\mathcal{H}_A$ and $\mathcal{H}_B$, respectively, and N_A, N_B their corresponding dimension. Notice that the coefficients C_{ij} can be arranged in a rectangular matrix of dimension $N_A \times N_B$ which admits a *singular value decomposition* (SVD),

$$C = U\Lambda V^\dagger, \tag{A.2}$$

where U and V are unitary matrices of dimension $N_A \times N_A$ and $N_B \times N_B$, respectively. The matrix Λ, which has dimension $N_A \times N_B$, is diagonal and shows real and positive elements, $\Lambda_{kk} = \sigma_k$, called *singular values* of matrix C. Therefore, it can be expressed as

$$C_{ij} = \sum_{k=1}^{\min(N_A,N_B)} U_{ik}\sigma_k V^*_{kj}, \tag{A.3}$$

and we can rewrite Eq. (A.1)

$$|\Psi\rangle = \sum_{ij}\sum_{k} U_{ik}\sigma_k V^*_{kj} \left|a_i b_j\right\rangle = \sum_k \sigma_k \left(\sum_i U_{ik} |a_i\rangle\right) \otimes \left(\sum_j V^*_{kj} \left|b_j\right\rangle\right). \tag{A.4}$$

Let us define now $|\alpha_k\rangle = \sum_i U_{ik} |a_i\rangle$ and $|\beta_k\rangle = \sum_j U_{kj} \left|b_j\right\rangle$ so it follows

$$|\Psi\rangle = \sum_{k=1}^{\min(N_A,N_B)} \sigma_k |\alpha_k\rangle \otimes |\beta_k\rangle. \tag{A.5}$$

This is the so-called *Schmidt decomposition* of a pure state in $\mathcal{H} = \mathcal{H}_A \otimes \mathcal{H}_B$.

Let us assume σ_k are ordered in decreasing order such as only the first n_S are non-zero. Then, the sum in Eq. (A.5) can only take values up to n_S, which is called

the *Schmidt number*. If $n_S = 1$, the state can be factorized and $|\Psi\rangle = |\alpha_1\rangle \otimes |\beta_1\rangle$. If $n_S > 1$, the state is entangled.

From Eq. (A.5) one can compute the reduced density matrices

$$\begin{aligned}
\rho_A &= \mathrm{Tr}_B \, |\Psi\rangle \langle\Psi| \\
&= \mathrm{Tr}_B \sum_{k,k'=1}^{n_S} \sigma_k \sigma_{k'} \, |\alpha_k\rangle \otimes |\beta_k\rangle \langle\alpha_{k'}| \otimes \langle\beta_{k'}| \\
&= \sum_{k,k'=1}^{n_S} \sigma_k \sigma_{k'} \left(|\alpha_k\rangle \langle\alpha_{k'}| \otimes |\beta_k\rangle \langle\beta_{k'}| \right) \\
&= \sum_{k,k'=1}^{n_S} \sigma_k \sigma_{k'} \left(|\alpha_k\rangle \langle\alpha_{k'}| \right) \mathrm{Tr} \left(|\beta_k\rangle \langle\beta_{k'}| \right) \\
&= \sum_{k,k'=1}^{n_S} \sigma_k \sigma_{k'} \, |\alpha_k\rangle \langle\alpha_{k'}| \, \delta_{kk'} \\
&= \sum_{k=1}^{n_S} \sigma_k^2 \, |\alpha_k\rangle \langle\alpha_k| \, .
\end{aligned} \tag{A.6}$$

The reduced density matrix ρ_A is diagonal in the basis of $\{\alpha_k\}$, with eigenvalues σ_k^2.

Analogously, we can compute

$$\rho_B = \sum_{k=1}^{n_S} \sigma_k^2 \, |\beta_k\rangle \langle\beta_k| \, . \tag{A.7}$$

It is important to pay attention at the fact that both density matrices, ρ_A and ρ_B, of a given system in a pure state have the same spectrum[1], $\{\sigma_k^2\}$, which is the so called *entanglement spectrum*.

[1] If we do not take into account the vanishing eigenvalues.

Appendix B

Energy for OBC

The energy of the system is given by Eq. (3.8) where $\varepsilon_k = -2\cos(k)$. For open boundary conditions, the allowed modes are given by Eq. (3.28). In order to compute the energy of the GS, we need to fill in only those modes with negative energy, *i.e.*, $k \in \left[1, N/2\right]$. Therefore, the endpoints of the interval we are considering in order to apply Euler-MacLaurin expression, Eq. (3.34),

$$\sum_{n=a}^{b} f(n) \sim \int_a^b f(x)dx + \frac{f(a)+f(b)}{2} + \sum_{q=1}^{\infty} \frac{B_{2q}}{(2q)!}\left(f^{(2q-1)}(b) - f^{(2q-1)}(a)\right), \quad \text{(B.1)}$$

are $a = 1$ and $b = N/2$.

The first term of the asymptotic expansion is given by

$$\int_a^b f(x)dx = 2\int_1^{N/2} \cos\left(\frac{m\pi}{N+1}\right) dm, \quad \text{(B.2)}$$

where $m \in \left[1, N/2\right]$ and N is the size of the system. It is a straightforward calculation to compute this term so the result after integrating Eq. (B.2) is given by

$$\frac{2(N+1)}{\pi}\left(\cos\left(\frac{\pi}{2(N+1)}\right) - \sin\left(\frac{\pi}{N+1}\right)\right) \approx \frac{2N}{\pi} + \left(\frac{2}{\pi} - 2\right) - \frac{\pi}{4(N+1)}, \quad \text{(B.3)}$$

where the cosine and sine functions must be expanded to second and first order, respectively, in order to ensure no missing contributions in $1/N$. Higher terms in the expansion of the trigonometric functions lead to higher order corrections which are not relevant in this work.

The second term of the expansion is given by

$$\frac{f(a)+f(b)}{2} = \cos\left(\frac{N\pi}{2(N+1)}\right) + \cos\left(\frac{\pi}{N+1}\right) \approx \frac{\pi}{2(N+1)} + 1. \quad \text{(B.4)}$$

The third term of the Euler-MacLaurin asymptotic expansion includes the Bernoulli terms that take into account all high order derivatives involved. However, for our

purposes we only need to compute the term corresponding to $k = 1$

$$\frac{B_2}{2}\left(f'(b) - f'(a)\right) = \frac{\pi}{6(N+1)}\left(\sin\left(\frac{\pi}{N+1}\right) - \cos\left(\frac{\pi}{2(N+1)}\right)\right) \approx \frac{-\pi}{6(N+1)}, \tag{B.5}$$

where $B_2 = 1/6$.

From Eq. (B.3), (B.4) and (B.5), we end up with the following expression for the energy of the GS at half-filling with open boundary conditions in the thermodynamic limit where $N \to \infty$,

$$E^{\mathrm{OBC}}(N) \approx -\frac{2N}{\pi} - \left(\frac{2}{\pi} - 1\right) - \frac{\pi}{12}. \tag{B.6}$$

The calculation is analogous for PBC but now $k = \dfrac{2m\pi}{N}$. Furthermore, we must distinguish two cases: $N = 4n$ and $N = 4n + 2$. When $N = 4n$, the endpoints of the interval we are considering are $a = -N/4$ and $b = N/4$. On the other hand, for $N = 4n+2$ we must use $a = -(N-2)/4$ and $b = (N-2)/4$. This difference in a and b leads to different results for the energy of the GS when computing the three terms corresponding to the asymptotic expansion of Euler-MacLaurin expression given in equations (3.36) and (3.37).

We showed in Section **??** that the energy for APBC is equivalent to the PBC case by changing the roles of $N = 4n$ and $N = 4n + 2$, and taking into account the allowed modes in each case, which are different for the anti-periodic and periodic cases.

Appendix C

Virasoro algebra as a central extension

If we consider a matrix Lie group M, which is formed by $n \times n$ invertible matrices with entries in $\mathbb{C}$, the elements G of its Lie algebra $\mathbf{m}$ are given by

$$G = \frac{d}{dt}\left(g(t)\right)|_{t=0}, \tag{C.1}$$

where g is a differentiable path in M that goes through the identity element at $t = 0$. The commutators of elements of the Lie algebra can be computed using two paths, g_1 and g_2,

$$[G_1, G_2] = \frac{d}{dt}\left(g_1(t)g_2(t)g_1(t)^{-1}g_2(t)^{-1}\right)|_{t=0}, \tag{C.2}$$

with $G_1 = g_1'(0)$ and $G_2 = g_2'(0)$. Given a group representation $U(M)$, the commutator of two elements, U_1 and U_2, of its Lie algebra $\mathbf{u(m)}$ is computed by

$$[U_1, U_2] = \frac{d}{dt}\left(U\left(g_1(t)\right)U\left(g_2(t)\right)U\left(g_1(t)\right)^{-1}U\left(g_2(t)\right)^{-1}\right)|_{t=0}. \tag{C.3}$$

From equations (C.2) and (C.3), one can read that there is a Lie algebra isomorphism between $\mathbf{m}$ and $\mathbf{u(m)}$: $\mathbf{u}$ is a faithful representation of $\mathbf{m}$.

Let us consider now $U(M)$ as a projective representation where the multiplication rule reads

$$U(g_1)U(g_2) = \omega(g_1, g_2)U(g_1, g_2) = e^{i\xi(g_1,g_2)}U(g_1, g_2). \tag{C.4}$$

The function ω is often required to be smooth and it is called a 2-cocycle in M so it satisfies

$$\omega(g, e) = \omega(e, g) = 1, \tag{C.5}$$

$$\omega(g_1, g_2g_3)\omega(g_2, g_3) = \omega(g_1, g_2)\omega(g_1g_2, g_3), \tag{C.6}$$

$$\omega\left(g, g^{-1}\right) = \omega\left(g^{-1}, g\right). \tag{C.7}$$

If we now use the multiplication rule (C.4) in Eq. (C.3), we end up with

$$[U_1, U_2] = \frac{dU\left(g_1(t)g_2(t)g_1(t)^{-1}g_2(t)^{-1}\right)}{dt}|_{t=0} + \frac{d\Omega(g_1, g_2)}{dt}|_{t=0}\, c, \tag{C.8}$$

where $\Omega(g_1, g_2) = e^{i\xi(g_1,g_2)\xi(g_1^{-1},g_2^{-1})\xi(g_1g_2,g_1^{-1}g_2^{-1})}$ and c is called the *central charge*.

The operators in a Lie algebra form a linear vector space. Since the linear vector space is closed under commutations, the commutator of any two basis vectors can be expressed as a linear superposition of basis vectors. Following Eq. (C.2) and Eq.(C.8), this leads to

$$[G_i, G_j] = C_{ij}^k G_k, \tag{C.9}$$

$$[U_i, U_j] = C_{ij}^k U_k + D_{ij} c, \tag{C.10}$$

where C_{ij}^k are the so-called *structure constants*. In order for $\mathbf{u}$ to be closed under the bracket and become a Lie algebra, a central charge c must be included.

The central charge arises naturally in the context of projective representations. Let us consider the most general central extension of the Witt algebra, which is given by

$$[L_m, L_n] = (m-n)L_{m+n} + c(m,n). \tag{C.11}$$

It is straightforward to check $c(m,n) = -c(n,m)$.

We can write any general central charge extension into the standard form where $c(m,n)$ is a c-number if we appropriately redefine the generators L_m. The algebra remains the same under the transformation $L_m \to L_m + a(m)$, where $a(m)$ is a c-number function. Under this redefinition,

$$c(m,n) \to c(m,n) + (m-n)a(m+n), \tag{C.12}$$

and we choose

$$a(m) = -\frac{1}{m} c(m,0), m \neq 0 \tag{C.13}$$

$$a(0) = -\frac{1}{2} c(1,-1). \tag{C.14}$$

Therefore, we find

$$c(m,0) \to c(m,0) + ma(m) = 0, m \neq 0 \tag{C.15}$$

$$c(1,-1) \to c(1,-1) + 2a(0) = 0. \tag{C.16}$$

The conformal algebra then takes the form

$$[L_m, L_0] = mL_m, \tag{C.17}$$

$$[L_1, L_{-1}] = 2L_0. \tag{C.18}$$

The remaining generators satisfy the same algebra written in Eq. (C.11).

Let us consider the Jacobi identity for $m, n \neq 0$ and $m+n \neq 0$,

$$0 = \big[[L_m, L_n]\, L_0\big] + \big[[L_n, L_0]\, L_m\big] + \big[[L_0, L_m]\, L_n\big] = -(m+n)c(m,n). \tag{C.19}$$

Since $m+n \neq 0$, $c(m,n) = 0$. Taking all of this into account, we find that

$$c(m,n) = a(m)\delta_{m+n,0}, \tag{C.20}$$

$$[L_m, L_n] = (m-n)L_{m+n} + a(m)\delta_{m+n,0}, \tag{C.21}$$

where $a(\pm 1) = 0$ and $a(m) = -a(-m)$.

Let us now look at a generic Jacobi identity,

$$0 = \big[[L_m, L_n]\, L_p\big] + \Big[\big[L_p, L_m\big]\, L_n\Big] + \Big[\big[L_n, L_p\big]\, L_m\Big], \tag{C.22}$$

$$0 = (m-n)a(m+n) + (2m+n)a(n) - (m+2n)a(m). \tag{C.23}$$

For $m = 1$,

$$a(n+1) = \frac{n+2}{n-1}a(n). \tag{C.24}$$

This leads to

$$a(n) = \frac{a(2)}{6}n(n^2-1), \tag{C.25}$$

with $a(2)$ chosen to be $a(2) = \dfrac{c}{2}$. Therefore,

$$[L_m, L_n] = (m-n)L_{m+n} + \frac{c}{12}m(m^2-1)\delta_{m+n,0}. \tag{C.26}$$

If hermiticity conditions are imposed on Virasoro operators in order to deal with a proper quantum system, then the CFT is called unitary. This implies

$$L_n^\dagger = L_{-n}, \tag{C.27}$$

$$\bar{L}_n^\dagger = \bar{L}_n. \tag{C.28}$$

Appendix D

Casimir energy

D.1 CFT derivation of the Casimir energy in curved backgrounds

Let us provide a theoretical justification for our deformed extension of expression (5.23), given in Eq. (5.24). The two first terms are non-universal: $c_0(N-1) \mapsto c_0 S_N$, while $c_B \mapsto (c_B/2)(J_1+J_N)$ are just a consequence of first-order perturbation theory. Yet, the finite-size correction term $(c\pi v_F/24N)$ is universal, i.e. fixed by conformal invariance, and requires further explanation. In what follows we will assume that the Fermi velocity (the speed of light) is $v_F = 1$.

According to CFT, the variation of the energy-momentum tensor T under a local conformal transformation, $z \to w(z)$, in flat space-time is given by [21]

$$T'(w) = \left(\frac{dw}{dz}\right)^{-2} \left[T(z) - \frac{c}{12}\{w; z\}\right], \tag{D.1}$$

where c is the central charge of the CFT and $\{w; z\}$ is the Schwarzian derivative,

$$\{w; z\} = \frac{d^3w/dz^3}{dw/dz} - \frac{3}{2}\left(\frac{d^2w/dz^2}{dw/dz}\right)^2. \tag{D.2}$$

Let us consider a CFT defined on the whole complex plane, with vanishing energy density $\langle T(z)\rangle \sim 0$. Now, we would like to map it into a strip of width L (see Section 4.6), using

$$z \to w = \frac{L}{\pi}\ln z. \tag{D.3}$$

This yields a nonzero vacuum energy density on the strip

$$\langle T_{strip}(w)\rangle = -\frac{c\pi^2}{24\,L^2}. \tag{D.4}$$

Now, the energy density can be evaluated (check Eq. (5.40) of [21]),

$$\left\langle T^{00}\right\rangle = \langle T_{zz}\rangle + \langle T_{\bar{z}\bar{z}}\rangle = -\frac{1}{\pi}\langle T\rangle = \frac{\pi c}{24L^2}, \tag{D.5}$$

which corresponds to the universal term in Eq. (5.23). Yet, our z variable is composed of a deformed space variable and time, $z = \tilde{x} + it$, so the length appearing in this expression is, in fact, $\tilde{L}$, as required.

Let us provide an alternative derivation, only valid for infinitesimal deformations of the metric, $g_{\mu\nu} \mapsto g_{\mu\nu} + \delta g_{\mu\nu}$. The free energy density of a conformal system, F, varies as

$$\delta F = -\frac{1}{2}\int d^2x\, \sqrt{g}\, \delta g_{\mu\nu} \langle T^{\mu\nu}\rangle\,, \tag{D.6}$$

where $\sqrt{g} = \det\left(g_{\mu\nu}\right)^{1/2}$ is required by the invariance of the space-time integration measure. Let consider the Minkowski energy density, given by

$$T^{00} = \frac{\pi c}{24\, L^2}, \tag{D.7}$$

and deform the metric, mapping $g_{00} = -1$ to $g_{00} + \delta g_{00} = -J^2(x) \approx -1 - 2\delta J(x)$. This leads to a new free energy,

$$\delta F = \int d^2x\, \delta J(x) \frac{\pi c}{24\, L^2}, \tag{D.8}$$

where the integration must be performed on a strip $[0, L] \times \mathbb{R}$, where the vertical direction is trivial. The total energy is given by the new free energy per unit length (in the transverse direction),

$$E = F_L + \delta F_L = \left(\frac{1}{L}\int_0^L (1 + \delta J(x))\right) \frac{\pi c}{24\, L}, \tag{D.9}$$

i.e. the energy gets corrected by a new Fermi velocity, which is equal to the average value of $J(x)$ in the interval. This is the main result of Eq. (5.25).

Of course, this result is only valid for very small deformations, $J(x) \approx 1 + \delta J(x)$. The full expression (5.24) can be obtained by integrating it, $F = \int \delta F$. We may parametrize the change from $g_{00} = -1$ to $g_{00} = -J^2(x)$ in a continuous way, considering a one-parameter metric family, $g_{00}(s) = J^2(x, s)$ such that $J^2(x, 0) = -1$ and $J^2(x, 1) = J^2(x)$, so that the final energy correction takes the form

$$\Delta F = \int_0^1 ds \int dx \sqrt{g(s)} \left(\frac{\pi c}{24 L(s)^2}\right) \frac{\partial J(x, s)}{\partial s}, \tag{D.10}$$

where $L(s)$ and $\sqrt{g(s)}$ correspond respectively to the effective length and the volume factor at each stage of the deformation process.

D.2 Casimir force measured by local observer

Let E be the Casimir energy for the whole system. When it is measured by a local observer at site x will be given by $E(x) = E/g_{00}(x)^{1/2} = E/J(x)$, following Eq. (5.26). Let us remember that the energy is not a scalar, but a vector pointing along the time axis: $(E(x), 0)$. The force is defined as the spatial component of the covariant derivative of the energy,

$$F(x) = -D_x E(x), \tag{D.11}$$

where the covariant derivative of a vector is defined as

$$D_\mu V^\alpha = \partial_\mu V^\alpha + \Gamma^\alpha_{\mu\nu} V^\nu, \tag{D.12}$$

where the $\Gamma^\alpha_{\mu\nu}$ are the Christoffel symbols, given by

$$\Gamma^\alpha_{\mu\nu} = \frac{1}{2} g^{\alpha\beta} \left(g_{\beta\mu,\nu} + g_{\beta\nu,\mu} - g_{\mu\nu,\beta} \right). \tag{D.13}$$

for the metric connection. In the case of an optical metric, Eq. (5.2), the only relevant Christoffel symbol is

$$\Gamma^0_{10} = \frac{J'(x)}{J(x)}. \tag{D.14}$$

Thus, we can find the force

$$F(x) = -\frac{\partial_x E(x)}{J(x)} + \frac{J'(x)}{J(x)} E(x) - \frac{J'(x)}{J(x)} E(x) = -\frac{\partial_x E(x)}{J(x)}. \tag{D.15}$$

And from this equation we can find a possible definition of the Casimir force felt by a local observer at the boundary,

$$F_N \approx -\frac{E_N - E_{N-1}}{J_N \Delta x}, \tag{D.16}$$

where we set $\Delta x = 1$, since it is arbitrary. Yet, the strong parity oscillations suggest that a better alternative is to take the discrete derivative over two lattice spacings,

$$F_N \equiv -\frac{E_N - E_{N-2}}{J_{N-2} + J_{N-1}}. \tag{D.17}$$

Appendix E

Eigenstates of first order continuum approximation

In order to find the eigenstates of the Hamiltonian

$$H(\tilde{x}) = -\int_0^{\mathcal{N}} d\tilde{x} \left[2ai \sin(k_F a) \left(\tilde{\Psi}_L^\dagger \partial_{\tilde{x}} \tilde{\Psi}_L(\tilde{x}) - \tilde{\Psi}_R^\dagger(\tilde{x}) \partial_{\tilde{x}} \tilde{\Psi}_R(\tilde{x}) \right) \right.$$
$$\left. + \cos(k_F a) \left(2\tilde{J}(\tilde{x}) - a \frac{\tilde{J}'(\tilde{x})}{\tilde{J}(\tilde{x})} \right) \left(\tilde{\Psi}_L^\dagger(\tilde{x}) \tilde{\Psi}_L(\tilde{x}) + \tilde{\Psi}_R^\dagger(\tilde{x}) \tilde{\Psi}_R(\tilde{x}) \right) \right], \tag{E.1}$$

we need to solve the corresponding equations of motion

$$\partial_t \tilde{\Psi}_{R/L}(\tilde{x}, t) = i \left[H, \tilde{\Psi}_{R/L}(\tilde{x}, t) \right]. \tag{E.2}$$

We will make use of the following property

$$[AB, C] = A\,[B, C] + [A, C]\,B = A\{B, C\} - \{A, C\}B, \tag{E.3}$$

and the knowledge that fermionic fields obey cannonical anticommutation relations given by

$$\{\Psi_{R/L}(x), \Psi_{R/L}(x')\} = \{\Psi_{R/L}^\dagger(x), \Psi_{R/L}^\dagger(x')\} = 0, \tag{E.4}$$

$$\{\Psi_{R/L}^\dagger(x), \Psi_{R/L}(x')\} = \delta(x - x'), \tag{E.5}$$

$$\{\partial_x \Psi_{R/L}(x), \Psi_{R/L}(x')\} = 0. \tag{E.6}$$

Therefore, we only need

$$\left[\Psi_{R/L}^\dagger(x) \partial_x \Psi_{R/L}(x), \Psi_{R/L}(x') \right] = -\delta(x - x') \partial_x \Psi_{R/L}(x), \tag{E.7}$$

and

$$\left[\Psi_{R/L}^\dagger(x) \Psi_{R/L}(x), \Psi_{R/L}(x') \right] = -\delta(x - x') \Psi_{R/L}(x). \tag{E.8}$$

Now we can compute the commmutator of the fields with the Hamiltonian in order to write the equations of motion given by Eq. (E.2),

$$\left[H, \tilde{\Psi}_L(\tilde{x},t)\right] = \int_0^{\mathcal{N}} d\tilde{x} \left[-2ai\sin(k_F a)\partial_{\tilde{x}}\tilde{\Psi}_L(\tilde{x},t) - \cos(k_F a)\left(2\tilde{J}(\tilde{x}) - a\frac{\tilde{J}'(\tilde{x})}{\tilde{J}(\tilde{x})}\right)\tilde{\Psi}_L(\tilde{x},t)\right], \tag{E.9}$$

$$\left[H, \tilde{\Psi}_R(\tilde{x},t)\right] = \int_0^{\mathcal{N}} d\tilde{x} \left[2ai\sin(k_F a)\partial_{\tilde{x}}\tilde{\Psi}_R(\tilde{x},t) - \cos(k_F a)\left(2\tilde{J}(\tilde{x}) - a\frac{\tilde{J}'(\tilde{x})}{\tilde{J}(\tilde{x})}\right)\tilde{\Psi}_R(\tilde{x},t)\right]. \tag{E.10}$$

From the equations above, it follows that

$$\partial_t\tilde{\Psi}_L(\tilde{x},t) = -i\left[2ai\sin(k_F a)\partial_{\tilde{x}}\tilde{\Psi}_L(\tilde{x},t) + cos(k_F a)\left(2\tilde{J}(\tilde{x}) - a\frac{\tilde{J}'(\tilde{x})}{\tilde{J}(\tilde{x})}\right)\tilde{\Psi}_L(\tilde{x},t)\right], \tag{E.11}$$

$$\partial_t\tilde{\Psi}_R(\tilde{x},t) = i\left[2ai\sin(k_F a)\partial_{\tilde{x}}\tilde{\Psi}_R(\tilde{x},t) + cos(k_F a)\left(2\tilde{J}(\tilde{x}) - a\frac{\tilde{J}'(\tilde{x})}{\tilde{J}(\tilde{x})}\right)\tilde{\Psi}_R(\tilde{x},t)\right]. \tag{E.12}$$

Let us assume we can write $\tilde{\Psi}_{R/L}(\tilde{x},t) = \tilde{\psi}_{R/L}(\tilde{x})e^{-i\omega t}$. Plugging it in Eq. (E.11) and Eq. (E.12), and considering we are working at $t = 0$ and, thus, $\tilde{\Psi}_{R/L}(\tilde{x}) = \tilde{\psi}_{R/L}(\tilde{x})$,

$$\tilde{\psi}_L(\tilde{x}) = \exp\left[\frac{-i}{2a\sin(k_F a)}\left(\omega\tilde{x} - \int\cos(k_F a)\left(2\tilde{J}(\tilde{x}) - a\frac{\tilde{J}'(\tilde{x})}{\tilde{J}(\tilde{x})}\right)d\tilde{x}\right)\right], \tag{E.13}$$

$$\tilde{\psi}_R(\tilde{x}) = \exp\left[\frac{i}{2a\sin(k_F a)}\left(\omega\tilde{x} - \int\cos(k_F a)\left(2\tilde{J}(\tilde{x}) - a\frac{\tilde{J}'(\tilde{x})}{\tilde{J}(\tilde{x})}\right)d\tilde{x}\right)\right], \tag{E.14}$$

where ω is an integration constant. In other words, the wavefunctions are modulated planes wave in $\tilde{x}$.

Appendix F

Correlators for OBC

We have seen that for OBC the eigenstates are given by

$$\phi_n = A\sin(kn) = A\frac{e^{ikn} - e^{-ikn}}{2i}, \tag{F.1}$$

with $k = \dfrac{m\pi}{N+1}$ where m is an integer number, n represents the sites along the chain, and A is a normalization constant: $\sum_{n=1}^{N} |\phi_n|^2 = 1 \rightarrow A = \sqrt{\dfrac{2}{N+1}}$.

The nearest neighbors correlators can be written in terms of unitary matrices U_{kn}, which columns are the eigenstates given by Eq. (F.1),

$$\left\langle c_n^\dagger c_{n+1} \right\rangle = \sum_{k=1}^{N/2} \bar{U}_{kn} U_{k,n+1}. \tag{F.2}$$

We need to sum over all the occupied modes and, as we are at half-filling, the sum goes up to $k = N/2$. Thus, plugging the eigenstates of Eq. (F.1) in Eq. (F.2), it follows that

$$\left\langle c_n^\dagger c_{n+1} \right\rangle = \frac{1}{N+1}\sum_{m=1}^{N/2} \cos\left(\frac{m\pi}{N+1}\right) - \frac{1}{N+1}\sum_{m=1}^{N/2} \cos\left(\frac{m\pi}{N+1}(2n+1)\right). \tag{F.3}$$

One can compute the sum of both terms of the expression above by making use of the relation

$$\sum_{m=0}^{N_t} \cos(m\alpha) = \frac{1}{2} + \frac{\sin\left(\dfrac{2N_t+1}{2}\alpha\right)}{2\sin\left(\dfrac{\alpha}{2}\right)}, \tag{F.4}$$

where α is a constant that may depend on n. Therefore,

$$\left\langle c_n^\dagger c_{n+1} \right\rangle = \frac{1}{2(N+1)\sin\left(\dfrac{\pi}{2(N+1)}\right)} - \frac{\sin\left(\dfrac{\pi}{2}(2n+1)\right)}{2(N+1)\sin\left(\dfrac{\pi}{2(N+1)}(2n+1)\right)}. \tag{F.5}$$

We must be aware that the sine functions present in the previous equation may have n in their argument. In that case, we can not perform a series expansion as the result must be valid for all values of n and not just in the small regime. However, it is possible to expand $\sin\left(\frac{\pi}{2(N+1)}\right)$ as there is no n-dependence.

Taking into account that

$$\begin{aligned} n \text{ even} &\rightarrow \sin\left(\frac{\pi}{2}(2n+1)\right) = 1, \\ n \text{ odd} &\rightarrow \sin\left(\frac{\pi}{2}(2n+1)\right) = -1, \end{aligned} \tag{F.6}$$

we end up with

$$\left\langle c_m^\dagger c_{m+1} \right\rangle_{\text{OBC}} \simeq \frac{1}{\pi} + \frac{\pi}{24\left(N+1\right)^2} - \frac{(-1)^n}{2\left(N+1\right)\sin\left(\frac{\pi\left(n+1/2\right)}{N+1}\right)}. \tag{F.7}$$

We can check that the terms responsible of the parity oscillations is symmetric under the exchange $n \rightarrow N-n$ as expected.

This procedure remains the same for PBC and ABC by just using the corresponding eigenstates in each case.

Appendix G

Passive energy calculation

The passive energy $\widetilde{E}_A$ can be written as

$$\widetilde{E}_A = \sum_{k=1}^{\ell} \nu_k \varepsilon_k^A ., \tag{G.1}$$

where ε_k^A and ν_k are given by Eq. (7.35) and Eq. (7.36), respectively. Thus, the passive energy for a general system of size N is given by

$$\widetilde{E}_A = \sum_{p=1}^{N} \varepsilon_p^A \nu_p^A \approx \sum_{p=1}^{N} \frac{-2\cos(\pi p/(N+1))}{1+e^{-\beta(p-N/2)}}. \tag{G.2}$$

In order to compute this sum we need to take the continuum limit, making use of the Sommerfeld expansion [158] and the Euler-Maclaurin formula given by Eq. (3.34). The Sommerfeld expansion can be written as

$$\int_{-\infty}^{+\infty} \frac{H(\varepsilon)}{e^{\beta(\varepsilon-\mu)+1}} d\varepsilon = \int_{-\infty}^{\mu} H(\varepsilon) d\varepsilon + \frac{\pi^2}{6}\left(\frac{1}{\beta}\right)^2 H'(\mu) + O\left(\frac{1}{\beta\mu}\right)^4. \tag{G.3}$$

Therefore,

$$\widetilde{E}_A \approx -2\left[\int_1^{N/2} \cos\left(\frac{p\pi}{N+1}\right) dp - \frac{\pi^3}{6\beta(N+1)} \sin\left(\frac{\pi N}{2(N+1)}\right)\right] \tag{G.4}$$

It is straightforward to calculate the integral of the expression above as

$$
\begin{aligned}
-2\int_1^{N/2}\cos\left(\frac{p\pi}{N+1}\right)dp &= \frac{-2(N+1)}{\pi}\left[\sin\left(\frac{N\pi}{2(N+1)}\right)-\sin\left(\frac{\pi}{N+1}\right)\right] \\
&= \frac{-2(N+1)}{\pi}\left[\sin\left(\frac{\pi}{2}-\frac{\pi}{2(N+1)}\right)-\sin\left(\frac{\pi}{N+1}\right)\right] \\
&= \frac{-2(N+1)}{\pi}\left[\cos\left(\frac{\pi}{2(N+1)}\right)-\sin\left(\frac{\pi}{N+1}\right)\right] \\
&\approx -\frac{2N}{\pi}-\left(\frac{2}{\pi}-2\right)+\frac{\pi}{4(N+1)}.
\end{aligned}
\tag{G.5}
$$

However, when we approximate a sum by an integral we may have other contributions which can be calculated by the Euler-MacLaurin formula previously used given by Eq. (3.34). Thus,

$$
\frac{f(N)+f(1)}{2}\approx -1, \tag{G.6}
$$

$$
\frac{B_2}{2}\left(f'(b)-f'(a)\right)\approx\frac{\pi}{6N}, \tag{G.7}
$$

where $B_2 = 1/6$ still stands for one of the Bernouilli's numbers.

Taking into account all the aforementioned contributions, we can write the passive energy as

$$
\widetilde{E}_A \approx -\frac{2N}{\pi}-\left(\frac{2}{\pi}-2\right)+\frac{5\pi}{12N}+\frac{\pi^3}{3N\beta^2}. \tag{G.8}
$$

However, we are interested in considering a system of size $N/2$. For that aim, we should replace $N \to N/2$ in Eq. (G.8) and subtract the central link energy as we have done previously to calculate the associated energy to block A, E_A.

Finally, the expression for $\widetilde{E}_A$ is given by

$$
\widetilde{E}_A \approx -c_0\left(\frac{N}{2}-1\right)-c_B-\frac{c\pi v_F}{12N}+\frac{2\pi^3}{3N\beta^2}, \tag{G.9}
$$

which can be also written as

$$
\widetilde{E}_A \approx -c_0\left(\frac{N}{2}-1\right)-c_B-\frac{\pi}{6N}+\frac{\log^2(\gamma N)}{6\pi N}, \tag{G.10}
$$

where $\beta = \dfrac{2\pi^2}{\log(\gamma N)}$.

Bibliography

[1] P.M. Chaikin, T.C. Lubensky, *Principles of condensed matter*, Cambrige University Press (1995).

[2] L.D. Landau, *The theory of a Fermi liquid*, Sov. Phys. JETP **3**, 920 (1957).

[3] G.B. Mbeng, A. Russamanno, G.E. Santoro, *The quantum Ising chain for beginners*, arXiv:2009.09208.

[4] R.I. Nepomechie, *A spin chain primer*, Int. J. Mod. Phys. **B13**, 2973 (1999).

[5] O. Boada, A. Celi, J.I. Latorre, M. Lewenstein, *Dirac equation for cold atoms in artificial curved space-times*, New J. Phys. **13**, 035002 (2011).

[6] J. Rodríguez-Laguna, L. Tarruell, M. Lewenstein, A. Celi, *Synthetic Unruh effect in cold atoms*, Phys. Rev. A **95**, 013627 (2017).

[7] M. Lewenstein, A. Sanpera, V. Ahufinger, *Ultracold atoms in optical lattices*, Oxford University Press (2012).

[8] H.B.G. Casimir, D. Polder, *The Influence of Retardation on the London-van der Waals Forces*, Phys. Rev. **73**, 360 (1948).

[9] O. Kenneth, I. Klich, *Opposites Attract: A Theorem about the Casimir Force*, Phys. Rev. Lett. **97**, 160401 (2006).

[10] B. V. Derjaguin, I. I. Abrikosova, E. M. Lifshitz, *Direct measurement of molecular attraction between solids separated by a narrow gap*, Progress in Surface Science **40**, 77 (1992).

[11] M.J. Sparnaay, *Measurements of attractive forces between flat plates*, Physica **24**, 751 (1958).

[12] i.e. Dzyaloshinskii, E.M. Lifshitz, L.P. Pitaevskii, *Van der Waals Forces in Liquid Films*, JETP **10**, 161 (1960).

[13] J.N. Munday, D. Iannuzzi, Y. Barash, F. Capasso, *Torque on birefringent plates induced by quantum fluctuations*, Phys. Rev. A **71**, 042102 (2005).

[14] F. Capasso, J. N. Munday, D. Iannuzzi, H.B. Chan, *Casimir Forces and Quantum Electrodynamical Torques: Physics and Nanomechanics*, IEEE Journal of Selected Topics in Quantum Electronics, **13**, 2, 400 (2007).

[15] H. G. Stanley, *Introduction to Phase Transitions and Critical Phenomena*, Oxford University Press, Oxford (1971).

[16] M. Krech, *The Casimir Effect in Critical Systems*, World Scientific, Singapore (1994).

[17] I. Brankov, D. M. Danchev, N. S. Tonchev, J. G. Brankov, *Theory of Critical Phenomena in Finite-Size Systems: Scaling and Quantum Effects*, Series in Modern Condensed Matter Physics **9**, World Scientific, Singapore, (2000).

[18] A. Ajdari, B. Duplantier, D. Hone, L. Peliti, J. Prost, *Pseudo-Casimir effect in liquid crystals*, J. Phys. II France **2**, 487 (1992).

[19] J.L. Cardy, *Conformal invariance and universality in finite-size scaling*, J. Phys. A: Math. Gen. **17**, L385 (1984).

[20] H.W.J. Blöte, J.L. Cardy, M.P. Nightingale, *Conformal Invariance, the Central Charge, and the Universal Finite-Size Amplitudes at Criticality*, Phys. Rev. Lett. **56**, 742 (1986).

[21] P. di Francesco, P. Matthieu, D. Sénéchal, *Conformal Field Theory*, Springer (1997).

[22] G. Mussardo, *Statistical Field Theory*, Oxford Graduate Texts (2010).

[23] G. Bimonte, T. Emig, M. Kardar, *Conformal field theory of critical Casimir interactions in 2D*, EPL **104**, 21001 (2013).

[24] B.S. DeWitt, *Quantum field theory in curved space-time*, Phys. Rep. **19**, 295 (1975).

[25] F. Sorge, *Casimir effect in a weak gravitational field*, Class. Quantum Grav. **22**, 5109 (2005).

[26] F. Sorge, *Casimir effect in weak gravitational field: Schwinger's approach*, Classical and Quantum Gravity **36**, 23 (2019).

[27] M. Nouri-Zonoz, B. Nazari, *Vacuum energy and the space-time index of refraction: A new synthesis*, Phys. Rev. D **82**, 044047 (2010).

[28] B. Nazari, M. Nouri-Zonoz, *Electromagnetic Casimir effect and the space-time index of refraction*, Phys. Rev. D **85**, 044060 (2012).

[29] A. Einstein, *Über einen die Erzeugung und Verwandlung des Lichtes betreffenden heuristischen Gesichttspunkt*, Annalen der Physik **17**, 132 (1905).

[30] E. Schrodinger, *An ondulatory theory on the mechanics of atoms and molecules*, Phys. Rev. **28**, 1049 (1926).

[31] W. Heisenberg, *Über den anschaulichen Inhalt der quantentheoretischen Kinematik und Mechanik*, Z. Physik **43**, 172 (1927).

[32] A. Einstein, B. Podoslki, N. Rosen, *Can quantum-mechanical description of physical reality be considered complete?*, Phys. Rev. **47**, 777 (1935).

[33] E. Schrödinger, *Die gegenwärtige situation in der Quantenmechanik*, Naturwissenschaften 23, 844 (1935). English translation: J.D. Trimmer, *The Present Situation in Quantum Mechanics: A Translation of Schrödinger's "Cat Paradox" Paper*, Proceedings of the American Philosophical Society, **124**, 5 (1980).

[34] C.S. Wu, I. Shaknov, *The Angular Correlation of Scattered Annihilation Radiation*, Phys. Rev. **77**, 136 (1950).

[35] D. Bohm, *Quantum Theory*, Englewood Cliffs, Prentice-Hall (1951).

[36] D. Bohm, Y. Aharonov, *Discussion of Experimental Proof for the Paradox of Einstein, Rosen, and Podolsky*, Phys. Rev. **108**, 1070 (1957).

[37] J.S. Bell, *On the Einstein Podolsky Rosen paradox*, Physics Physique Fizika **1**, 3, 195 (1964).

[38] J.F. Clauser, M.A. Horne, A. Shimony, R.A. Holt, *Proposed Experiment to Test Local Hidden-Variable Theories*, Phys. Rev. Lett. **23**, 880 (1969).

[39] A. Aspect, J. Dalibard, G. Roger, *Experimental Test of Bell's Inequalities Using Time-Varying Analyzers*, Phys. Rev. Lett. **49**, 1804 (1982).

[40] D.M. Greenberger, M.A. Horne, A. Zeilinger, *Going beyond Bell's theorem*, in: *Bell's Theorem, Quantum Theory, and Conceptions of the Universe*, M. Kafatos, Kluwer, Dordrecht, 69 (1989).

[41] J. von Neumann, *Matematische Grundlagen der Quantenmechanik*, Springer, (1932).

[42] C.E. Shannon, *A Mathematical Theory of Communication*, Bell System Technical Journal **27**, 379 (1948).

[43] J.D. Bekenstein, *Black Holes and Entropy*, Phys. Rev. D **7**, 2333 (1973).

[44] M. Srednicki, *Entropy and area*, Phys. Rev. Lett. **71**, 666 (1993).

[45] D.N. Page, *Average entropy of a subsystem*, Phys. Rev. Lett. **71**, 1291 (1993).

[46] M.B. Hastings, *An area law for one-dimensional quantum systems*, J. Stat. Mech. (2007) P08024.

[47] I. Affleck, T. Kennedy, E.H. Lieb, H. Tasaki, *Valence bond ground states in isotropic quantum antiferromagnets*, Comm. Math. Phys. **115** (1988).

[48] M. Fannes, B. Nachtergaele, R.F. Werner, *Finitely correlated states on quantum spin chains*, Commun. Math. Phys. **144**, 443 (1992).

[49] SR White, *Density matrix formulation for quantum renormalization groups*, Phys. Rev. Lett. **69**, 2863 (1992).

[50] S.R. White, *Density matrix algorithms for quantum renormalization groups*, Phys. Rev. B **48**, 10345 (1993).

[51] R. Orus, *A practical introduction to Tensor Networks: Matrix Product States and Projected Entangled Pair States*, Annals of Physics **349**, 117 (2014).

[52] B. Swingle, *Entanglement Renormalization and Holography*, Phys. Rev. D **86**, 065007 (2012).

[53] J. Maldacena, L. Susskind, *Cool horizons for entangled black holes*, Fortsch. Phys. **61**, 781 (2013).

[54] G. Vitagliano, J.I. Latorre, *Violation of area-law scaling for the entanglement entropy in spin* 1/2 *chains*, New J.Phys. **12** 113049 (2010).

[55] G. Ramírez, J. Rodríguez-Laguna, G. Sierra, *Breaking the Area Law: The Rainbow State*, Strongly Coupled Field Theories for Condensed Matter and Quantum Information Theory: 395 (2020).

[56] S.W. Hawking, *Black Hole Explosions?*, Nature **248**, 30 (1974).

[57] S.W. Hawking, *Particle creation by black holes*, Commun. Math. Phys. **43**, 199 (1975).

[58] S.A. Fulling, *Nonuniqueness of Canonical Field Quantization in Riemannian Space-Time*, Phys. Rev. D **7**, 2850 (1973).

[59] P.C.W. Davies, *Scalar production in Schwarzschild and Rindler metrics*, J. Phys. A: Math. Gen. **8**, 609 (1975).

[60] W.G. Unruh, *Notes on black-hole evaporation*, Phys. Rev. D **14**, 870 (1976).

[61] L. Susskind, J. Lindesay, *An introduction to black holes, information and the string theory revolution*, World Scientific (2005).

[62] D. Singleton, S. Wilburn, *Hawking Radiation, Unruh Radiation, and the Equivalence Principle*, Phys. Rev. Lett. **107**, 081102 (2011).

[63] T. Jacobson, *Thermodynamics of space-time: The Einstein Equation of State*, Phys. Rev. Lett. **75**, 1260 (1995).

[64] J.S. Bell, J.M. Leinaas, *Electrons as accelerated thermometers*, Nucl. Phys. B **212**, 131 (1983).

[65] J.S. Bell, J.M. Leinaas, *The Unruh Effect and Quantum Fluctuations of Electrons in Storage Rings*, Nucl. Phys. B **284**, 488 (1987).

[66] A. Wehrl, *General properties of entropy*, Rev. Mod. Phys. **50**, 221 (1978).

[67] N. Laflorencie, *Quantum entanglement in condensed matter systems*, Phys. Rep. **646**, 1 (2016).

[68] H. Li, F.D.M. Haldane, *Entanglement spectrum as a generalization of entanglement entropy: Identification of topological order in non-abelian fractional quantum Hall effect states*, Phys. Rev. Lett. **101**, 010504 (2008).

[69] P. Calabrese, J.L. Cardy, *Entanglement entropy and quantum field theory*, J. Stat. Mech. P06002 (2004).

[70] Y. Chen, G. Vidal, *Entanglement contour*, J. Stat. Mech P10011 (2014).

[71] A. Auerback, *Interacting Electrons and Quantum Magnetism*, Springer (1998).

[72] L. Onsager, *Crystal Statistics. I. A Two-Dimensional Model with an Order-Disorder Transition*, Phys. Rev. **65**, 117 (1944).

[73] N.D. Mermin, H. Wagner, *Absence of Ferromagnetism or Antiferromagnetism in One- or Two-Dimensional Isotropic Heisenberg Models*, Phys. Rev. Lett. **17**, 1133 (1966).

[74] L. Néel, *Influence des fluctuations du champ moléculaire sur les propriétés magnétiques des corps*, Ann. Phys. **10**, 18 (1932).

[75] E. Lieb, T. Schultz, D. Mattis, *Two solvable models of an antiferromagnetic chain*, Annals of physics **16**, 407 (1961).

[76] P. Jordan, E. Wigner, *Über das Paulische Äquivalenzverbot*, Z. Physik **47**, 631 (1928).

[77] B. A. Cipra, *An Introduction to the Ising Model*, The American Mathematical Monthly, **94**, 10, 937 (1987).

[78] K. Joel, D. Kollmar, L.F. Santos, *An introduction to the spectrum, symmetries, and dynamics of spin-1/2 Heisenberg chains*, Am. J. Phys. **81**, 450 (2013).

[79] J. Cardy, *Scaling and Renormalization in Statistical Physics*, Cambridge University Press (1996).

[80] A.A. Belavin, A.M. Polyakov, A.B. Zamolodchikov, *Infinite conformal symmetry in two-dimensional quantum field theory*, Nucl. Phys. B **241**, 333 (1984).

[81] J.D. Qualls, *Lectures on Conformal Field Theory*, arXiv:1511.04074 (2015).

[82] M.F. Sohnius, P.C. West, *Conformal invariance in $N = 4$ supersymmetric Yang-Mills theory*, Phys. Lett. B **100**, 3 (1981).

[83] J. Maldacena, *The Large N Limit of Superconformal Field Theories and Supergravity*, Adv. Theor. Math. Phys. **2**, 231 (1998).

[84] Luke Cybulki, *Sugawara's construction of Virasoro algebra for $c = 1$, $h = 0$*, J. Math. Phys. **32**, 1121 (1991).

[85] R.C. Brower, G.T. Fleming, H. Neuberger, *Radial Quantization for Conformal Field Theories on the Lattice*, Proc. Sci. LATTICE2012 061 (2012).

[86] C. Holzhey, F. Larsen, F. Wilczek, *Geometric and renormalized entropy in conformal field theory*, Nucl. Phys. B **424**, 443 (1994).

[87] G.L. Klimchitskaya, V.M. Mostepanenko, *Experiment and theory in the Casimir effect*, Contemp. Phys. **47**, 131 (2006).

[88] M. Kardar, R. Golestanian, *The friction of vacuum, and other fluctuation-induced forces*, Rev. Mod. Phys. **71**, 4, 1233 (1999).

[89] M. Asorey, J.M. Muñoz-Castañeda, *Attractive and repulsive Casimir vacuum energy with general boundary conditions*, Nucl. Phys. B **874**, 852 (2013).

[90] P. Sundberg, R.L. Jaffe, *The Casimir effect for fermions in one dimension*, Ann. Phys. **309**, 442 (2004).

[91] D. Zhabinskaya, J.M. Kinder, EJ Mele, *Casimir effect for massless fermions in one dimension: A force-operator approach*, Phys. Rev. A **78**, 060103 (2008).

[92] U. Leonhardt, *Lifshitz theory of the cosmological constant*, Ann. Phys. **411**, 167973 (2019).

[93] U. Leonhardt, *The case for a Casimir cosmology*, Phil. Trans. R. Soc. A **378**, 20190229 (2020).

[94] S. Takagi, *Vacuum noise and stress induced by uniform accelerator: Hawking-Unruh effect in Rindler manifold of arbitrary dimensions*, Prog. Theor. Phys. Supp. **88**, 1 (1986).

[95] J. Louko, *Thermality from a Rindler quench*, Class. Quant. Grav. **35** 205006 (2018).

[96] J. Eisert, M. Cramer, M.B. Plenio, *Colloquium: Area laws for the entanglement entropy*, Rev. Mod. Phys. **82**, 1, 277 (2010).

[97] G. Vitagliano, A. Riera, J.I. Latorre, *Volume-law scaling for the entanglement entropy in spin-1/2 chains*, New J. of Phys. **12**, 113049 (2010).

[98] G. Ramirez, J. Rodriguez-Laguna, G. Sierra, *From conformal to volume-law for the entanglement entropy in exponentially deformed critical spin 1/2 chains*, J. Stat. Mech. P10004 (2014).

[99] G. Ramirez, J. Rodriguez-Laguna, G. Sierra, *Entanglement over the rainbow*, J. Stat. Mech. P06002 (2015).

[100] G. Vidal, J.I. Latorre, E Rico, A Kitaev, *Entanglement in quantum critical phenomena*, Phys. Rev. Lett. **90**, 227902 (2003).

[101] P. Calabrese, J.Cardy, *Entanglement entropy and conformal field theory*, J. Phys. A: Math. Theor. **42**, 504005 (2009).

[102] J. Rodríguez-Laguna, J. Dubaîl, G. Ramírez, P. Calabrese, G. Sierra, *More on the rainbow chain: entanglement, space-time geometry and thermal states*, J. Phys. A: Math. Theor. 50, 164001 (2017).

[103] E. Tonni, J. Rodríguez-Laguna, G. Sierra, *Entanglement hamiltonian and entanglement contour in inhomogeneous 1D critical systems*, J. Stat. Mech. 043105 (2018).

[104] I. MacCormack, A.L. Liu, M. Nozaki, S Ryu, *Holographic Duals of Inhomogeneous Systems: The Rainbow Chain and the Sine-Square Deformation Model*, J. Phys. A: Math. Theor. **52**, 505401 (2019).

[105] R.M. Wald, *General relativity*, The University of Chicago Press (1984).

[106] I. Peschel, *Calculation of reduced density matrices from correlation functions*, J. Phys. A **36**, L205 (2003).

[107] B.-Q. Jin, V.E. Korepin, *Quantum Spin Chain, Toeplitz Determinants and the Fisher—Hartwig Conjecture*, J. Stat. Phys. **116**, 79 (2004).

[108] M. Fagotti, P. Calabrese, *Universal parity effects in the entanglement entropy of XX chains with open boundary conditions*, J. Stat. Mech. P01017 (2011).

[109] P.D. Nation, J.R. Johansson, M.P. Blencowe, F. Nori, *Stimulating uncertainty: Amplifying the quantum vacuum with superconducting circuits*, Rev. Mod. Phys. **84**, 1 (2012).

[110] J. Rodríguez-Laguna, S.N. Santalla, G. Ramírez, G. Sierra, *Entanglement in correlated random spin-chains, RNA folding and kinetic roughening*, New J. Phys. **18**, 073025 (2016).

[111] V. Alba, S.N. Santalla, P. Ruggiero, J. Rodríguez-Laguna, P. Calabrese, G. Sierra, *Unusual area-law violation in random inhomogeneous systems*, J. Stat. Mech. 023105 (2019).

[112] N. Samos Sáenz de Buruaga, S.N. Santalla, J. Rodríguez-Laguna, G. Sierra, *Piercing the rainbow: entanglement on an inhomogeneous spin chain with a defect*, Phys. Rev. B **101**, 205121 (2020).

[113] G. Ramírez, J. Rodríguez-Laguna, G. Sierra, *Entanglement in low-energy states of the random-hopping model*, J. Stat. Mech. P07003 (2014).

[114] B. Mula, S.N. Santalla, J. Rodríguez-Laguna, *Casimir forces on deformed fermionic chains*, Phys. Rev. Res. **3**, 013062(9) (2021).

[115] C. Dasgupta, S.-K. Ma, *Low-temperature properties of the random Heisenberg antiferromanetic chain*, Phys. Rev. B **22**, 1305 (1980).

[116] F. Finkel, A. González-López, *Entanglement entropy of inhomogeneous XX spin chains with algebraic interactions*, JHEP 184(35) (2021).

[117] L. Dagurre, R. Medina, M. Solís, G. Torroba, *Aspects of quantum information in finite density field theory*, JHEP 79 (2021).

[118] M. Mintchev, D. Pontello, A. Sartori, E. Tonni, *Entanglement entropies of an interval in the free Schrödinger field theory at finite density*, JHEP 120 (2022).

[119] N. Samos Sáenz de Buruaga, S.N. Santalla, J. Rodríguez-Laguna, G. Sierra, *Entanglement in non-critical inhomogeneous quantum chains*, Phys. Rev. B **104**, 195147 (2021).

[120] N. Samos Sáenz de Buruaga, S.N. Santalla, J. Rodríguez-Laguna, G. Sierra, *Symmetry protected phases in inhomogeneous spin chains*, J. Stat. Mech. 093102 (2019).

[121] G. Refael, J.E. Moore, *Entanglement entropy of random quantum critical points in one dimension*, Phys. Rev. Lett. **93**, 260602 (2004).

[122] N. Laflorencie, *Scaling of entanglement entropy in the random singlet phase*, Phys. Rev. B **72**, 140408(R) (2005).

[123] A. Hoyos, A.P. Vieira, N. Laflorencie, E. Miranda, *Correlation amplitude and entanglement entropy in random spin chains*, Phys. Rev. B **76**, 174425 (2007).

[124] S. Rosenberg, *The laplacian on a riemannian manifold*, Cambridge Univ. Press (2009).

[125] J. Gemmer, M. Michel, G. Mahler, *Quantum Thermodynamics*, Springer (2004).

[126] F. Binder, L.A. Correa, C. Gogolin, J. Anders, G. Adesso, *Thermodynamics in the quantum regime*, Springer (2018).

[127] M.N. Bera, A. Riera, M. Lewenstein, Z.B. Khanian, A. Winter, *Thermodynamics as a consequence of information conservation*, Quantum **3**, 121 (2019).

[128] M. Scully, M.S. Zubairy, G.S. Agarwal, H. Walther, *Extracting work from a single heat bath via vanishing quantum coherence*, Science **299**, 862 (2003).

[129] A. Ghosh, V. Mukherjee, W. Niedenzu, G. Kurizki, *Are quantum thermodynamic machines better than their classical counterparts?* Eur. Phys. J. Special Topics **227**, 2043 (2019).

[130] J.J. Fernández, *Optimization of energy production in two-qubit heat engines using the ecological function*, Quantum Sci. Technol. **7**, 035002 (2022).

[131] A.E. Allahverdyan, R. Balian, Th.M. Nieuwenhuizen, *Maximal work extraction from finite quantum systems*, Europhys. Lett. **67**, 565 (2004).

[132] R. Alicki, M. Fannes, *Entanglement boost for extractable work from ensembles of quantum batteries*, Phys. Rev. E **87**, 042123 (2013).

[133] F. Campaioli, F.A. Pollock, F.C. Binder, L. Céleri, J. Goold, S. Vinjanampathy, K. Modi, *Enhancing the charging power of quantum batteries*, Phys. Rev. Lett. **118**, 150601 (2017).

[134] G.M. Andolina, M. Keck, A. Mari, M. Campisi, V. Giovannetti, M. Polini, *Extractable work, the role of correlations, and asymptotic freedom of quantum batteries*, Phys. Rev. Lett. **122**, 047702 (2019).

[135] D. Rosa, D. Rossini, G.M. Andolina, M. Polini, M. Carrega, *Ultra-stable charging of fast-scrambling SYK quantum batteries*, JHEP **11**, 067 (2020).

[136] G. Francica, J. Goold, F. Plastina, M. Paternostro, *Daemonic ergotropy: enhanced work extraction from quantum correlations*, npj Quantum Information **3**, 12 (2017).

[137] G. Francica, F.C. Binder, G. Guarnieri, M.T. Mitchison, J. Goold, F. Plastina, *Quantum coherence and ergotropy*, Phys. Rev. Lett. **125**, 180603 (2020).

[138] S. Tirone, R. Salvia, V. Giovannetti, *Quantum energy lines and the optimal output ergotropy problem*, Phys. Rev. Lett. **127**, 210601 (2021).

[139] A. Touil, B. Çakmak, S. Deffner, *Ergotropy from quantum and classical correlations*, J. Phys. A: Math. Theor. **55**, 025301 (2022).

[140] G. Francica, *Quantum correlations and ergotropy*, Phys. Rev. E **105**, L052101 (2022).

[141] G. Manzano, F. Plastina, R. Zambrini, *Optimal work extraction and thermodynamics of quantum measurements and correlations*, Phys. Rev. Lett. **121**, 120602 (2018).

[142] A. Solfanelli, L. Buffoni, A. Cuccoli, M. Campisi, *Maximal energy extraction via quantum measurement*, J. Stat. Mech. 094003 (2019).

[143] J.J. Bisognano, E.H. Wichmann, *On the duality condition for a Hermitian scalar field*, J. Math. Phys. **16**, 985 (1975).

[144] J.J. Bisognano, E.H. Wichmann, *On the duality condition for quantum fields*, J. Math. Phys. **17**, 303 (1976).

[145] I. Peschel, M.-C. Chung, *Density Matrices for a Chain of Oscillators*, J. Phys. A **32** 8419 (1999).

[146] M.-C. Chung, I. Peschel, *On Density-Matrix Spectra for Two-Dimensional Quantum Systems*, Phys. Rev. B **62**, 4191 (2000).

[147] M.-C. Chung, I. Peschel, *Density-Matrix Spectra of Solvable Fermionic Systems*, Phys. Rev. B **64**, 064412 (2001).

[148] H. Casini, M. Huerta, *Reduced density matrix and internal dynamics for multicomponent regions*, Class. Quant. Grav. **26**, 185005 (2009).

[149] H. Casini, M. Huerta, R. Myers, *Towards a derivation of holographic entanglement entropy*, JHEP **1105**, 036 (2011).

[150] V. Eisler, I. Peschel, *Analytical results for the entanglement Hamiltonian of a free-fermion chain*, J. Phys. A: Math. Theor. **50**, 284003 (2017).

[151] H. Santos, J.E. Alvarellos, J. Rodríguez-Laguna, *Entanglement detachment in fermionic systems*, Eur. Phys. J. D **72**, 203 (2018).

[152] J. Cardy, E. Tonni, *Entanglement hamiltonians in two-dimensional conformal field theory*, J. Stat. Mech. 123103 (2016).

[153] S. Singha Roy, S.N. Santalla, J. Rodríguez-Laguna, G. Sierra, *Link representation of the entanglement entropies for all bipartitions*, J. Phys. A: Math. Theor. **54**, 305301 (2021).

[154] S. Singha Roy, S.N. Santalla, J. Rodríguez-Laguna, G. Sierra, *Entanglement as geometry and flow*, Phys. Rev. B **101**, 195134 (2020).

[155] A. Zamora, J. Rodríguez-Laguna, M. Lewenstein. L. Tagliacozzo, *Splitting a critical spin chain*, J. Stat. Mech. P09035 (2014).

[156] T. Shimaji, T. Takayanagi, Z. Wei, *Holographic quantum circuits from splitting/joining local quenches*, JHEP **03**, 165 (2019).

[157] A. Rolph, *Local measures of entanglement in black holes and CFTs*, SciPost Phys. **12**, 079 (2022).

[158] N.W. Ashcroft, N.D. Mermin, *Solid state physics*, Harcourt College Publ. (1976).

[159] U. Schollwöck, *The density-matrix renormalization group in the age of matrix product states*, Ann. Phys. **326**, 96 (2011).

[160] W.G. Unruh, *Notes on black-hole evaporation*, Phys. Rev. D **14**, 870 (1976).